

EXPERIMENTAL STUDIES OF FLUID TURBULENCE DURING THE
ENTRAINMENT OF AN INDIVIDUAL GRAVEL PARTICLE

A THESIS
SUBMITTED TO THE FACULTY OF THE GRADUATE SCHOOL
OF THE UNIVERSITY OF MINNESOTA
BY

KIRBY E. TEMPLIN

IN PARTIAL FULFILLMENT OF THE REQUIREMENTS
FOR THE DEGREE OF
MASTER OF SCIENCE

ADVISER: KIMBERLY HILL
CO-ADVISER: FERNANDO PORTÉ-AGEL

JUNE 2011

© KIRBY E. TEMPLIN 2011

Acknowledgements

I would first like to thank my advisers, Dr. Kimberly Hill and Dr. Fernando Porté-Agel. Thank you, Kimberly, for all your guidance and advice on this project. You were an invaluable help with the experimental design and data analysis. Fernando, thank you for your suggestions and guidance. Without both of you, this project would not have flowed as well as it did. I would also like to thank Chris Paola for serving on my defense committee.

To the technical staff at the St. Anthony Falls Laboratory, thank you for providing an enormous amount of help and making the lab a fun place to work.

Thank you fellow graduate students for creating a fun work atmosphere, your friendships have been essential to my success.

Lastly, I would like to thank the National Science Foundation for providing the funding for this project under the NSF grant No. 0756480.

Dedication

This thesis is dedicated to my family and friends for their love and support.

Abstract

Experiments were performed in a laboratory flume to investigate the relative importance of different turbulence mechanisms for the entrainment of an individual gravel particle into bed-load transport. The bed conditions tested in these experiments were a mobile gravel bed with a rough-to-smooth (R-S) transition, a fixed gravel bed with a R-S transition, and a fixed gravel bed with a smooth-to-rough (S-R) transition. One location of interest was in a region of steady uniform flow located away from the transition (SS location), and the other location of interest was in a region of steady non-uniform flow located near the roughness transition (T location). Fluid velocity measurements were taken directly above a tracer particle during entrainment into bed-load. Turbulence statistics of interest in this investigation included the downstream velocity (u), vertical velocity (w), downstream normal Reynolds stress ($u'u'$), vertical normal Reynolds stress ($w'w'$), and the Reynolds shear stress ($u'w'$). Conditionally averaged results show a strong correlation of particle entrainment with increases in u and decreases in w for all SS and T locations over the bed conditions tested. The fixed bed R-S transition results also show a correlation between initial motion and increases in $u'u'$, and $u'w'$ for the SS location but not the T location. The peaks seen in the trends of the conditionally averaged u results primarily occur prior to initial motion, and the time difference increases with distance above the bed. This suggests that inclined coherent structures are responsible for the entrainment of individual gravel particles.

Table of Contents

List of Tables	vi
List of Figures	viii
Chapter 1 Introduction and Background	1
1.1 Introduction	1
1.2 Bed-load Transport Models and Methods	2
1.3 Quadrant Analysis Background	6
1.4 Other Turbulence Statistics as Bed-load Transport Mechanisms	9
1.5 Coherent Structures	13
1.6 Uncertainties Inherent to Bed-load Transport and Thesis Focus	15
Chapter 2 Experimental Setup	17
2.1 The Laboratory Flume	17
2.2.1 Experimental Details - Experiment 1	18
2.2.2 Instrumentation - Experiment 1	27
2.2.3 Experimental Procedure - Experiment 1	30
2.2.4 Data Analysis - Experiment 1	35
2.3.1 Experimental Details - Experiment 2	38
2.3.2 Instrumentation - Experiment 2	38
2.3.3 Experimental Procedure - Experiment 2	40
Chapter 3 Experimental Results	43
3.1 Measurements of Turbulence Statistics and Tracer Particle Entrainment Under Uniform and Non-Uniform Conditions	43
3.1.1 Mobile Bed R-S Transition	44
3.1.2 Fixed Bed R-S Transition	49
3.1.3 Fixed Bed S-R Transition	54
3.1.4 Coherent Structure Analysis	60
3.1.5 Quadrant Analysis	70
3.2 Experiment 2	77

3.2.1	Fixed Bed Transition Location 1	77
3.2.2	Fixed Bed Transition Location 2	84
Chapter 4 Discussion		93
4.1	Considerations of Trends in Downstream Velocity Pulses.....	93
4.2	Alternate Bed-load Transport Models	99
4.3	Implications of Results	101
4.4	Frequency of Transport Events.....	102
Chapter 5 Summary and Conclusions.....		104
References		107
Appendix 1 Data from Fixed Bed R-S Transition Location 2		112

List of Tables

Table 2.1. Flume dimensions and experimental conditions relevant to the R-S transition mobile bed flume set-up. A, B, C, and D reference specific points in the flume as indicated in Figure 2.2a. Many details are specific to the reach of the flume. h refers to the average depth of the water, U is the mean flow velocity, Q is the water discharge, S is the bed slope, Re is the average Reynolds number of the flow, Fr is the average Froude number, D_{16} is the particle diameter of the 16 th percentile, D_{50} is the particle diameter of the 50 th percentile, D_{65} is the particle diameter of the 65 th percentile, D_{84} is the particle diameter of the 84 th percentile, D_{90} is the particle diameter of the 90 th percentile.....	24
Table 2.2. Flume dimensions and experimental conditions relevant to the R-S transition fixed bed flume set-up. The variables are defined in the caption of Table 2.1 and the relevant bed dimensions are referenced in Figure 2.2a.....	25
Table 2.3. Flume dimensions and experimental conditions relevant to the S-R transition fixed bed flume set-up. The variables are defined in the caption of Table 2.1 and the relevant bed dimensions are referenced in Figure 2.2b. (“-” indicates the property is not constant for the section).....	26
Table 2.4. Shear stresses calculated to validate system threshold transport conditions for the R-S transition bed configurations.	26
Table 2.5. Calculated values and instrument limitations which framed the decision on selecting the sediment feed rate, as well as the two sediment feed rates used for the experiments.	42
Table 3.1. Average turbulence statistics for the two locations investigated over the mobile bed R-S transition configuration.	49
Table 3.2. Average turbulence statistics for the two locations investigated over the fixed bed R-S transition configuration.....	53
Table 3.3. Average turbulence statistics for the two locations investigated over the fixed bed S-R transition configuration. The flow rate was increased by 15 % to collect data at the T location.	59
Table 3.4. Angles of inclined coherent structures associated with the offset of the peak seen in conditionally averaged downstream velocity u relative to when initial motion occurred. (*) denotes angles are oblique which represent angles towards the bed. (-) represents no clear trend in the conditionally averaged	

downstream velocity u . (+) represents an outlier, where a trend was present in the conditionally averaged downstream velocity u but the peak is not closely related to when initial motion occurred.	67
Table 3.5. Comparison of average angles representative of the data sets for the SS locations. The average angles are associated with the offsets of the peak which were determined from different methods. The second method described in the text to determine the angles was used to obtain these results.	70
Table 3.6. Comparison of average angles representative of the data sets for the T locations. The average angles are associated with the offsets of the peak which were determined from different methods. The second method described in the text to determine the angles was used to obtain these results. (*) Denotes that angles were determined without the outlier point.....	70
Table 3.7. Quadrant Analysis results for the SS location. The table represents the percentage of time associated with each quadrant event for a 2 sec window and 0.5 sec window surrounding when initial motion occurred.	76
Table 3.8. Quadrant Analysis results for the T location. The table represents the percentage of time associated with each quadrant event for a 2 sec window and 0.5 sec window surrounding when initial motion occurred.	77
Table 3.9. Slopes and intercepts for the linear trend lines of form $y = ax + b$ in Figure 3.19.	84
Table 3.10. Slopes and intercepts for the linear trend lines of form $y = ax + b$ in Figure 3.22.	91
Table A.1. R-S transition location 2 fixed bed flume dimensions and experimental properties. This table corresponds to Table 2.2. Refer to Figure 2.2a for flume dimensions.	113
Table A.2. Average turbulence statistics for the investigation to confirm the results of the fixed bed. This table corresponds to Table 3.2.	116
Table A.3. Angles of inclined coherent structures associated with the offset of the peak seen in conditionally averaged downstream velocity u relative to when initial motion occurred. This table corresponds to Table 3.4. (*) denotes angles are oblique which represent angles towards the bed.	116
Table A.4. Quadrant analysis results for the investigation to confirm the results of the fixed bed. This table corresponds to Tables 3.7 and 3.8 for the SS location and the T location, respectively.	117

List of Figures

Figure 1.1. Diagram representing the quadrant analysis and the corresponding quadrant and event names.....	9
Figure 1.2. Example of a fluid structure with coherent movement within a distinct region inclined away from the bed. Modeled after <i>Theodorsen</i> [1952] as seen in <i>Robinson</i> [1991].....	15
Figure 2.1. Photograph of the flume used for the experiments.	18
Figure 2.2. a.) Flume set-up for R-S transition configuration. Tables 2.1 and 2.2, and A.1 contain specific values of A, B, C, and D for the experiments. b.) Flume set-up for S-R transition configuration. Table 2.3 contain specific values of A, B, C, and D for the experiments.....	23
Figure 2.3. Photograph of one of the tracer gravel particles used for the experiments. The reference dimensions in the picture are cm.	23
Figure 2.4. A photograph of the seeding system.....	29
Figure 2.5. a.) A photograph of the instrument cart which the ADV and camera are mounted to. The instrument cart could move up and down the length of the flume. b.) Front and side view of the system configuration and the system relationships under the water surface.	30
Figure 2.6. a.) Photograph of the parts grabber used to place the tracer particle in location. b.) Photograph of the parts grabber grabbing mechanism extended..	34
Figure 2.7. Running average of a.) u and b.) $u'w'$. Each plot shows the average of a two minute long sample and six different sets of 100 points tested for the number of events needed to determine trends in the results.	35
Figure 2.8. Shown in the photograph is the setup to collect a minute long sample to determine the sediment feed rate.	40
Figure 3.1. Bed profile and WSP for the experiments performed over the mobile bed R-S transition configuration. The data markers are at the points where data were collected. The equations represent the linear trend lines associated with the rough and smooth sections of the bed and provide the slopes of those sections. The two locations where data was collected are marked with an “X”. A line was used for the WSP to guide the eye.....	46

Figure 3.2. Velocity profiles for the two locations investigated over the mobile bed R-S transition configuration. Lines were used to guide the eye.	47
Figure 3.3. Conditionally averaged results for the turbulence statistics u , w , $u'u'$, $u'w'$, and $w'w'$ for the two locations investigated over the mobile bed R-S transition configuration. The left column of figures is the results for the SS location. The right column of figures is the results for the T location.	48
Figure 3.4. Bed profile and WSP for the experiments performed over the fixed bed R-S transition configuration. The data markers are at the points where data were collected. The equations represent the linear trend lines associated with the rough and smooth sections of the bed and provide the slopes of those sections. The two locations where data were collected are marked with an “X”. A line was used for the WSP to guide the eye.....	51
Figure 3.5. Velocity profiles for the two locations investigated over the fixed bed R-S transition configuration. Lines were used to guide the eye.	51
Figure 3.6. Conditionally averaged results for the turbulence statistics u , w , $u'u'$, $u'w'$, and $w'w'$ for the two locations investigated over the fixed bed R-S transition configuration. The left column of figures is the results for the SS location. The right column of figures is the results for the T location.	53
Figure 3.7. Bed profile and WSP for the experiments performed over the fixed bed S-R transition configuration. The two WSP’s correspond to the two conditions used for these experiments as described in the text. Specifically, the flow rate was increased by 15 % to collect data at the T location. The data markers are at the points where data were collected. The equations represent the linear trend lines associated with the rough and smooth sections of the bed and provide the slopes of those sections. The two locations where data were collected are marked with an “X”. A line was used for the WSP to guide the eye.....	57
Figure 3.8. Velocity profiles for the two locations investigated over the fixed bed S-R transition configuration. The flow rate was increased by 15 % to collect data at the T location. Lines were used to guide the eye.....	57
Figure 3.9. Conditionally averaged results for the turbulence statistics u , w , $u'u'$, $u'w'$, and $w'w'$ for the two locations investigated over the fixed bed S-R transition configuration. The left column of figures is the results for the SS location. The right column of figures is the results for the T location. The flow rate was increased by 15 % to collect data at the T location. Special thanks to A. Iversen who collected the data for the height 2.1 cm at the T location.	59

Figure 3.10. A system diagram showing the dimensions and configuration that has been studied and the representation of an inclined structure. The ADV has a cylindrical control volume. The height of the control volume is 7 mm and the diameter is 6 mm.	66
Figure 3.11. Offset associated with the peak seen in the conditionally averaged u results as it is affected by the number of smoothing iterations. a.) Example where multiple iterations are required for the peak to stabilize. b.) Example where no smoothing iterations were necessary for the stabilization of the peak, and an example of a large scale shift in the peak not relevant to when initial motion occurred.	67
Figure 3.12. All uncorrected offsets associated with the peak in the u velocity of the conditionally averaged results. The limits corresponding to the 0.033 sec window of uncertainty are also plotted.....	68
Figure 3.13. Plots associated with the second method for determining the average angle of inclination representative for the data sets at the SS location and the T location. The equation for the linear trend lines is $y = Ax + B$. a.) Fixed bed R-S transition. SS location: $A = -0.2012, B = 0.643$. T location: $A = -0.1171, B = 0.1249$. b.) Fixed bed S-R transition. SS location: $A = -0.0972, B = 0.3943$. T location: $A = -0.145, B = -0.0102$. c.) Mobile bed R-S transition. SS location: $A = -0.085, B = 0.1647$. T location: $A = -0.1238, B = 0.2111$	69
Figure 3.14. Quadrant analysis plots for a.) 2 second window and b.) 0.5 second window of the SS location for the height 1.4 cm over the fixed bed R-S transition....	74
Figure 3.15. Quadrant analysis plots for a.) 2 second window and b.) 0.5 second window of the T location for the height 1.37 cm over the fixed bed R-S transition....	75
Figure 3.16. The 2 sec and 0.5 sec window of the conditionally averaged w' results for locations a.) SS at 1.4 cm above the fixed bed, and b.) T at 1.37cm above the fixed bed.	75
Figure 3.17. a.) WSP's, b.) Bed profile, c.) Depth of flow. Lines were used to guide the eye.....	81
Figure 3.18. a.) Bed elevation change with respect to the pre-experiment local average bed profile. b.) Zoomed in look at the near transition region of the bed elevation change with respect to the pre-experiment local average bed profile. c.) Bed elevation change with respect to the hr 7 local average bed profile. d.) The percentage of the hr 7 local average bed elevation. Lines were used to guide the eye.	82

Figure 3.19. Zoomed in bed profiles with linear fit trend lines of form $y = ax + b$ where the slope “ a ” and intercept “ b ” are in Table 3.9. a.) 1.17 m. b.) 0.3 m upstream of the R-S transition. c.) the slope changes plotted verses time..... 84

Figure 3.20. a.) WSP’s, b.) Bed profile, c.) Depth of flow. Lines were used to guide the eye. 88

Figure 3.21. a.) Bed elevation change with respect to the pre-experiment local average bed profile. b.) Zoomed in look at the near transition region of the bed elevation change with respect to the pre-experiment local average bed profile. c.) Bed elevation change with respect to the hr 8 local average bed profile. d.) The percentage of the hr 8 local average bed elevation. Lines were used to guide the eye. 89

Figure 3.22. Zoomed in bed profiles with linear fit trend lines of form $y = ax + b$ where the slope “ a ” and intercept “ b ” are in Table 3.10. a.) 1.12 m. b.) 0.3 m upstream of the R-S transition. c.) the slope changes plotted verses time..... 91

Figure 3.22. Photograph of the streaks of gravel upstream of the fixed bed R-S transition as mentioned in the text. 92

Figure 4.1. Case which demonstrates how event time series can lead to a trend in u and trend in $u'u'$. a.) u velocity run samples and conditionally averaged u . b.) u' velocity fluctuation run samples and conditionally averaged u' . c.) $u'u'$ of the run samples and the conditionally averaged $u'u'$. Lines were used to guide the eye. 97

Figure 4.2. Case which demonstrates how event time series can lead to a trend in u and no trend in $u'u'$. a.) u velocity run samples and conditionally averaged u . b.) u' velocity fluctuation run samples and conditionally averaged u' . c.) $u'u'$ of the run samples and the conditionally averaged $u'u'$. Lines were used to guide the eye. 98

Figure 4.3. Case which demonstrates how event time series can lead to no trend in u and trend in $u'u'$. a.) u velocity run samples and conditionally averaged u . b.) u' velocity fluctuation run samples and conditionally averaged u' . c.) $u'u'$ of the run samples and the conditionally averaged $u'u'$. Lines were used to guide the eye. 99

Figure A.1. Bed profile and WSP for the experiments performed to confirm the results over the fixed bed. The data markers are at the points where data were collected. The equations represent the linear trend lines associated with the rough and smooth sections of the bed and provide the slopes of those sections. The two locations where data were collected are marked with an “X”. A line

was used for the WSP to guide the eye. This figure corresponds to Figure 3.4.	114
Figure A.2. Velocity profiles for the two locations investigated to confirm the results over the fixed bed. Lines were used to guide the eye. This figure corresponds to Figure 3.5.....	114
Figure A.3. Conditionally averaged results for the turbulence statistics, u , w , $u'u'$, $u'w'$, $w'w'$, for the two locations investigated to confirm the results over the fixed bed. The left column of figures is the results for the SS location. The right column of figures is the results for the T location. This figure corresponds to Figure 3.6.....	116

Chapter 1

Introduction and Background

1.1 Introduction

Systems that transport sediment by wind and water play a major role in shaping the earth's surface. Sediment transport is also important for certain engineered systems and the health of ecosystems. Thus sediment transport has attracted a wide range of interest in scientific and engineering communities. Sediment transport is often broken up into two distinctly different modes for modeling purposes, suspended-load and bed-load. When particles are transported through suspended-load they are transported within the fluid column with little contact with other particles. When particles are transported through bed-load, they are in frequent contact with other particles and with the system boundaries. Bed-load transport is a critical component in river engineering and stream restoration practices. Methods used to predict bed-load transport are used to help understand erosion and deposition in natural systems, and in altered or engineered systems. An assessment of channel stability is derived from the understanding of bed-load transport, and bed-load is often the chief mode of transport in low flows and gravel bed streams [Hill *et al.*, 2010]. Bed-load is also important for predicting suspended-load, because bed-load sets the scale for the amount of sediment being transported in suspended-load [Van Rijn, 1984b]. The most common models of bed-load transport were derived empirically using data obtained under steady state and uniform conditions. It is

important to expand the understanding of bed-load transport to complex flow situations more commonly found in nature. To do so requires a better understanding of the relationship between turbulent fluid and the movement of particles in bed-load transport. In this chapter, first, the most common framework for modeling and predicting bed-load transport in the field is briefly summarized. Then recent attempts to understand complex fluid/particle interactions relevant to bed-load transport are discussed.

1.2 Bed-load Transport Models and Methods

The bed-load process can be broken up into three stages and involves the entrainment of a particle into motion, displacement of the particle during motion, and distraintment of the particle from motion [*Drake et al.*, 1988]. *Drake et al.* [1988] defined the different modes of entrainment as entrainment by rollover, liftoff, and impact ejection. The different modes of displacement were defined as displacement by saltation, rolling, and sliding. They described the different modes of distraintment as a sudden halt for the distraintment of saltating and sliding particles, and a gradual deceleration for rolling particles. Current bed-load predictive methods follow a general framework which uses relatively simple measures to determine a system's potential to transport particles in bed-load and then provides a predictive measure of their transport [*Meyer-Peter and Müller*, 1948; *Einstein*, 1950; *Ashida and Michiue*, 1971; *Engelund and Friesoe*, 1976; *Van Rijn*, 1984a; *Parker*, 1990; *Wong and Parker*, 2006; *Francalanci and Solari*, 2008]. The primary physical mechanism used in most well established bed-load transport models is a measure of the average shear stress exerted by the fluid on the bed, τ_0 . In these models, when τ_0 is too small, no particles move. When τ_0 exceeds a critical shear

stress threshold value τ_c determined, as discussed below, by particles in the bed barely starting to move. Many bed-load discharge models are based on empirical and semi-empirical bed-load relationships that relate the bed-load discharge rate q_s to the difference of τ_0 and τ_c . As mentioned, there are many applications where the bed-load relationships do not provide great results because complex flow dynamics do not relate well with the flow situations under which the bed-load relationships were developed. To understand why, it is helpful to briefly review the key parameters τ_0 and τ_c and how the relationships for q_s were derived.

There are many methods to determine τ_0 and selecting the most appropriate method depends on the systems flow characteristics. Among many methods, some common methods used to estimate τ_0 are as follows: (1) the so-called depth-slope average expression, appropriate assuming gravity driven steady uniform flow:

$$\tau = \rho ghS \quad (1)$$

(2) the Reynolds shear stress:

$$\tau = -\rho \langle u'w' \rangle \quad (2)$$

(3) a shear stress derived using the shear velocity determined from the log law of the wall:

$$\tau = \rho u_*^2 \quad (3)$$

where the log law of the wall may be written

$$\frac{\langle u \rangle}{u_*} = \frac{1}{\kappa} \ln \left(\frac{z}{z_0} \right) \quad (4)$$

In these equations, ρ is the fluid density, g is gravity, h is the fluid depth, S is the bed slope, u' is the instantaneous downstream turbulent fluctuation, w' is the instantaneous

vertical turbulent fluctuation, u^* is the shear velocity, u is the downstream velocity, κ is the Karman constant equal to 0.4, z is the height above the bed, z_0 is the bed roughness characteristic length, and $\langle \rangle$ denotes time averaged quantity. At this point it is useful to note that all terms in equations (1)-(4) are considered time-averaged quantities. Time average is specified for $\langle u \rangle$ and $\langle u'w' \rangle$, since the assumption of turbulence velocities is implicit in the form of these expressions. Thus each velocity $u(t)$ can be expressed in terms of an average $\langle u \rangle$ and an instantaneous fluctuation $u'(t) = u(t) - \langle u \rangle$.

A critical piece in determining bed-load transport is predicting τ_c . For relatively narrowly distributed particle sizes Brownlie's formula works well [Brownlie, 1981].

$$\tau_c^* = .22Re_p^{-.6} + .06 \cdot 10^{(-7.7Re_p^{-.6})} \quad (5)$$

where,

$$Re_p = \frac{\sqrt{(s-1)gD^2}}{\nu} \quad (6)$$

and,

$$\tau_c^* = \frac{\tau_c}{\rho(s-1)gD} \quad (7)$$

where τ_c^* is the non-dimensional critical shear stress, Re_p is the Reynolds particle number, s is the specific weight of the particle, g is gravity, ν is kinematic viscosity, D is the median particle diameter of the bed, and τ_c is the critical shear stress. For less narrowly distributed particle sizes, there are a number of suggested modifications of this form [Wilcock and Crowe, 2003]. However they are not relevant to the focus of this thesis and will not be discussed further here.

Whether or not bed-load transport is predicted in a particular system is typically determined by comparing τ_0 with τ_c . To summarize, if τ_0 is greater than τ_c it is predicted

that bed-load transport will occur in the system, and if τ_0 is less than τ_c it is predicted that there will be no bed-load transport in the system. The next step in assessing bed-load transport is to provide an estimate for the bed-load discharge expected to occur in the system.

There are several methods which have been proposed to predict sediment discharge. A common method is the Meyer-Peter and Müller method [*Meyer-Peter and Müller, 1948; Wong and Parker, 2006*].

$$q_s^* = k(\tau_0^* - \tau_c^*)^{3/2} \quad (8)$$

where,

$$q_s^* = \frac{q_s}{[g(s-1)D]^{1/2}D} \quad (9)$$

where q_s^* is the non-dimensional bed-load sediment discharge per unit width, q_s is the bed-load sediment discharge per unit width, k is a constant 3.97, and τ_0^* is the non-dimensional bed shear stress, τ_c^* is the non-dimensional critical shear stress, g is gravity, s is the specific weight of the particle, and D is the median particle diameter of the bed.

There are a number of other analogous formulas, but all take similar forms. See, for example [*Meyer-Peter and Müller, 1948; Einstein, 1950; Ashida and Michiue, 1971; Engelund and Feresoe, 1976; Van Rijn, 1984a; Parker, 1990; Wong and Parker, 2006; Francalanci and Solari, 2008*].

There are several different ways to modify these expressions to encompass a wider range of systems. For example, corrections to Brownlie's formula [*Wilcock and Crowe, 2003*], and equation (9) take somewhat different forms depending on particle size distributions and the presence of bed forms, etc [*Meyer-Peter and Müller, 1948; Einstein,*

1950; Ashida and Michiue, 1971; Engelund and Feresoe, 1976; Van Rijn, 1984a; Parker, 1990; Wong and Parker, 2006; Francalanci and Solari, 2008]. There is difficulty in selecting the most appropriate equations and method for estimating τ_0 to predict bed-load transport in a particular system. Even while these modifications to the general bed-load transport model described above expand its applicability, physical measurements and numerically modeled results do not agree in many applications [Nelson *et al.*, 1995; McLean *et al.*, 1994]. In particular, under non-uniform conditions, the relationships suggested by equations (1)-(9) based on steady conditions break down.

1.3 Quadrant Analysis Background

As mentioned, the general framework for predicting bed-load transport has been developed using empirical and semi-empirical relationships from data acquired primarily under steady conditions. Further investigations have focused on one measure that can account for a variable flow, specifically the Reynolds stress, Equation (2). There has been a lot of interest in better understanding the bed shear stress predictor $\langle u'w' \rangle$ and the relationship between specific turbulent velocities and bed-load transport. To understand this, it is helpful to note a specific form of $\langle u'w' \rangle$ as it relates to discrete data points which may have positive or negative values of u' and w' .

$$\langle u'w' \rangle = \frac{1}{N} \sum_{i=1}^N (u_i - \langle u \rangle)(w_i - \langle w \rangle) \quad (10)$$

where u' is the instantaneous downstream turbulent fluctuation, w' is the instantaneous vertical turbulent fluctuation, N is the number of discrete data points, u_i is the instantaneous downstream velocity, u is the downstream velocity, w_i is the instantaneous vertical velocity, w is the vertical velocity, and $\langle \rangle$ denotes time averaged quantity.

A method known as the quadrant method was introduced to investigate the significance of the statistics of instantaneous $u'-w'$ pairs measured with flow measurement instruments [Willmarth and Lu, 1971]. The quadrant method describes the relationships of positive and negative values of u' and w' , and involves a plot of each instantaneous $u'-w'$ pair with u' plotted on the horizontal axis, and w' plotted on the vertical axis, as in Figure 1.1. The relationships corresponding with each quadrant are identified as follows. If $u' > 0$ and $w' > 0$, this data point falls in Quadrant 1 and is sometimes referred to as a “Q₁ event” or outward interaction. If $u' < 0$ and $w' > 0$, this data point falls in Quadrant 2 and is sometimes referred to as a “Q₂ event” or ejection. If $u' < 0$ and $w' < 0$, this data point falls in Quadrant 3 and is sometimes referred to as a “Q₃ event” or inward interaction. If $u' > 0$ and $w' < 0$, this data point falls in Quadrant 4 and is sometimes referred to as a “Q₄ event” or sweep. Q₂ and Q₄ events result in $u'w' < 0$ and contribute positively to the Reynolds stress, and Q₁ and Q₃ events result in $u'w' > 0$ and contribute negatively to the Reynolds stress.

Quadrant analyses of velocity time series have provided more information about the general statistics of the $u'-w'$ pair than a simple average calculation of $\langle u'w' \rangle$ can provide. Quadrant analyses have shown that the dominant quadrant events of a velocity time series typical for turbulent flow are Q₂ and Q₄ [Nelson et al., 1995; Paiement-Paradis et al., 2010; Williams et al., 1989; Thorne et al., 1989; Wallace et al., 1972]. Although Q₂ and Q₄ events have been shown to be the dominant quadrant events under several different system conditions, it has also been shown that in a bed of particles the dominant quadrant events can be different depending on the bed packing densities

[*Papanicolaou et al.*, 2001].

Recent research has paired quadrant analyses of velocity time series with analysis of bed-load transport. The primary focus has been in identifying specific quadrant events that correlate with bed-load transport events. The results have varied somewhat. Some research results indicate that Q₂ events are the primary $u'w'$ events that correlate with bed-load transport events [*Paiement-Paradis et al.*, 2010; *Sechet and Le Guennec*, 1999]. Other investigations have favored Q₄ events as the primary $u'w'$ events correlating with bed-load transport events [*Nelson et al.*, 1995; *Hofland et al.*, 2005; *Williams et al.*, 1989; *Thorne et al.*, 1989; *Drake et al.*, 1988; *Heathershaw and Thorne*, 1985]. Some of the research results indicate that while Q₄ events are the primary $u'w'$ events correlated with bed-load transport events, Q₁ events are important as well [*Nelson et al.*, 1995; *Thorne et al.*, 1989; and *Heathershaw and Thorne*, 1985].

Nelson et al. [1995] specifically investigated these issues for a very non-uniform system. They used a quadrant analysis in an investigation of bed-load transport in a complex flow field following a backward facing step. They took highly resolved measurements of the rate of sand transported simultaneously with fluid velocities. Then they performed an analysis of the bed-load transport associated with velocity events falling in each quadrant. Specifically, they performed a quadrant analysis during bed-load transport events that correlate the percentage of sediment transported during each kind of turbulence event with the percentage of time occupied by each kind of turbulence event. Their analysis showed that Q₄ and Q₁ events were the primary Reynolds stress contributors that correlated with sediment transport. In this analysis Q₁ events occupied

less time than Q_4 events, but the amount of sediment transport correlated equally between the two quadrant events. This suggests that an increase in the frequency of Q_1 events would cause an increase in sediment transport in the system, but cause a reduction in $\langle u'w' \rangle$ (average Reynolds stress) [Nelson *et al.*, 1995].

This analysis expresses the uncertainty which has been associated with the bed shear stress as the predictor for bed-load transport and it has proven difficult to develop a systematic approach which predicts bed-load transport well in complex flow fields.

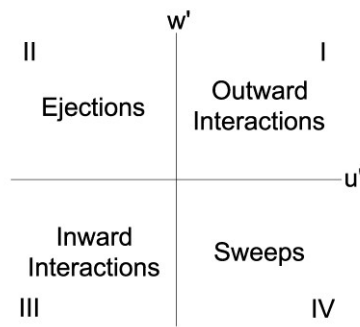


Figure 1.1. Diagram representing the quadrant analysis and the corresponding quadrant and event names.

1.4 Other Turbulence Statistics as Bed-load Transport Mechanisms

In addition to the research linking specific $u'w'$ events to bed-load transport described in the previous section, there have been a number of additional studies investigating other aspects of turbulence statistics for their relevance to bed-load transport. Many of these are motivated by the observation that bed-load transport tends to be dominated by intermittent movements, and it has been hypothesized that these are linked to sporadic instantaneous turbulence events not captured by time averaged quantities, especially in complex flow fields [Valyrakis *et al.*, 2010; Paiement-Paradis *et al.*, 2010; Schmeeckle *et al.*, 2007; Hofland *et al.*, 2005; Nelson *et al.*, 1995; Williams,

1990; *Williams et al.*, 1989]. Although bed-load relationships use the bed shear stress as a primary indicator of the quantity of particles transported in bed-load, recent investigations have suggested that the bed shear stress is not well correlated with important transport events. Instead, a number of investigations have suggested that other turbulence mechanisms may be more relevant to bed-load transport [*Nelson et al.*, 1995; *Papanicolaou et al.*, 2001; *Paiement-Paradis et al.*, 2010; *Schmeeckle et al.*, 2007; *Bottacin-Busolin et al.*, 2008; *Clifford et al.*, 1991]. Visual observations of bed-load transport suggested that increases in the horizontal turbulent velocity fluctuations are the reason for increases in $u'w'$ which causes sediment transport [*Thorne et al.*, 1989; *Drake et al.*, 1988; *Williams*, 1990]. Subsequent investigations have indicated that $u'w'$ is either weakly correlated with bed-load transport or that there is no correlation between sediment transport and $u'w'$ even under conditions when bed-load transport events are strongly correlated with u (instantaneous downstream velocity) [*Nelson et al.*, 1995] and [*Williams et al.*, 1989]. Research performed by *Schmeeckle et al.* [2007] investigating fluid forces at the particle scale support the findings that u , rather than $u'w'$, provides the physical mechanism responsible for moving particles in bed-load transport. *Schmeeckle et al.* [2007] measured fluid velocities around a stationary particle while simultaneously measuring instantaneous net vertical and horizontal forces on the particles. They found that the instantaneous horizontal force measured on stationary particles correlated well with u , but not with $u'w'$. These results point to the limitation in the bed-load transport framework described by Equations (1)-(9). In situations where turbulence fluctuations scale statistically similarly with the local average velocity, whether or not $\langle u'w' \rangle$ is

mechanistically responsible for bed-load movement, it may very well be correlated with average bed-load transport and thus work as a predictive parameter in a model. On the other hand, if $u'w'$ is neither the mechanism responsible for bed-load transport nor well correlated with the mechanism that is responsible for bed-load transport, it is important to understand the mechanism responsible for bed-load transport. Additional research has implicated other turbulence statistics as important for predicting bed-load transport. The research is still in its infancy, so there has been no corresponding bed-load transport models built on these findings, but it is still useful to consider them.

While the research described above has cast some uncertainty on the predictive relevance of $u'w'$ for bed-load transport, and there is no clear replacement, there is evidence for other statistics that can take the place of $u'w'$ under certain situations. In addition to the instantaneous downstream velocity, there is some evidence that point toward $u'u'$ (instantaneous downstream normal stress) as an important mechanism for bed-load transport. Specifically, *Papanicolaou et al.* [2001], and *Clifford et al.* [1991] have shown that $u'u'$ is the most dominant Reynolds stress term. It has also been suggested that different turbulence statistics are responsible for specific modes of bed-load transport such as sliding, rolling, and saltating [*Paiement-Paradis et al.*, 2010; *Valyrakis et al.*, 2010; *Drake et al.*, 1988]. Investigations by *Valyrakis et al.* [2010] measured impulse, defined as the magnitude and duration of turbulent events, for rolling and saltating transport events which showed that saltating events required a larger impulse in order to occur than rolling events. *Paiement-Paradis et al.* [2010] investigated the difference between rolling and sliding transport events, and noticed that

rolling events correlated mostly with Q_2 events and sliding events correlate mostly with Q_4 and Q_3 events. *Paiement-Paradis et al.* [2010] further suggested that the mode-specific turbulence mechanisms vary with the size of the particle. *Drake et al.* [1988] also found that the size of the gravel influenced the specific mode of transport. The specific modes of transport included rolling, sliding, and saltating.

In addition to understanding which turbulence statistics are important for bed-load transport, there is evidence that characteristics of the physical fluid turbulence events are important to understanding their influence on bed-load transport. That is, even if either u (instantaneous downstream velocity) or $u'u'$ (instantaneous downstream normal stress) alone might be shown most important, it seems that some sort of average over time may not be sufficient. It has been shown that both magnitude and duration of individual turbulence events [*Valyrakis et al.*, 2010], and/or fluid acceleration/deceleration [*Paiement-Paradis et al.*, 2010] may be most important for individual sediment transport events, and these may not scale simply with the mean statistics. Relative exposure of a particle can impact the necessary flow conditions for entrainment to occur [*Fenton and Abbott*, 1977, *Hofland et al.*, 2005], and what has been referred to as “pocket geometry”, may not be reflected in the turbulence statistics. There are many variable system characteristics important in bed-load transport, which includes flow characteristics and physical bed conditions that influence bed-load transport and the threshold of initial motion. Linking flow characteristics and physical bed conditions requires a deeper understanding of the fluid-bed interaction, especially concerning bed-load transport.

1.5 Coherent Structures

Some have suggested that larger correlated fluid structures are responsible for most of particle movement. A separate research subject by itself is studying the physical understanding of fluid organization, coherent structures. This presents additional complications for the next generation of models for bed-load transport, as there is a lot of uncertainty within the field on how the fluid organizes itself and the implications different system variables have on the organization of fluid and coherent structures. One important fluid structure appears to involve coherent movement within a distinct region inclined to the plane, perhaps first modeled by *Theodorsen* [1952]. An example of an inclined coherent structure, modeled after *Theodorsen* [1952] as seen in *Robinson* [1991], is shown in Figure 1.2. Since then, many models for inclined coherent structures have been proposed, though of similar appearance to that originally proposed by *Theodorsen* [1952] with relatively minor differences. Some of these differences involve the angles of inclination of these structures relative to the bed surface. Angles of inclination which have been published associated with the flow of water include an average of 14° [*Niño and García*, 1996; *García et al.*, 1995], 16° - 20° [*Lu and Willmarth*, 1973], average of 25° [*Roy et al.*, 2004], and 36° [*Buffin-Bélanger et al.*, 2000a]. Dye experiments have shown that there is not necessarily a unique angle associated with these inclined coherent structures, and several tangential angles can correspond to a single structure depending on the height above the bed. The angles associated with these different heights range between 6° - 67° [*Haidari and Smith*, 1994], and 15° - 75° with 45° being average [*Adrian et al.*, 2000]. Angles of inclination associated with the flow of air in wind tunnel

experiments include 13° [Rajagopalan and Antonia, 1979], 18° [Brown and Thomas, 1977], and large eddy simulation (LES) results from Marusic *et al.* [2001] agree with these results. Other variations in the descriptions of these inclined structures involve the specific turbulence events associated with the structure. Some physical models have linked specific $u'w'$ events to the inclined fluid structures (e.g., Q_2 events in [Kline *et al.*, 1967]). More recent physical models involve a more complex bursting cycle with the different $u'w'$ contributors as different features of the fluid organization and coherent structure (e.g., Q_2 events in the inside of the structure and Q_4 events around the inside of the structure) [Robinson, 1991]. Relating these and other fluid structures to quantitative measures of bed-load transport is difficult. While some have suggested these specific structures are relevant to bed-load transport, there are very few examples in the literature that present clear evidence linking sediment transport directly with inclined coherent structures. Most examples have been qualitative. For example, Niño and García, [1996] used dye and seeding experiments to visualize fluid structure simultaneously with the bed and individual particles. Also, Williams [1990] recorded video showing intermittent bursts of bed-load transport over a relatively wide spatial area, suggesting that an organization of fluid is responsible [Williams, 1990]. However, there has not yet been a predictive model built on these observations.

Fluid organization has major implications for sediment transport and the flow dynamics will likely be important for bed-load sediment transport. An example where fluid organization is important is in scour processes, and this has been extensively investigated around bridge piers. Horseshoe vortices similar to the structure shown in

Figure 1.2 are the primary mechanism involved in the scour process just upstream of the bridge pier, and predictive relationships remain difficult to establish for this well documented case because of the numerous variables influencing the complex flow field [Dargahi, 1990].

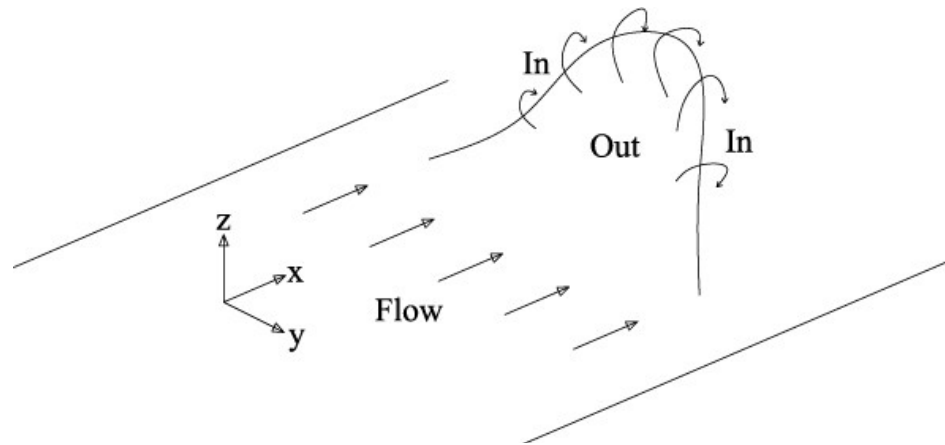


Figure 1.2. Example of a fluid structure with coherent movement within a distinct region inclined away from the bed. Modeled after *Theodorsen* [1952] as seen in *Robinson* [1991].

1.6 Uncertainties Inherent to Bed-load Transport and Thesis Focus

Bed-load sediment transport is difficult to predict because there are many interacting mechanisms important to bed-load transport, and their relative importance for the movement of particles in bed-load transport is not understood and apparently varies somewhat from one system to the next. One of the challenges in the study of bed-load transport is in the design of a system that isolates some of the mechanisms sufficiently well to study their effect on bed-load transport while maintaining a system that is sufficiently relevant to a natural system for eventual use in effective model building for natural systems. As discussed above, variables that influence the apparent mechanisms responsible for bed-load transport appear to include particle size, grain size distributions, the presence of bedforms and other details that give rise to an unsteady system in nature.

Thus an effective model for bed-load transport must include a representation of how various system variables (e.g., boulders, grain size distributions, roughness transitions, etc.) influence the complex flow fields that in turn transport the particles that comprise the bed, bedforms, roughness transitions, etc.

Understanding the interaction between the bed and the fluid during bed-load transport will help improve predictive models greatly. The role of turbulent coherent structures in sediment transport appears important, yet there is little existing data on which to build a predictive model, and much of it has been derived under relatively uniform or specialized conditions. Because the time scales of some of the turbulence statistics is so short, data collection systems need to have the capability of collecting data at a relatively high frequency to provide sufficiently resolved turbulence information.

The general purpose of the research described in this thesis is to identify the important turbulence mechanisms for the entrainment of particles into bed-load transport. The investigation is focused on the initial motion of particles at an individual gravel particle scale and how a roughness transition affects the apparent important turbulence mechanisms. To do so, fluid velocities were recorded at a high resolution near an individual gravel particle and correlated with particle entrainment. To investigate the fluids interaction with the bed during initial motion, the flow conditions were set near the critical threshold for motion. The rest of the thesis is organized as follows: In Chapter 2, the experimental set-up and most of the analysis methods are described in detail. In Chapter 3, the experimental results are presented. In Chapter 4, the discussion relevant to the results, and in Chapter 5, the summary and conclusion.

Chapter 2

Experimental Setup

2.1 The Laboratory Flume

The experiments were performed in an experimental flume at the St. Anthony Falls Laboratory at the University of Minnesota, pictured in Figure 2.1. The dimensions of the flume are 22.5 m long and 0.5 m wide, and the walls extend, at their lowest point 0.2 m above the established bed. The slope of the bed is nearly the same for all the experiments, but since it varies slightly, it will be discussed with the details of the particular experiment. The water supply to the channel is capable of a volumetric discharge of water of up to $0.125 \text{ m}^3/\text{s}$, though the discharge does not come anywhere near this value in these experiments. The water is not re-circulated as it is supplied directly from the Mississippi River and is returned to the river after it passes once through the flume. There were two qualitatively different types of experiments performed in this study. The experimental setup for the first type of experiments is discussed in section 2.2, and the experimental setup for the second type of experiments is discussed in section 2.3.

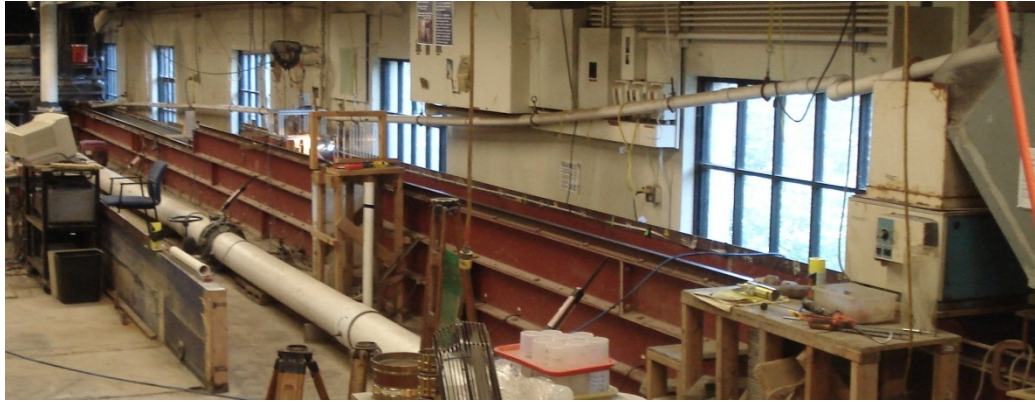


Figure 2.1. Photograph of the flume used for the experiments.

2.2.1 Experimental Details - Experiment 1

The work performed in the experiments of the first type was focused on correlations between turbulence statistics and sediment entrained under steady uniform and non-uniform roughness conditions in an otherwise flat bed. To achieve this, two consecutive long sections of the bed were prepared with a uniform roughness, and there was a relatively sharp transition between the two sections. The flow was considered relatively uniform far from the transition (as will be justified shortly).

There were two different roughness transitions investigated: (1) a rough to smooth (R-S) transition, and a smooth-to-rough (S-R) transition. There were two different bed conditions tested for the R-S transition experiments: (1) a mobile gravel bed for the upstream rough part of the transition and a smooth board for the downstream smooth part of the transition, and (2) a fixed gravel bed for the upstream rough part of the transition, and a fixed gravel bed comprised of smaller particles for the downstream smooth part of the transition. For the S-R transition experiments, only a fixed gravel bed comprised of small particles upstream for the smooth part of the transition, and a fixed gravel bed comprised of large particles for the downstream rough part of the transition was

investigated. In all cases for these experiments, the bed slope was approximately 0.5 %.

The roughness transitions were located towards the middle of the flume for both roughness transition cases. The specific locations were chosen to be far enough downstream of the headbox so that the flow reached a steady state several meters upstream of the transition, and also located far enough upstream of the tailbox so that associated backwater effects were minimized starting from several meters downstream of the transition. The characteristics of the different roughness configurations, bed conditions, and the flow conditions were kept as similar as possible from one set of experiments of type 1 to the next. A sketch of the bed for each of the two types of transitions is shown in Figure 2.2. More details for each are included below.

The first R-S transition bed configuration tested used a mobile gravel bed for the rough half of the R-S transition and a smooth plastic board downstream of the transition, so that the transition was extreme. The D_{50} and D_{90} of the mobile gravel bed section are 6.8 mm and 7.9 mm, respectively, where D_i refers to the particle size for which i % of the particles are smaller. The gravel bed was prepared by running water over the bed at a high enough flow rate that the bed was relatively flat and could be considered water worked. The experimental flow conditions were selected so that particle entrainment from the mobile bed would be rare, specifically, the flow conditions were set to be near the critical threshold for motion. A more detailed list of characteristics for the mobile bed conditions are summarized in Table 2.1, and the reference for the bed dimensions can be seen in Figure 2.2a.

The second bed condition tested with a R-S bed configuration was the fixed gravel

bed, with a R-S transition from larger gravel to smaller gravel. The D_{50} and D_{90} for the larger gravel section were 7.1 mm and 8.0 mm, respectively, and the D_{50} and D_{90} for the smaller gravel section were 2.5 mm and 3.3 mm, respectively. The preparation of the fixed gravel bed included the construction of the different roughness panels that were installed in the flume. The base of the fixed bed panels were constructed out of sheet metal, and the gravel was attached to the sheet metal by using a two-part epoxy paint. The preparation of each panel was done prior to installation into the flume. The sheet metal was cut to 1.22 m lengths so adjustment of the panels while placing them in the flume would be easier. The epoxy paint was spread onto the sheet metal panels, then the large gravel was placed on half of the panels and the small gravel was placed on the other half of the panels. Each panel was installed carefully into the flume to achieve a local and global slope of 0.5 %, equal to that of the mobile bed experiments. A polyurethane adhesive was used to secure the panels to the walls of the flume, and was also used to secure each pair of panels together where they met end to end. While most of the experiments were performed with the transition at one location, a second transition location was tested to assure the results were not dependent on location in the flume, for example, on any local flaws in the flume. A more detailed list of characteristics for the fixed bed conditions where most of the data were taken are summarized in Table 2.2, where the reference for the bed dimensions can be seen in Figure 2.2a. A detailed list of the characteristics for the second R-S transition fixed bed condition is in Table A.1.

For the S-R transition bed configuration only a single fixed bed configuration was tested. The S-R transition was from smaller gravel to larger gravel. The gravel used was

the same as the gravel used for the R-S transition fixed bed condition. To facilitate the installation, the gravel and paint of the R-S transition fixed bed was scraped off the sheet metal while the sheet metal was still in place and attached to the flume. A few adjustments were made to a couple panels. Then the two-part epoxy paint was painted on the sheet metal *in situ* and the large and small gravel were placed on the sheet metal to be secured as the epoxy paint dried. The transition location was arbitrarily decided and small gravel particles were glued upstream of the transition and large particles were glued downstream of the transition. A more detailed list of characteristics for the S-R fixed bed conditions are summarized in Table 2.3, where the reference for the bed dimensions can be seen in Figure 2.2b.

The flow conditions for the experiments were initially set up to be near the critical threshold for transport of the large gravel mobile bed. This was determined by adjusting the flow rate so that bed-load transport events occurred only infrequently. Validation of the flow and transport conditions for the different bed conditions was done by comparing different measures of τ_0 computed from several methods listed in Chapter 1 including the gravity driven steady uniform flow equation (Equation (1)), the Reynolds shear stress equation (Equation (2)), and the shear velocity method equation (Equation (3)) determined from the log law of the wall (Equation (4)). For the velocity measurements, an Acoustic Doppler Velocimeter (ADV) was used, and will be described in more detail below. The measure of τ_0 was then compared with τ_c computed using Brownlie's formula equation (5) for the D_{50} and D_{90} of the two bed conditions. The values obtained from these methods for the purpose of this comparison are in Table 2.4. The flow conditions

were determined to be near the critical threshold for bed-load transport and the flow rate was held constant at $0.0387 \text{ m}^3/\text{s}$ for nearly all of the experiments with one exception where the flow rate had to be increased. As will be detailed below, for one set of experiments, involving the S-R transition, the flow rate had to be increased by 15 % to $0.0445 \text{ m}^3/\text{s}$ for feasible data acquisition rates.

In these experiments of type 1, an individual tracer gravel particle was monitored for all bed conditions and roughness transition configurations studied. The diameter of the tracer particle used for the experiments was from the 90th percentile for both bed conditions and was 8 mm in diameter. The larger particle size was chosen to help assure that strong turbulence events were needed to cause transport which would assure cleaner results. The larger particle size also proved helpful in easing the placing of the gravel particle in the specific locations of interest during the experiments. Over the course of all of the experiments, only two tracer particles were used (e.g., Fig. 2.3) and they were similar in general shape, and size: 8 mm in diameter. Only one tracer particle was used at any one time. Two tracer particles were required because the initial tracer particle was lost in action.

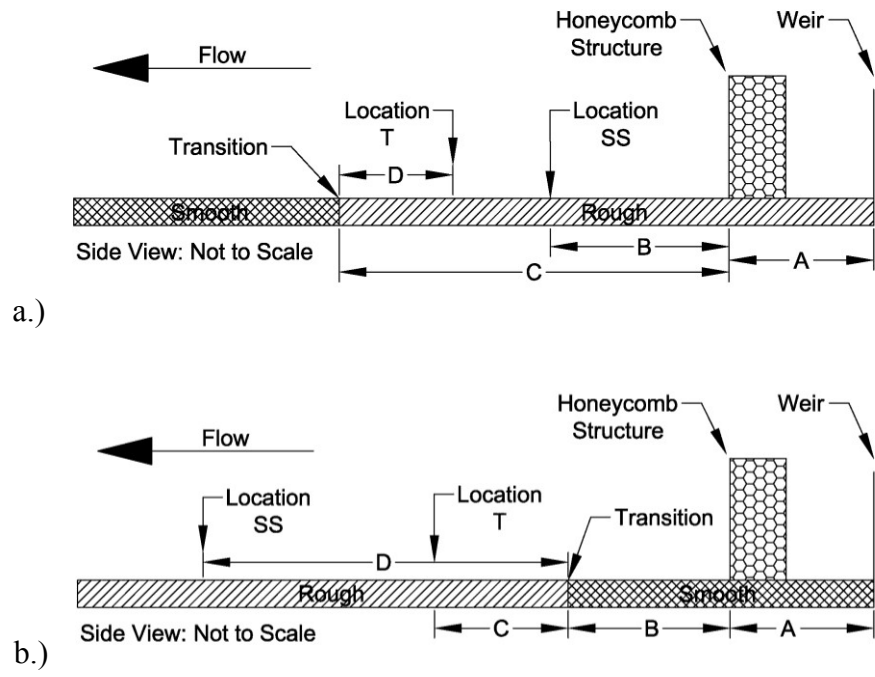


Figure 2.2. a.) Flume set-up for R-S transition configuration. Tables 2.1 and 2.2, and A.1 contain specific values of A, B, C, and D for the experiments. b.) Flume set-up for S-R transition configuration. Table 2.3 contain specific values of A, B, C, and D for the experiments.



Figure 2.3. Photograph of one of the tracer gravel particles used for the experiments. The reference dimensions in the picture are cm.

R-S Transition Mobile Bed			
Flume Dimensions			
A	0.6		m
B	5.4		m
C	9.53		m
D	5		cm
Experimental Properties			
	Rough Section	Smooth Section	
h	0.127	0.093	m
U	0.610	0.833	m/s
Q	0.0387	0.0387	m ³ /s
S	0.0052	0.0079	m/m
Re	77476	77476	
Fr	0.547	0.872	
D_{16}	5.9	Smooth Board	mm
D_{50}	6.8	Smooth Board	mm
D_{65}	7.2	Smooth Board	mm
D_{84}	7.8	Smooth Board	mm
D_{90}	7.9	Smooth Board	mm

Table 2.1. Flume dimensions and experimental conditions relevant to the R-S transition mobile bed flume set-up. A, B, C, and D reference specific points in the flume as indicated in Figure 2.2a. Many details are specific to the reach of the flume. h refers to the average depth of the water, U is the mean flow velocity, Q is the water discharge, S is the bed slope, Re is the average Reynolds number of the flow, Fr is the average Froude number, D_{16} is the particle diameter of the 16th percentile, D_{50} is the particle diameter of the 50th percentile, D_{65} is the particle diameter of the 65th percentile, D_{84} is the particle diameter of the 84th percentile, D_{90} is the particle diameter of the 90th percentile.

R-S Transition Fixed Bed			
Flume Dimensions			
A	0.6		m
B	5.4		m
C	8.57		m
D	5		cm
Experiment Properties			
	Rough Section	Smooth Section	
h	0.113	0.110	m
U	0.683	0.704	m/s
Q	0.0387	0.0387	m ³ /s
S	0.0048	0.0050	m/m
Re	77476	77476	
Fr	0.648	0.677	
$D16$	6.2	1.9	mm
$D50$	7.1	2.5	mm
$D65$	7.4	2.8	mm
$D84$	7.8	3.1	mm
$D90$	8.0	3.3	mm

Table 2.2. Flume dimensions and experimental conditions relevant to the R-S transition fixed bed flume set-up. The variables are defined in the caption of Table 2.1 and the relevant bed dimensions are referenced in Figure 2.2a.

S- R Transition Fixed Bed			
Flume Dimensions			
A	0.6		m
B	7.9		m
C	5		cm
D	6.5		m
Experiment Properties			
	Smooth Section	Rough Section	
h	-	0.119	m
U	-	0.651	m/s
Q	0.0387	0.0387	m ³ /s
S	0.0051	0.0047	m/m
Re	77476	77476	
Fr	-	0.603	
$D16$	1.9	6.2	mm
$D50$	2.5	7.1	mm
$D65$	2.8	7.4	mm
$D84$	3.1	7.8	mm
$D90$	3.3	8.0	mm

Table 2.3. Flume dimensions and experimental conditions relevant to the S-R transition fixed bed flume set-up. The variables are defined in the caption of Table 2.1 and the relevant bed dimensions are referenced in Figure 2.2b. (“-” indicates the property is not constant for the section).

Bed Condition		Location B m	τ (equation)			
			(1) Nm ⁻²	(2) Nm ⁻²	(3) Nm ⁻²	(5) Nm ⁻² D_{50}, D_{90}
Mobile		6	6.479	5.25	6.32	5.79, 6.84
Fixed	Transition Location 1	6	5.340	4.29	6	6.08, 6.93
Fixed	Transition Location 2	9.12	5.542	7.88	9.22	6.08, 6.93

Table 2.4. Shear stresses calculated to validate system threshold transport conditions for the R-S transition bed configurations.

2.2.2 Instrumentation - Experiment 1

The purpose of the first type of experiment was to investigate the importance of the different measures of turbulence statistics including, specifically, instantaneous downstream and vertical velocities, u , w , and the velocity fluctuation correlations, $u'u'$, $u'w'$, and $w'w'$ during entrainment of an individual gravel particle under different bed conditions. The data required to perform the investigation of the different turbulence mechanisms required the collection of high resolution velocity data, and required the monitoring of an individual tracer particle with high resolution video in order to capture when initial motion occurred.

Fluid motion was measured using a Nortek Vectrino+ ADV (Acoustic Doppler Velocimeter) with a downward facing probe. The ADV collects three-dimensional velocity data at a frequency of 200hz. The ADV was used to collect the fluid velocities above the individual tracer particle at multiple heights above the bed, and at different locations along the flume. The velocities were collected over a long period of time during which several individual transport events occurred and were observed and measured. These data were used to correlate specific turbulence statistics directly with initial motion. The ADV was also used to collect velocity profiles at specific locations along the flume to aid in the investigation. Manual adjustment of ADV settings allows the user to increase the reliability of the velocity data collected under many different flow conditions. The setting “Nominal Velocity Range” (an expected range of velocities measured) impacted the quality of the velocity data under the flow conditions studied. The Nominal Velocity Range was set at “ ± 1.00 m/s” indicating the expected range of

velocities in any of the three directions was between 1 m/s and -1 m/s. Only the u and w signals were analyzed in this study. The ADV outputs 2 separate w velocity signals, z_1 and z_2 . Since the probe tip which is associated with the signal for u is in line with the probe tip that is associated with the z_1 signal, z_1 was the signal used for w in the analysis. The ADV needs particles in the water to be able to collect a clean signal. If there are not enough particles in the water, it is necessary to seed the water with particles. Since the water used in the experiments was directly from the Mississippi river, seeding the water was only required during the winter months. During the winter months there are fewer particles which are naturally suspended in the water. As a result, the ADV signal is contaminated with noise because there are not enough particles to backscatter the acoustic pulse. The contamination of noise was reduced greatly and often avoided when seeding was used. The seeding material used was a coffee creamer, which was mixed with water and fed upstream of the location of data collection. Figure 2.4 is a picture of the seeding system used to disperse the water-coffee creamer mixture.

Particle motion was measured using an Epix SV9M001C camera. The capture rate was 30 fps. The camera was used to help with the placement of the individual tracer particle at the specific locations where the ADV was collecting velocity measurements and to record the details of the tracer particle movement when initial motion occurred.

The camera and ADV were mounted to an instrument cart that could move up and down the flume (Figure 2.5a). A viewing tube to house the camera was constructed to provide clear sight to the bed below, where the tracer particle was placed. A clear plastic plate at the end of the viewing tube interacted with the surface of the water, and the

upstream edge of the plate was beveled to reduce the impact the plate had on the water surface. The beveled edge greatly reduced the impact the plate had on the flow and the subsequent influence on the results. Figure 2.5b shows a front and side view drawing of the system configuration.

The camera and ADV were setup to be triggered to start collecting data simultaneously. This allowed for a video reference time to correspond to the beginning of the velocity time series, so that transport events captured on video could be identified in the velocity time series accurately. This was necessary to eliminate the uncertainty in the analysis since the data was collected on separate computers and the time stamps were different from one computer to the other, and also because the timestamps associated with the ADV and camera were of different resolutions. The trigger for the system was a 0-5 V TTL (transistor-transistor logic) pulse which was controlled by a button.

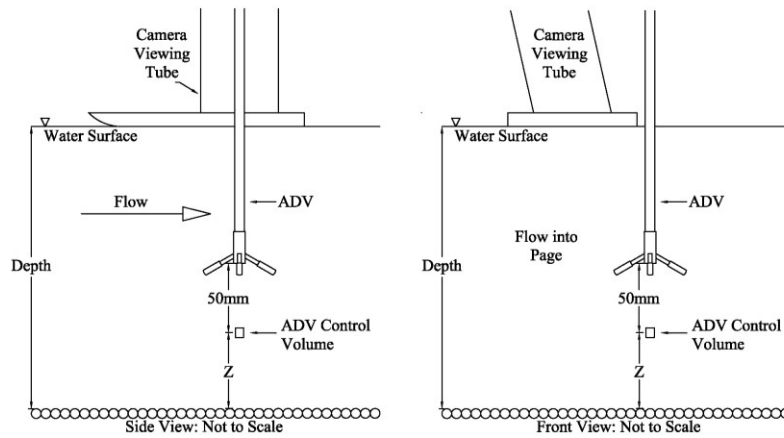
Reference bed elevations and water surface profiles were measured using a point gauge attached to the instrument cart. The point gauge could move up and down and had an incremental measurement resolution of 0.3048 mm (0.001 ft).



Figure 2.4. A photograph of the seeding system.



a.)



b.)

Figure 2.5. a.) A photograph of the instrument cart which the ADV and camera are mounted to. The instrument cart could move up and down the length of the flume. b.) Front and side view of the system configuration and the system relationships under the water surface.

2.2.3 Experimental Procedure - Experiment 1

Two locations were investigated for each bed configuration. The first location investigated was within a section of the flume where steady uniform flow existed, and the second location investigated was either at 5 cm before a R-S transition or 5 cm after a S-R transition where steady non-uniform flow existed. These two situations were investigated to identify similarities and differences in turbulence mechanisms that correlated with initial motion under uniform flow conditions and non-uniform flow

conditions induced by roughness transitions. The primary components of data collection involved monitoring the transport events and collecting velocity data in a manner which was conducive to the sporadic nature of the transport events.

For the purpose of these experiments, a transport event will be defined as the entrainment of a tracer particle into motion provided the tracer particle has been resting on the bed for a time sufficiently long after its initial placement, so that the movement is not initiated by any disturbance created by the placement of the particle. This minimum resting time interval was chosen to be approximately 20 sec so any disturbance of the velocity statistics associated with the particle placement was no longer recognizable. The movement was only considered to be an entrainment event when the tracer particle became completely dislodged from its location and traveled downstream. Most of the events occurred when the tracer particle had been in location for much longer than 20 sec. The tracer particle was placed into location by using a parts grabber Figure 2.6. Using the parts grabber allowed for very little impact to the flow while placing the tracer particle, and it offered high precision and control while placing the tracer particle in location. After an event took place, the tracer particle was collected and placed back into the location of interest so another event could be collected.

Collection of the velocity data was done with the ADV described in the instrumentation section. The ADV data was not nearly as big as the video data, so it was collected in a continuous velocity time series over the entire time of each run set. A two hour period of time was selected because the file size was manageable and also the duration of time was large enough that there was likelihood that several transport events

would occur in the time frame. The long velocity time series corresponds to the triggered system which started the ADV and camera to begin collecting data simultaneously. This velocity time series included the velocity data that was relevant to specific transport events which were identified in the event videos. Baseline velocity samples were collected prior to the long velocity time series and immediately after the long velocity time series. The length of the baseline velocity samples was 2 min. The 2 min long samples served as a check to make sure flow conditions had not changed during the time the long velocity time series was collected. There are a few exceptions to this rule of thumb which will be detailed where appropriate.

Monitoring of the particle during transport events was done using the camera configuration described in the instrumentation section. While the particle was monitored on the bed for an extensive period of time (approximately 2 hours) the particle movements took place intermittently and only during a small fraction of the time. The video files are very large so, in order to reduce the storage capacity necessary, the collection of video was broken into two categories, a reference video and event videos. A reference video was taken at the beginning of each run set which corresponded to the initiation of the ADV for recording the velocities to provide a reference time stamp for that run set. Then, during the entire run set, a digital video was recorded in temporary storage in the form of a continuous loop of (20 seconds). When an event occurred, the event video would be manually stopped, and only after stopping the event video would the data be recorded for future analysis. The time stamp corresponding to the initial motion of each event was identified as the frame in the video immediately preceding the

frame in which motion occurred. The corresponding time in the fluid velocity time series was then determined by calculating the elapsed time between the reference time stamp and the transport event time stamp.

Data was collected at multiple heights above the bed for the two locations of interest for each bed configuration and condition. For each height and subsequent location, 25 events were averaged together to identify correlations between initial motion and the different turbulence mechanisms. Since the events occurred randomly and infrequently, it was necessary to collect the events over a period of days. For each day, monitoring the conditions of the experiment assured that the bed remained unchanged and the flow rate was set to be the same over the course of data acquisition for a particular location. For the three heights collected at the T location and the height 0.53 cm at the SS location for the mobile bed R-S condition, there was only one baseline velocity time series collected and it was collected after the long velocity time series.

To determine that the data from 25 events averaged together was adequate to identify correlations between initial motion and the different turbulence mechanisms, a random set of instantaneous velocities were sampled and analyzed. Specifically, under steady state conditions where no disturbances associated with rock placement or movement were generated, a series of ADV data was collected. Then, 100 data points were selected from this series. Then a running average was calculated for several measures of the velocity. Specifically, if q_i represents the i^{th} random reading of the variable q_i , the running average q_n is taken for the first n points in that random data set,

$$q_n = \sum \frac{q_i}{n} \quad (11)$$

Some of the results are plotted in Figure 2.7. From these plots, it is apparent that there is no longer a significant variation in the running average of each variable after 20-25 points. To test this conclusion, 50 events were collected for one particular location (0.79 cm above the bead at the SS location for the fixed bed R-S transition condition). The results are not significantly different than the results from collecting only 25 events for the conditional averaging analysis.

In addition to the data collected specific to the events, velocity profiles were collected at the specific locations at and around the locations where transport events were measured. The sample lengths for the velocity time series collected for the profiles were 2 min.

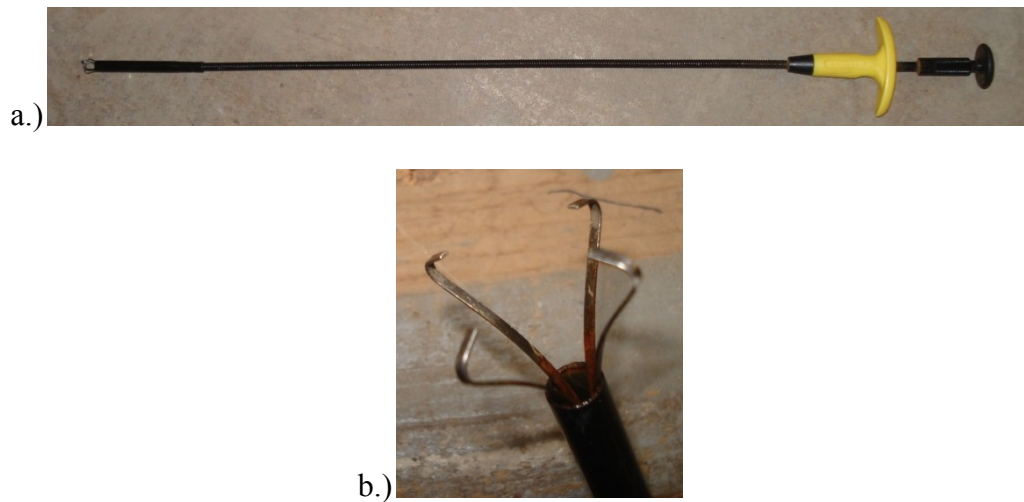


Figure 2.6. a.) Photograph of the parts grabber used to place the tracer particle in location. b.) Photograph of the parts grabber grabbing mechanism extended.

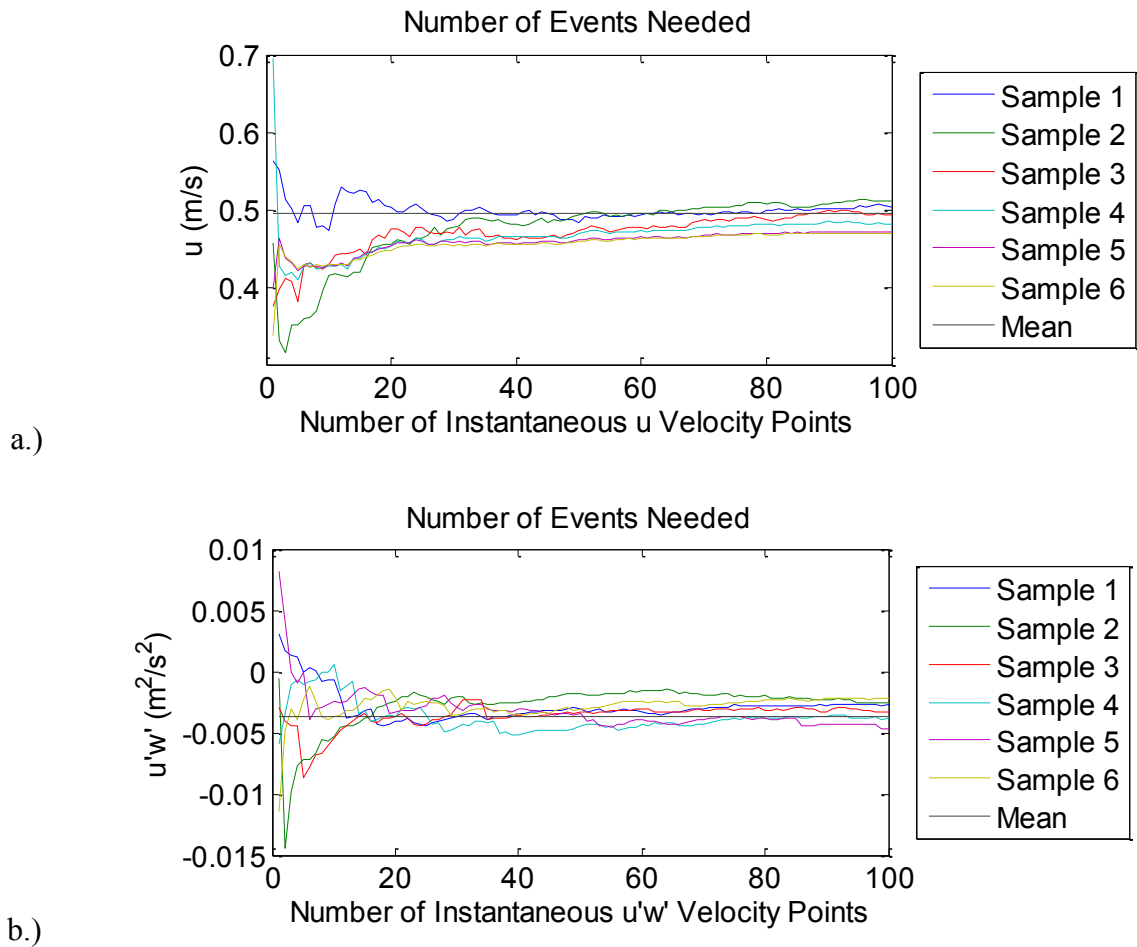


Figure 2.7. Running average of a.) u and b.) $u'w'$. Each plot shows the average of a two minute long sample and six different sets of 100 points tested for the number of events needed to determine trends in the results.

2.2.4 Data Analysis - Experiment 1

Data analysis techniques for experiments of type 1 include the methods used to calculate the turbulence statistics, the quadrant analysis, and determining the height above the bed at which velocity measurements were taken. The turbulence statistics investigated in this study include u (downstream velocity), w (vertical velocity), $u'u'$ (horizontal normal stress), $u'w'$ (Reynolds Stress), and $w'w'$ (vertical normal stress). Before the turbulence statistics were computed, each ADV time series was filtered using

a modified version of the Phase-Space-Thresholding method [*Parsheh et al.*, 2010].

Since the turbulence statistics are very important in this study, the calculation of the turbulence statistics is described here in detail. The first step in calculating the turbulence statistics is calculating the average turbulence statistics for each baseline velocity time series for before and after the run set time series. The average turbulence statistics representative of the flow characteristics during the collection of the run set time series are calculated by averaging the two baseline velocity time series. The 2 sec window of instantaneous velocities centered around the entrainment event is considered the instantaneous velocity time series corresponding to a particular event. A conditional average associated with the time series surrounding the events corresponding to the same condition (same bed condition, same downstream location from the transition point, and same height above the bed) was calculated using the instantaneous turbulent velocities at each time relative to the entrainment time of each event. The instantaneous downstream and vertical velocity fluctuations u' and w' , respectively, were determined by subtracting the average turbulence statistics representative of the run set from each event's instantaneous velocity time series. The different stresses $u'u'$, $u'w'$, and $w'w'$ were calculated by multiplying the corresponding velocity fluctuations to create the instantaneous stresses time series. Finally, for each height at each downstream location, the instantaneous velocity and stress time series of 25 events were conditionally averaged together to identify trends in the turbulence statistics which correlate to initial motion. The average turbulence statistics representative for each height at each location is calculated by averaging all the baseline average turbulence statistics for the given height.

A Quadrant Analysis was performed on the conditionally averaged instantaneous velocity fluctuations u' and w' . For each height and location the quadrant analysis was performed for the whole 2 sec window of conditionally averaged results, and also a 0.5 sec window surrounding initial motion time $t = 0$. The 0.5 sec window was considered because it is the region most relevant to when initial motion occurred.

The final part of the description of the experiments of type 1 involves the method developed for the research in this thesis and used to determine the height above the bed where velocity measurements were collected and to assure that this height is consistent for all the equipment used. The ADV device records an estimate of a height above the bed at which the velocity data is being collected, but the resolution of the reported height is in mm resolution. To improve the resolution, the following method was developed and a reference 0 bed elevation was determined. The ADV was lowered until the control volume was within the bed. When the ADV control volume is within the bed, the real-time velocities being reported resemble a flat line near zero. Two minute samples were then collected with the ADV at 0.3048 mm increments in the vertical direction until the ADV control volume was no longer in the bed as evidenced by the fact that the ADV was reporting significant real-time velocities. The reference bed elevation is finally determined post processing, and is defined as the sample height where the average u for the heights above the “determined bed elevation” are each increasing significantly. This method for determining the bed elevation proved consistent between downstream locations and therefore the bed elevation was determined this way for each location investigated. The difference between the vernier readings of the determined bed

elevation and the height the data were being collected is the reported height above the bed.

2.3.1 Experimental Details - Experiment 2

The purpose of the second type of experiment was to investigate the effects the R-S transition had on a mobile bed upstream of the transition. The investigation was to provide information that would be relevant in understanding the differences in the results obtained from experiment 1 R-S transition fixed bed. The second type of experiment was performed in the same flume as experiment 1. The general configuration for this experiment is one where sediment is fed into the flume under the same flow conditions as used in the experiments of type 1, with a water discharge of $0.0387 \text{ m}^3/\text{s}$, and the bed elevation adjusted to a new equilibrium bed slope in response to the new flux of sediment. The base bed, which was the initial condition for this experiment, was the R-S transition fixed bed condition. The bed slope was monitored as it changed until the new equilibrium state was reached. This experiment was performed two times, once for both R-S transition fixed bed transition locations. The sediment that was fed into the flume was the large gravel described as the rough section in experiment 1 for the R-S transition fixed bed condition, Table 2.2. The D_{50} and D_{90} for the large gravel are 7.1 mm and 8.0 mm, respectively.

2.3.2 Instrumentation - Experiment 2

The instrumentation needed for this experiment was used to monitor the bed and water surface elevations, and supply sediment to the system.

The bed and water surface elevations were measured using a point gauge. For the

first time the experiment was performed, one point was measured at each downstream location along the length of the flume to determine the bed and water surface elevations. The second time the experiment was performed, three separate points at each location along the length of the flume were averaged to determine the bed elevation, and one point was measured at each location to determine the water surface profile. One point was measured at each location for the water surface profile because the amount of time required to collect the water surface profile in this way was 20-30 minutes which already is a significant fraction of time compared to the time scale at which the mobile bed was changing.

The sediment supply was fed at a steady rate into the flume by a sediment recirculation feeder capable of supplying up to $1.28\text{E-}05 \text{ m}^3/\text{sec}$. The sediment system may be considered re-circulating because there is a sediment trap located just before the tailbox of the flume to collect sediment that has been transported down the entire length of the flume, and a venturi suction system moves the sediment back to the hopper at the beginning of the flume to feed the gravel back into the system. On the other hand, the sediment is fed at a constant rate, so that the re-circulating nature of the feed system does not affect the sediment supply. The sediment feed rate was determined by collecting a sample supplied by the feeder for several one-minute periods of time and weighing it for each sample, Figure 2.8.



Figure 2.8. Shown in the photograph is the setup to collect a minute long sample to determine the sediment feed rate.

2.3.3 Experimental Procedure - Experiment 2

Determining the rate to supply sediment into the system involved consideration of shear stresses at different locations along the bed. Since the flow rate for the system was selected to provide system conditions that were near the critical threshold for motion for the initial bed conditions, there was no need for sediment to be supplied for the bed to remain essentially in a steady state. Near the transition, where the flow experiences spatial acceleration, higher shear stresses were measured and were determined by using the log law of the wall (equations (3)-(4)). The sediment feed rate was selected by considering three things: (1) using the shear stress just upstream of the transition to calculate the bed-load discharge at that position using the Meyer-Peter and Müller method (equation (8)) modified by *Wong and Parker*, [2006], (2) the amount of sediment required to achieve a new steady state away from the transition point based on the depth slope average equation, and (3) the sediment supply capabilities of the sediment feeder. The amount of sediment required to achieve the new steady state was approximated by estimating the new steady state slope, and determining the amount of gravel required to fill the volume underneath the new estimated steady state slope in 2 hours. It was expected that it would take longer than 2 hours because sediment is transported through

the system as the bed is adjusting to the new steady state. Table 2.5 gives the calculated values and instrument limitations which framed the decision on selecting the sediment feed rate as outlined above, as well as the two sediment supply rates used for the experiments.

To determine the evolution of the bed and the time at which the system reached a steady state, water surface profiles and bed elevations were measured several times through the duration of the experiment. The first time the experiment was performed, water surface profiles and bed elevations were measured every hour of run time for the first 3 hours and then every 2 hours for the last 4 hours of run time. The second time the experiment was performed, the water surface profiles and bed elevations were measured every 1.5 hours of run time for the first 6 hours and then measured after the last 2 hours of run time. Breaking the duration of the experiment up in this way allowed the evolution of the system to be monitored, and steady state could be seen when there were no longer any significant changes to the bed elevations and water surface profiles. The first time the experiment was performed, measurements for water surface profiles and bed elevations were taken starting at the transition and measured in 5 cm increments away from the transition for 0.5 m. Then starting at the next 0.25 m interval marked along the flume (e.g., 8.25 m, 8.5 m, 8.75 m, 9 m, etc.), measurements were taken every 0.25 m. The second time the experiment was performed, measurements for water surface profiles and bed elevations were taken starting 0.25 m before the R-S transition and at 5 cm increments until 0.5 m after the R-S transition. Then starting at the next 0.25 m interval marked along the flume (e.g., 8.25 m, 8.5 m, 8.75 m, 9 m, etc.), measurements

were taken every 0.25 m.

Sediment feed rates were monitored throughout the duration of the experiment to ensure the feed rate was not changing over the course of the experiment. Sediment feed samples were collected every 20 min during the first time the experiment was performed, and sediment samples were collected every 30 min during the second time the experiment was performed. The sediment feed rates remained constant throughout the duration of both experiments.

Feed Rate Condition Argument	q_s m ² /s	Q_s m ³ /s
Meyer-Peter and Müller	4.56E-05	2.28E-05
Amount of Sediment to achieve steady state	1.71E-05	8.53E-06
Sediment Feeder (Maximum)	2.57E-05	1.28E-05
First Feed Rate	1.71E-05	8.56E-06
Second Feed Rate	1.57E-05	7.85E-06

Table 2.5. Calculated values and instrument limitations which framed the decision on selecting the sediment feed rate, as well as the two sediment feed rates used for the experiments.

Chapter 3

Experimental Results

Experimental results are presented for the two different types of experiments outlined in Chapter 2. The results for experiment 1 concerning the turbulence mechanisms which correlate directly with initial motion of an individual tracer gravel particle are detailed in section 3.1. The results for experiment 2 concerning how a R-S transition affects the buildup of gravel upstream of the transition are detailed in section 3.2.

3.1 Measurements of Turbulence Statistics and Tracer Particle Entrainment Under Uniform and Non-Uniform Conditions

As described in detail in Section 2.2, experiments of type 1 concern the correlation between turbulence statistics and the initial motion of an individual tracer gravel particle. Measurements were taken under uniform and non-uniform conditions for three different bed conditions: a R-S transition where the bed is partially mobile, a R-S transition where the bed is fixed, and a S-R transition where the bed is fixed. There were two locations investigated over each bed condition and roughness configuration, one location was located in a region far from the transition that was steady uniform flow, and the other location was located 5 cm before the R-S transition or 5 cm after the S-R transition in a region of steady non-uniform flow. The results are discussed in the context of the particular bed conditions in the first three subsections below. Then, additional turbulence

statistics are analyzed in the subsequent two subsections.

3.1.1 Mobile Bed R-S Transition

The first bed condition investigated was the R-S transition, where the rough half of the bed was a mobile gravel bed and the smooth half of the bed was a smooth plastic board. The bed profile and water surface profile (WSP) measured during the experiments are shown in Figure 3.1 and the positions where the particle entrainment studies were performed are marked on this plot with an “X”. From these results, a few interesting details are apparent. The dip in the bed just upstream of the transition is evidence that there is a little bed scour that is caused from the fixed smooth plastic board. Two different bed slopes exist between the mobile rough region, and the fixed smooth board region. This was not intended and was the consequence of oversight while preparing the initial bed configuration. The fluid surface indicates a sharp drop in the depth of the flow after the roughness transition, which, with continuity, indicates the fluid moves faster over the faster board. As mentioned, two positions along the bed were investigated in detail, a point several meters upstream of the transition where the conditions are essentially both steady and uniform referred to as the SS location and a point 5cm upstream of the transition referred to as the T location. The velocity profiles of the two locations investigated are plotted in Figure 3.2. The velocity profile for the T location is faster at all depths in the bottom part of the water column than the velocity profile at the SS location. The results of certain conditionally averaged velocities and velocity fluctuations corresponding to the 25 entrainment events are shown in Figure 3.3. Specifically, u , w , $u'u'$, $u'w'$, and $w'w'$ are plotted for the SS location in the left column

of Figure 3.3, and plotted in the right column of Figure 3.3 are the results for the T location. In all cases, $t = 0$, is the time just before the entrainment took place. At both locations, data were collected at three different heights above the bed. The average statistics of the flow associated with each height in Fig. 3.3 is presented in Table 3.1. This table allows the comparison of the average statistics, which for this case does not provide much detail in understanding the difference between the two locations. Evidence of a different flow pattern at the T location is seen in comparing the w velocities, where w is positive on average at the T location and negative on average at the SS location.

The most noticeable trend in these data is in u at the T location 5 cm before the R-S transition. For all heights, a peak in u correlates well with initial motion time $t = 0$. There appears to be small peaks in u for the SS location too, but the trends are not very clear or strong, so the correlation of u and initial motion is not considered strong for the data collected at this location. No trends are visible in the results for w , $u'u'$, $u'w'$, and $w'w'$ for both locations, so the correlation with initial motion is very weak at both the SS location and the T location for the mobile bed results.

Since the bed was mobile, it was difficult to get absolutely identical conditions from one run to the next. This, in combination with the limited data for each point of 25 entrainment events could together have resulted in poorly correlated data. For example, possible variations that could occur from one entrainment event to the next over the mobile bed included the slight changes in local bed configurations, local slope, and particle placement relative to the location data were being collected with the ADV. Additionally, it was difficult to place the tracer particle in precisely the same location for

each event given, in part to local rearrangements associated with bed movement, and it is unknown to what extent that impacted the results obtained over the mobile bed. These considerations motivated the subsequent experiments using a bed entirely comprised of fixed gravel particles.

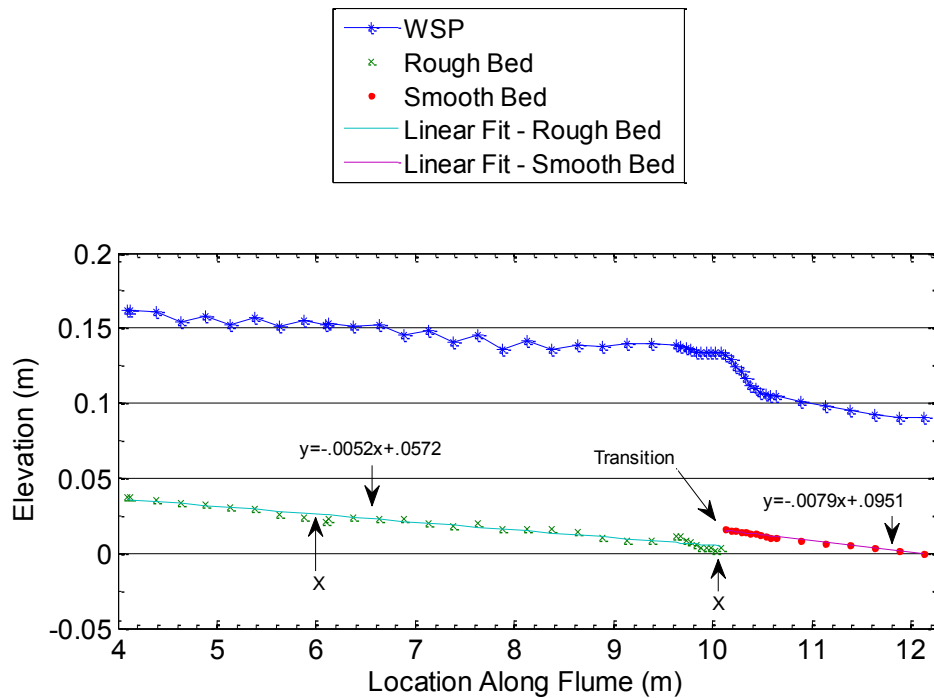


Figure 3.1. Bed profile and WSP for the experiments performed over the mobile bed R-S transition configuration. The data markers are at the points where data were collected. The equations represent the linear trend lines associated with the rough and smooth sections of the bed and provide the slopes of those sections. The two locations where data was collected are marked with an “X”. A line was used for the WSP to guide the eye.

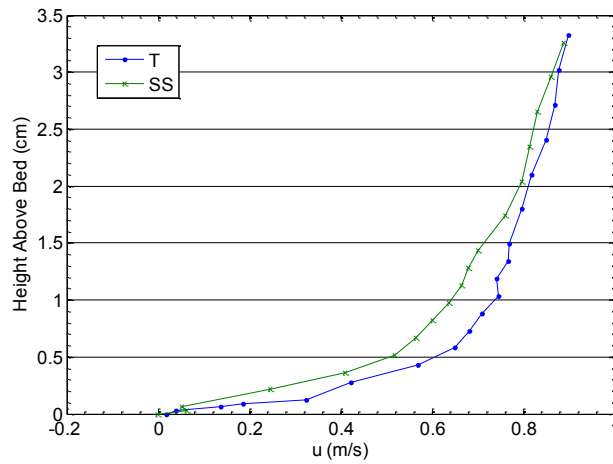
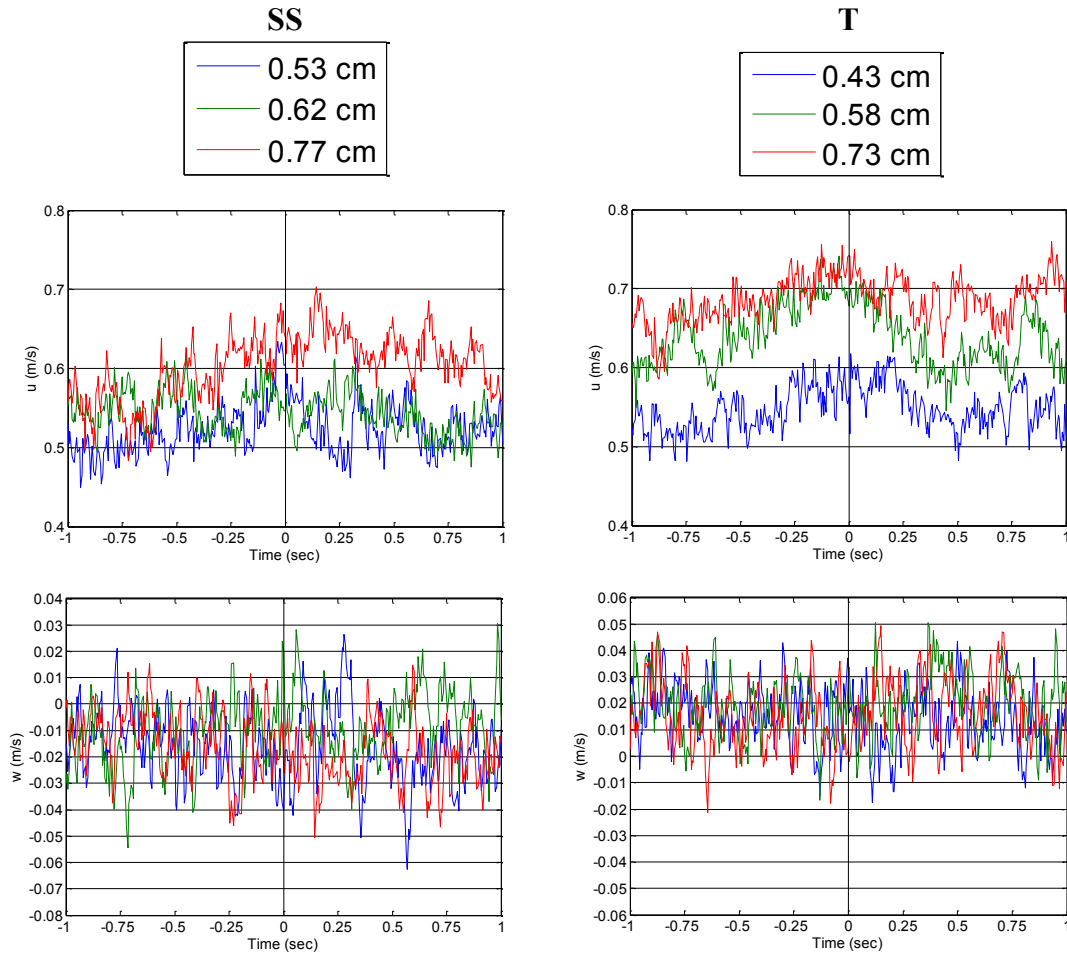


Figure 3.2. Velocity profiles for the two locations investigated over the mobile bed R-S transition configuration. Lines were used to guide the eye.



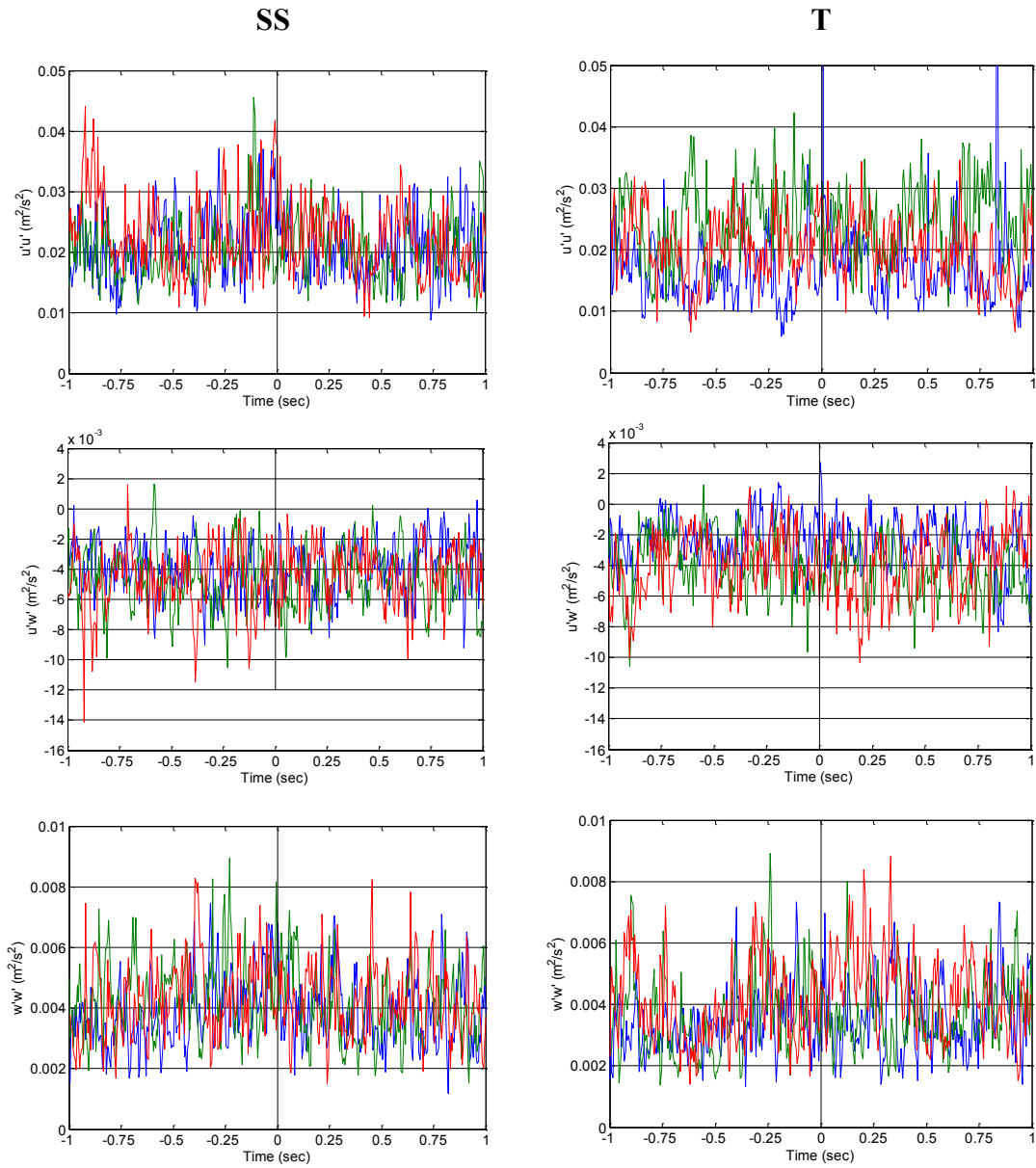


Figure 3.3. Conditionally averaged results for the turbulence statistics u , w , $u'u'$, $u'w'$, and $w'w'$ for the two locations investigated over the mobile bed R-S transition configuration. The left column of figures is the results for the SS location. The right column of figures is the results for the T location.

Bed Condition	Location	Height above bed	u	w	$u'u'$	$w'w'$	$u'w'$
		cm	m/s	m/s	m ² /s ²	m ² /s ²	m ² /s ²
Mobile	SS	0.53	0.52	-0.016	0.023	0.0037	-0.0045
		0.61	0.55	-0.017	0.019	0.0040	-0.0042
		0.77	0.59	-0.019	0.017	0.0041	-0.0038
Mobile	T	0.43	0.57	0.004	0.021	0.0032	-0.0038
		0.58	0.65	0.009	0.019	0.0033	-0.0035
		0.73	0.69	0.005	0.016	0.0035	-0.0032

Table 3.1. Average turbulence statistics for the two locations investigated over the mobile bed R-S transition configuration.

3.1.2 Fixed Bed R-S Transition

The second R-S transition bed condition investigated was the fixed bed with large gravel particles glued to a board placed over the bed in the upstream part of the flume and small gravel particles glued to a board placed over the bed in the downstream part of the flume. The bed profile and WSP during the experiments are shown in Figure 3.4 and the positions where the particle entrainment studies were performed are marked on this plot with an “X”. By default, there is no scour upstream of the rough-to-smooth transition and the bed slope is constant throughout. The velocity profiles for the two positions investigated in detail for entrainment are plotted in Figure 3.5. The velocity profiles are similar to the velocity profiles of the mobile bed R-S transition, because the profile associated with the T location has faster velocities throughout the profile than the profile associated with the SS location. This is a common characteristic between the two system configurations, even though a clear change in the WSP did not occur for the fixed bed R-S transition configuration. The results of certain conditionally averaged velocities u , w , and velocity fluctuation correlations $u'u'$, $u'w'$, and $w'w'$ corresponding to the

entrainment events are shown for the SS location in the left column of Figure 3.6, and for the T location in the right column of Figure 3.6. At both locations, data were collected at four different heights above the bed. The average turbulence statistics for both locations and each subsequent height investigated are listed in Table 3.2. This table allows the comparison of the average statistics, which show that the average statistics are larger for the T location.

The results associated with the SS location indicate there are strong correlations between initial motion and u , w , $u'u'$, and $u'w'$, and possibly weak correlations between particle movement and $w'w'$. At the T location, there is a strong correlation between initial particle motion and u , but comparably weak or no correlation between initial particle motion and w , $u'u'$, $u'w'$, and $w'w'$.

To verify that the difference was due to the difference between the bed at the two locations rather than something else such as a flaw in the flume, the boards were moved so that the R-S transition was repositioned to a new location 2.45 m downstream from the first roughness transition location. The results from the fixed bed transition location 2 are similar to the data reported above, confirming that the differences in the results between the SS location and the T location are not a result of flow imperfections introduced by the flume, and are not location specific. The results associated with the fixed bed transition location 2 investigation are presented and briefly discussed in Appendix 1.

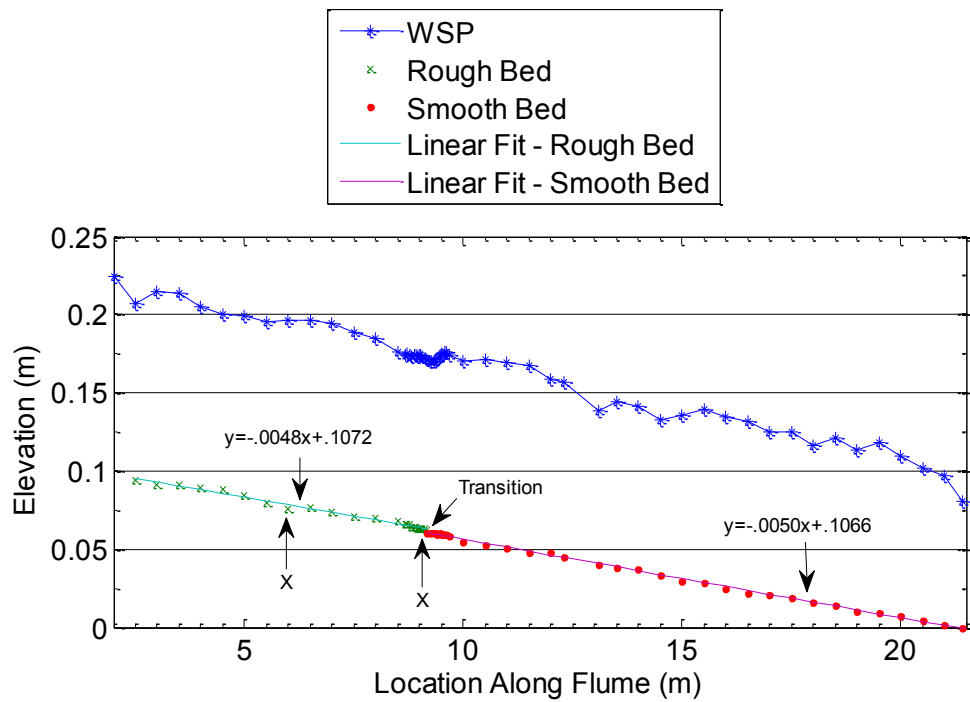


Figure 3.4. Bed profile and WSP for the experiments performed over the fixed bed R-S transition configuration. The data markers are at the points where data were collected. The equations represent the linear trend lines associated with the rough and smooth sections of the bed and provide the slopes of those sections. The two locations where data were collected are marked with an “X”. A line was used for the WSP to guide the eye.

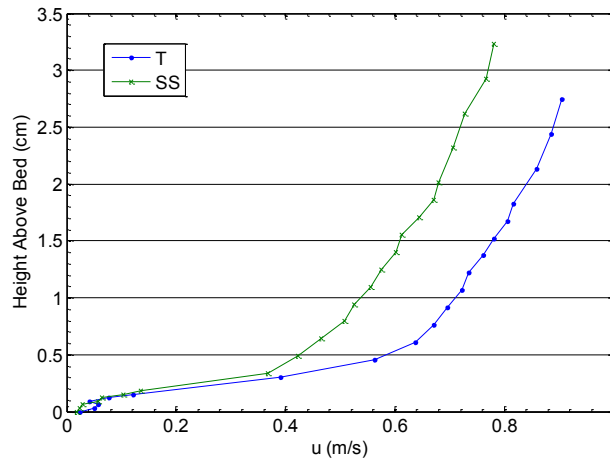
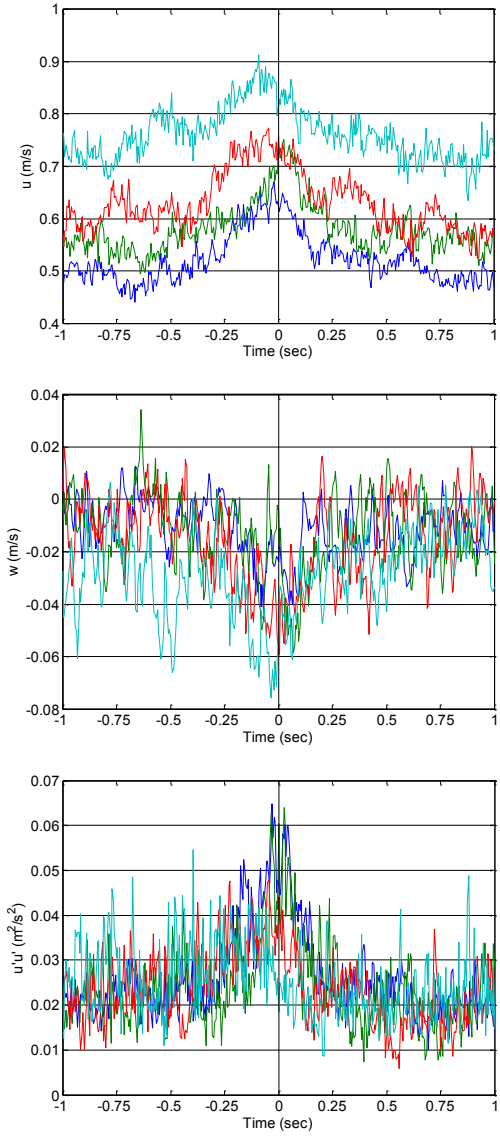
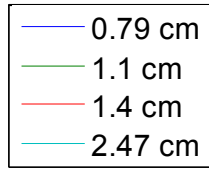
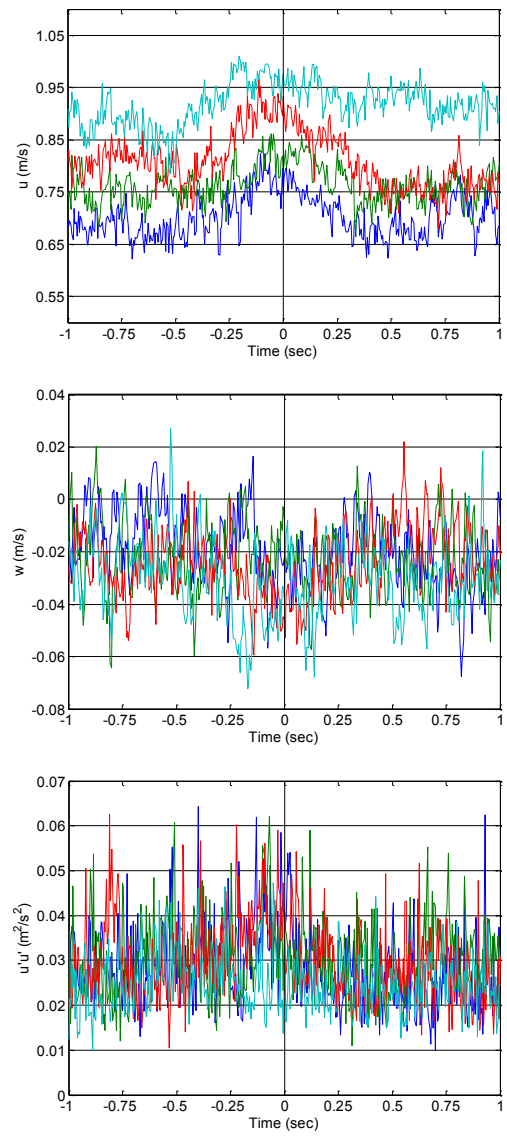
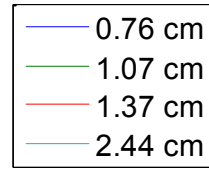


Figure 3.5. Velocity profiles for the two locations investigated over the fixed bed R-S transition configuration. Lines were used to guide the eye.

SS



T



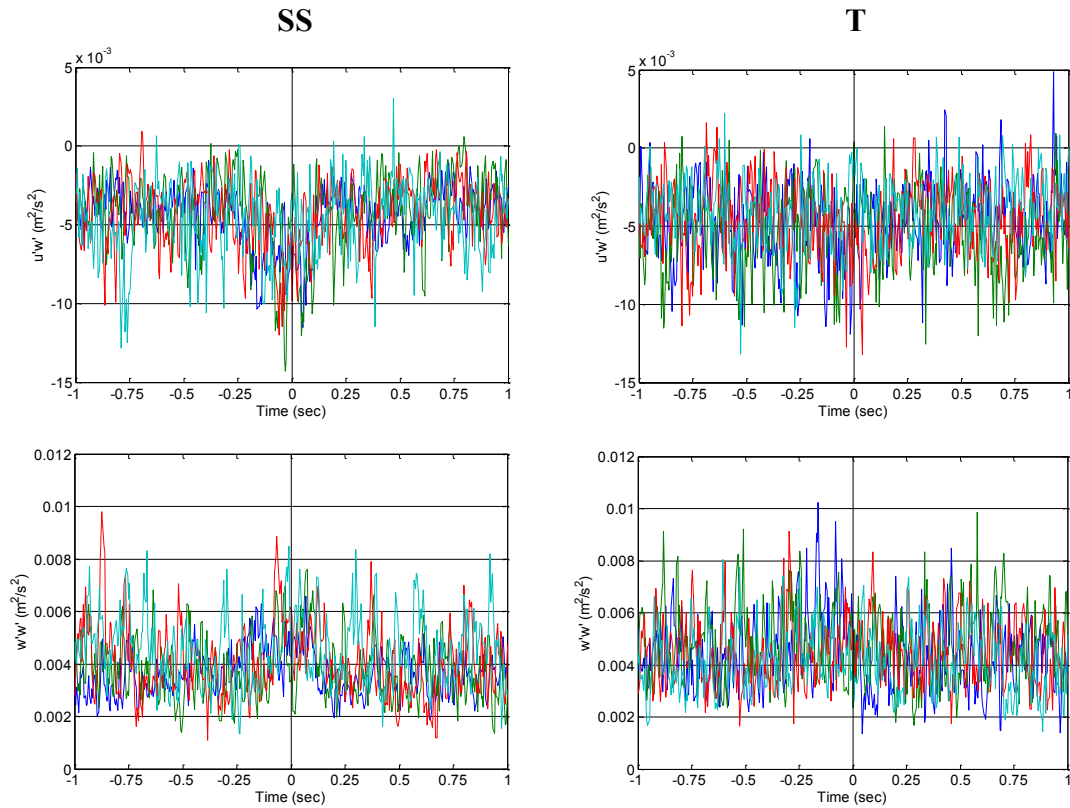


Figure 3.6. Conditionally averaged results for the turbulence statistics u , w , $u'u'$, $u'w'$, and $w'w'$ for the two locations investigated over the fixed bed R-S transition configuration. The left column of figures is the results for the SS location. The right column of figures is the results for the T location.

Bed Condition	Location	Height above	u	w	$u'u'$	$w'w'$	$u'w'$	
		bed						
			cm	m/s	m/s	m ² /s ²	m ² /s ²	m ² /s ²
Fixed	SS	0.79	0.50	-0.002	0.021	0.0031	-0.0036	
		1.1	0.55	-0.009	0.019	0.0037	-0.0038	
		1.4	0.61	-0.012	0.020	0.0040	-0.0040	
		2.47	0.74	-0.023	0.022	0.0042	-0.0039	
Fixed	T	0.76	0.68	-0.018	0.027	0.0041	-0.0047	
		1.07	0.73	-0.018	0.028	0.0043	-0.0046	
		1.37	0.78	-0.020	0.029	0.0043	-0.0045	
		2.44	0.90	-0.027	0.025	0.0041	-0.0041	

Table 3.2. Average turbulence statistics for the two locations investigated over the fixed bed R-S transition configuration.

3.1.3 Fixed Bed S-R Transition

The third bed condition investigated had a S-R transition bed configuration. In this case, the upstream part of the bed was comprised of small gravel particles glued to a board and the downstream part of the bed was comprised of large gravel particles glued to a board. The bed profile and WSP during the experiments are shown in Figure 3.7. The bed surface profile shows only a subtle difference in slopes associated with the two regions of the bed. The WSP shows some effects of the transitions. Specifically, the S-R transition affects the flow for a significant distance upstream of the transition which can be seen in Figure 3.7 because the WSP is horizontal upstream on the transition. The positions where the particle entrainment studies were performed are marked on this plot with an “X”. The velocity profiles of the two locations investigated are plotted in Figure 3.8. Similar to the previous transition velocity profiles, the velocity profile for the T location shows the flow is faster at the transition than at the SS location. For the T location, the particle entrainment events were extremely rare, so that it was impractical to acquire data under the same water flow rates as done for the SS location. Thus the flow rate was increased by 15% for these data points. Thus the difference in velocity profiles is not associated with the difference in the relative positions on the bed alone. Even with the increase in fluid flow, the particle entrainment rate was very slow. While the data were not taken under entirely consistent conditions, they are included here to provide a bit of information about what may or may not be unique about a R-S transition in the bed.

The conditionally averaged velocities u and w and velocity fluctuations $u'u'$, $w'w'$, and $u'w'$ are plotted for the SS location in the left column of Figure 3.9, and plotted for

the T location in the right column of Figure 3.9. At both locations, data were collected at three different heights above the bed. The average turbulence statistics for both locations and each subsequent height investigated are listed in Table 3.3. One might note that the average turbulence statistics are smaller at the T location even though the velocity profile shows faster velocities at the T location than the SS location. This is different than what was seen in Table 3.2 for the T location and SS location of the fixed bed R-S transition condition with similar velocity profile relationships. Strong trends indicating correlations between velocities and particle motion can be seen in u and w of Figure 3.9 for both the SS location and the T location. The trends are similar to the results that were obtained for the comparable locations over the fixed bed R-S transition condition. Specifically, there are no trends seen in $u'u'$, $u'w'$, and $w'w'$ for the locations 5 cm relative to the transition. On the other hand, while trends were strong for $u'u'$, $u'w'$, and weak for $w'w'$ for the SS location of the R-S transition condition in Figure 3.6, trends are not very prominent in the SS results of the S-R transition condition in Figure 3.9 for $u'u'$ and $u'w'$. There are no trends present in $w'w'$ of Figure 3.9 for the SS location. The average turbulence statistics for the SS location of the S-R transition in Table 3.3 are quantitatively very similar to the average turbulence statistics for the SS location of the R-S transition in Table 3.2. The average turbulence statistics for the T location of the S-R transition in Table 3.3 are quantitatively very different to the average turbulence statistics for the T location of the R-S transition in Table 3.2. The average turbulence statistics of the T location are smaller than the average turbulence statistics of the SS location for the S-R transition in Table 3.3. This is consistent with the less frequent transport rate at the location 5 cm

after the S-R transition compared to that of the SS location.

While the transition points are qualitatively different for the R-S transition set-up and the S-R transition set-up, the SS locations are qualitatively similar. Specifically, the system conditions are the same including water discharge, bed slope, and gravel size. However, even though the conditions for each are essentially uniform, there is a subtle difference: one SS location is located upstream of a roughness transition, and one SS location is located downstream of a roughness transition. One might expect the results for the SS location of the S-R transition to be similar to the results for the SS location of the fixed bed R-S transition results, but there are some subtle differences. There is a difference in the strength of the trends in the SS results of the S-R transition compared to the SS results of the R-S transition, and this may be associated with the flow not being completely steady for the SS location after the S-R transition. In other words, the difference indicates a somewhat longer-distance effect of a roughness transition than expected.

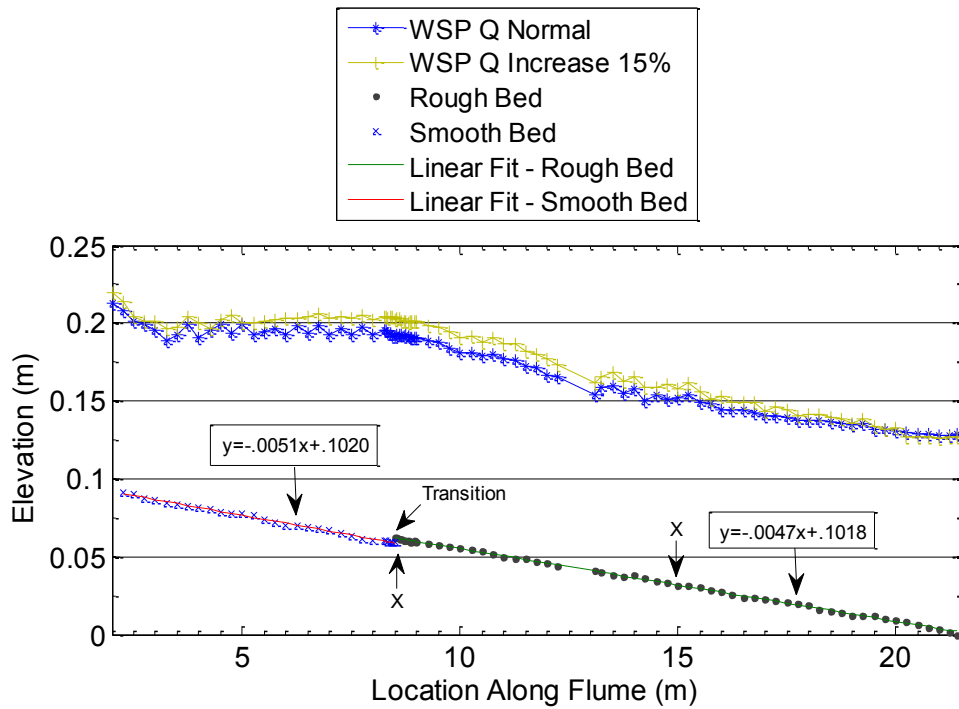


Figure 3.7. Bed profile and WSP for the experiments performed over the fixed bed S-R transition configuration. The two WSP's correspond to the two conditions used for these experiments as described in the text. Specifically, the flow rate was increased by 15 % to collect data at the T location. The data markers are at the points where data were collected. The equations represent the linear trend lines associated with the rough and smooth sections of the bed and provide the slopes of those sections. The two locations where data were collected are marked with an "X". A line was used for the WSP to guide the eye.

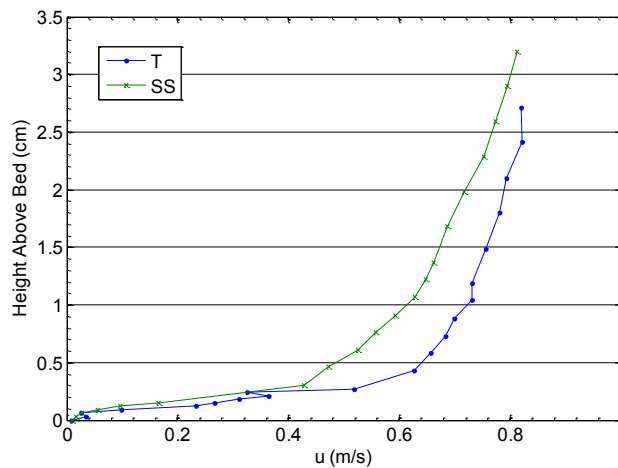
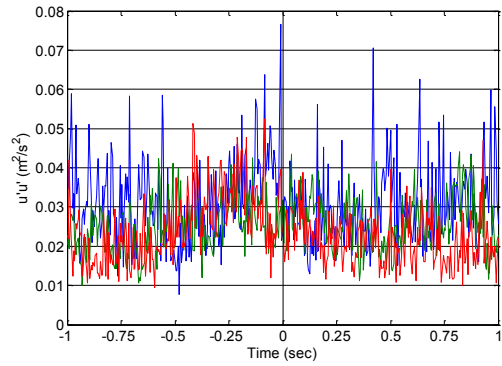
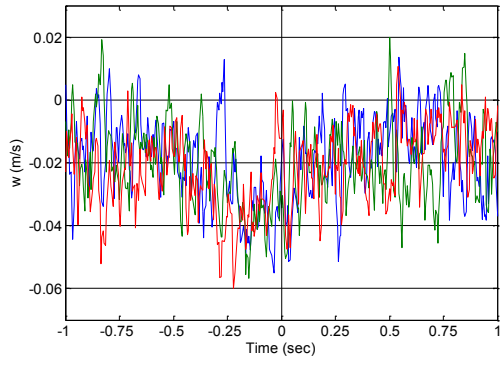
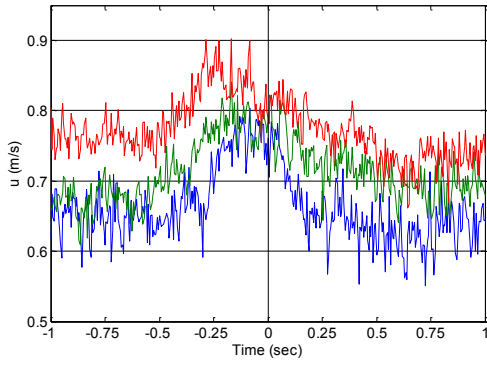
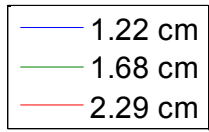
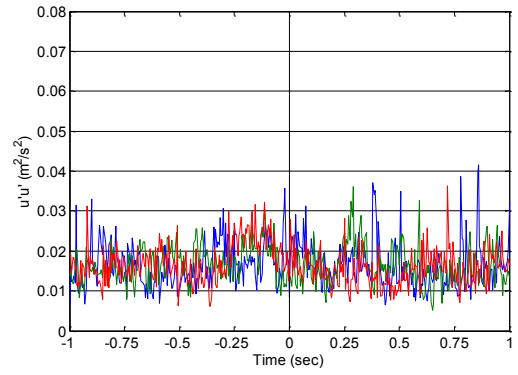
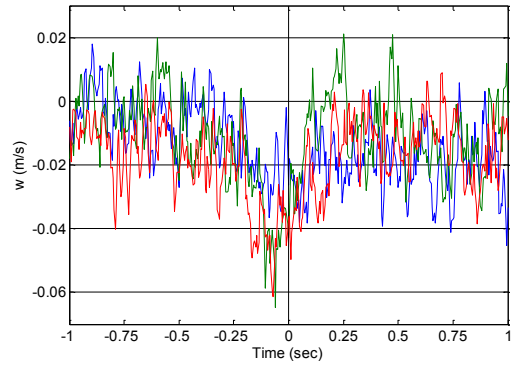
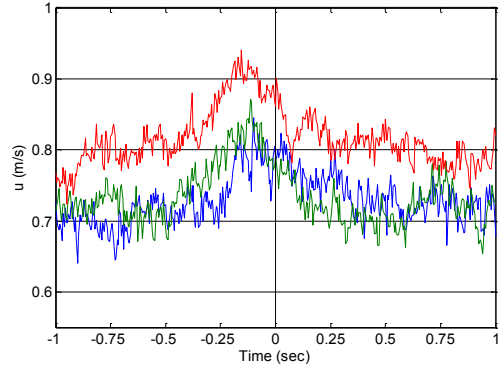
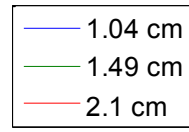


Figure 3.8. Velocity profiles for the two locations investigated over the fixed bed S-R transition configuration. The flow rate was increased by 15 % to collect data at the T location. Lines were used to guide the eye.

SS



T



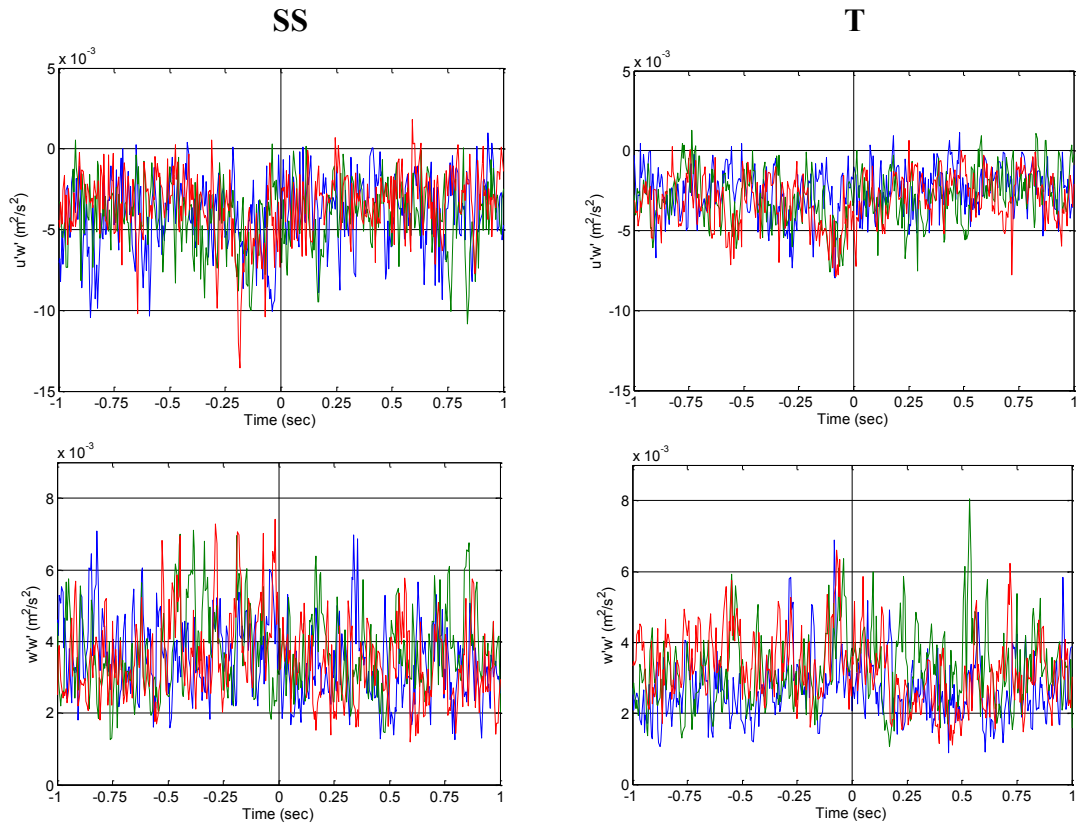


Figure 3.9. Conditionally averaged results for the turbulence statistics u , w , $u'u'$, $u'w'$, and $w'w'$ for the two locations investigated over the fixed bed S-R transition configuration. The left column of figures is the results for the SS location. The right column of figures is the results for the T location. The flow rate was increased by 15 % to collect data at the T location. Special thanks to A. Iversen who collected the data for the height 2.1 cm at the T location.

Bed Condition	Location	Height	u	w	u'u'	w'w'	u'w'
		above bed cm					
Fixed S-R	SS	1.22	0.64	-0.016	0.026	0.0034	-0.0038
		1.68	0.70	-0.017	0.022	0.0035	-0.0036
		2.29	0.75	-0.017	0.022	0.0034	-0.0033
Fixed S-R	5 cm	1.04	0.72	-0.009	0.019	0.0025	-0.0027
		1.49	0.74	-0.008	0.016	0.0029	-0.0028
		2.1	0.79	-0.011	0.015	0.0030	-0.0028

Table 3.3. Average turbulence statistics for the two locations investigated over the fixed bed S-R transition configuration. The flow rate was increased by 15 % to collect data at the T location.

3.1.4 Coherent Structure Analysis

For nearly all the conditionally averaged velocities that exhibit a trend correlating with particle entrainment, the trend is exhibited in the form of a peak that occurs just before the time of particle entrainment. That is, the highest point in the plots is typically located to the left of $t=0$, the time at which initial motion occurred. A possible explanation for this is that an inclined fluid structure such as a “hairpin” or “horse shoe” structure is responsible for both the peak in the conditionally averaged velocity and the particle entrainment Figure 3.10. In this case, part of the structure above the bed would pass through the single point (control volume) where velocity data were collected before the bottom part of it reached the bed. To test this hypothesis, the conditionally averaged downstream velocity data were analyzed further.

The purpose of this analysis is to identify features of coherent structures that correlate with the entrainment of the tracer particle. The feature investigated is the angle of inclination associated with the offset of the peak seen in the trends of the conditionally averaged u velocity results. The peak was determined by smoothing the conditionally average u results by doing a 5 point average. This was iterated one thousand times to investigate the behavior of the iteration method and how it impacted the results. Figure 3.11 shows two examples of how the offset associated with the peak seen in the conditionally averaged u results is impacted over several smoothing iterations. Figure 3.11a shows an example where multiple iterations are required until the peak stabilizes and begins to drift in the direction of the dominant side of the trend. Figure 3.11b shows an example where no iterations were necessary for the stabilization of the peak. In the

second case, the peak actually drifts in the direction of what could be called the dominant side of the trend, and a larger scale shift is experienced after several hundred iterations. The large scale shifts may not be relevant to the entrainment of the particle, and criteria were developed to identifying the peak most relevant with the coherent structure associated with the entrainment of the particle. The criteria used to determine the offset of the peak for the investigation of the angle of inclination met the following conditions: (1) the relevant value of the peak is the offset when the movement was temporarily stabilized, that is, the subsequent iterations caused the peak to drift towards the dominant side of the trend, (2) the stabilization point must occur within the first 50 iterations, or (3) when no initial stabilization occurred, the relevant value for the peak is taken to be the offset associated with the initial offset associated with the peak in the trend.

Two methods were used to investigate the angle of inclination associated with an inclined coherent structure. Since there is a window of uncertainty associated with the different capture resolutions of the ADV and the camera, the reported angles of inclination were corrected to represent the range of angles associated with the uncertainty. The window of uncertainty is described in more detail below.

The first method used, applied Taylor's hypothesis [Pope, 2005] to the offset of the peak seen in the trends in u of the conditionally averaged results. The average velocity u for the height being investigated was multiplied by the corrected offsets in time between initial motion time $t = 0$ and the peak in the trend seen in u . Using L and the height h , an associated angle $\theta = \tan^{-1}(L/z)$ can be determined. The angles of inclination discussed by this method were corrected by determining the maximum angle associated with the offset

of the peak seen in the trends of the u results, and the minimum angle associated with the uncertainty, by adding 0.033 sec to the offset of the peak seen in the trends of the u results, and applying Taylor's hypothesis. The average angle of the maximum and minimum angles is the representative angle. This angle is reported as the angle of inclination associated with an inclined coherent structure representative for each height. The analysis using Taylor's hypothesis may provide results that are larger than actual average angles of inclination. This is because the analysis effectively fixes the lowest point of the inclined structure at time $t = 0$, which may not be the case. As a result, another approach was used to estimate a single average angle of inclination representative of the two locations investigated for the three different bed conditions.

$$L = \langle u \rangle \Delta t \quad (12)$$

where L is the representative x-projection of the inclined coherent structure for a particular height of the coherent structure, u is the downstream velocity, Δt is the offset in the peak seen in the u trends of the conditionally averaged analysis, and $\langle \rangle$ denotes time averaged quantity.

The second method used to investigate the angle of inclination provides an average angle representative of the data sets for each location. The angles were corrected by centering each data point within the window of uncertainty in order to express the range of possible angles graphically more clearly. The uncertainty is limited to a single frame with a time elapse of 0.033 sec, so 0.0165 sec was added to the offsets associated with the peak of the trends seen in the conditionally averaged u results to provide representative angles. The average angle of inclination for each location was determined from the slope

of a linear best fit line through the data sets corresponding to each location with a data point added at height $h=0$ and time $t = 0$ to add weight at the location of interest. A comparison was made between the angles of inclinations represented by applying the method described directly above to similarly represented offsets determined by other methods including following: (1) the peak associated with the initial highest point in the trend, (2) the peak associated with the offset after ten smoothing iterations, and (3) the peak associated with the offset after twenty smoothing iterations.

To investigate the hypothesis that the time offset between the peak in downstream velocity and particle entrainment is associated with an inclined structure, first the height dependence of the time offset is considered at both the SS and T locations for all the bed conditions. The time offset for each height $\Delta t(z)$ is plotted in Fig. 3.12. The uncertainty associated with the finite data acquisition rate is also indicated in this figure. From these plots, it is apparent that Δt increases with height above the bed, supporting the hypothesis that there is an inclined structure associated with the peaks in the fluid velocity that correlate with particle movement.

Next, the first method described above was used to associate $\Delta t(z)$ with a physical distance $\Delta x(z)$ relative to the particle location on the bed. In this way, at a particular height z , the horizontal distance between the structure and the downstream particle distance is approximately $\sim u \Delta t(z)$. Finally, an angle of inclination $\theta(z) = \tan [z / u \Delta t(z)]$ was calculated for each height. Table 3.4 presents the angles of inclination which are associated with the peak in the u results for each bed condition, configuration, location, and height above the bed. In Figure 3.10, is a simple visual representation of the inclined

coherent structure relative to the instrument setup, and provides a sketch of the relevant parameters.

Figures 3.13a, b, and c plot these results with the best fit lines through the data sets as described by the second method above. The average angle of inclination associated with the slope of the linear best fit trend line for the fixed bed R-S transition condition SS location is 11.4° , and the angle for the T location is 6.7° (Figure 3.13a). The angle for the fixed bed S-R transition condition SS location is 5.6° , and the angle for the T location is 8.3° (Figure 3.13b). The angle for the mobile bed R-S transition condition SS location is 4.9° , and the angle for the T location is 7.1° (Figure 3.13c). These angles are smaller than the angles determined from using data only from a single point above the bed (given in Table 3.4). Both methods provide results that are consistent with previously published results based on experiments in water and air [Niño and García, 1996; García et al., 1995; Lu and Willmarth, 1973; Roy et al., 2004; Buffin-Bélanger et al., 2000a; Haidari and Smith, 1994; Adrian et al., 2000; Rajagopalan and Antonia, 1979; Brown and Thomas, 1977; Marusic et al., 2001] as summarized in Chapter 1. In Tables 3.5 and 3.6 are the angles determined using method 2 associated with offsets identified by different criteria. The average angles do not change by much under the different circumstances.

It is interesting to note that the angles associated with the results 5 cm before the fixed bed R-S transition are much smaller than the angles associated with the SS location. The difference in the angle of inclination between the two locations suggests that the coherent structure is modified and rotated toward the bed as it passes through the

transition region where the flow above the bed is faster downstream than upstream. Considering the widths of the peaks in the downstream velocity position in figure 3.6, the breadth of the SS location peak (± 0.25 sec) appears more narrow than that of the T location peak (± 0.50 sec) which indicates there may be additional elongation or stretching of the inclined coherent structure in the downstream direction as it moves through the region affected by the R-S transition. Also, the angle associated with the results 5 cm after the fixed bed S-R transition is slightly larger than the angle associated with the SS location. The S-R transition has an effect on the flow that is felt upstream of the transition. The transition region experiences a spatial deceleration in the flow and this may cause the coherent structure to tip away from the bed resulting in a larger angle at the T location than compared to the downstream SS location.

In considering the uncertainty in these results, it is helpful to note that the camera capture rate is finite: 30 fps. There is a small window of uncertainty associated with this in terms of when the actual time initial motion occurred corresponding to ± 0.0165 sec, likely responsible for the times associated with the positive shift of the peak relative to the time of initial particle movement (and thus the oblique angle in Table 3.4). Further, considering this uncertainty alone, this could have caused the trends in the u results of Figure 3.3, 3.6, and 3.9 to shift up to 0.033 sec to the left from where the trends currently occur. Even if this worst case scenario were to be true, the data would still provide support to the results that have been discussed. The uncertainty limits are identified in Figure 3.12 along with the time of the uncorrected offsets seen in the u results from the conditionally averaged analysis plotted versus height.

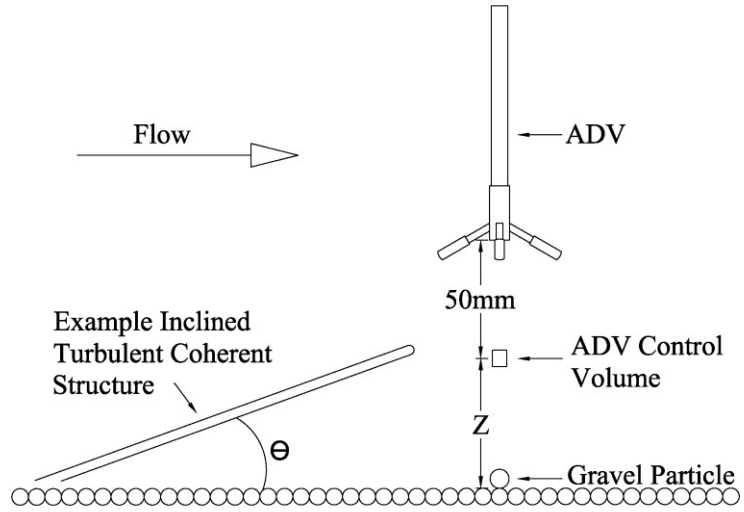
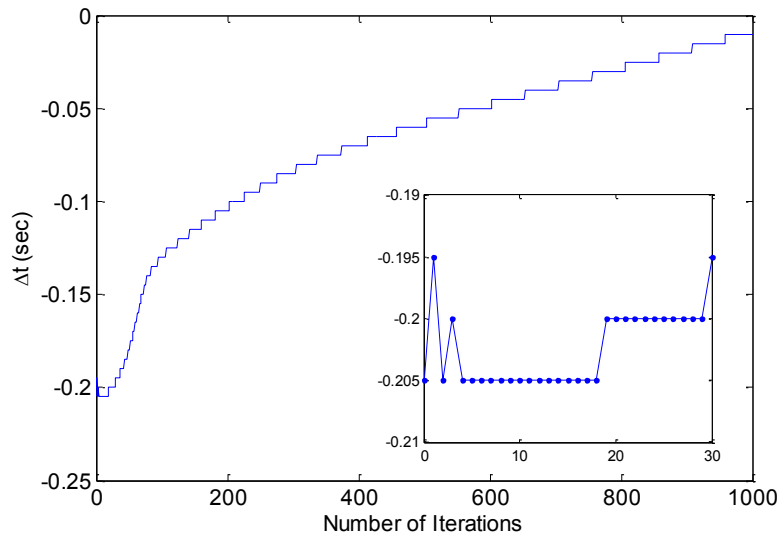
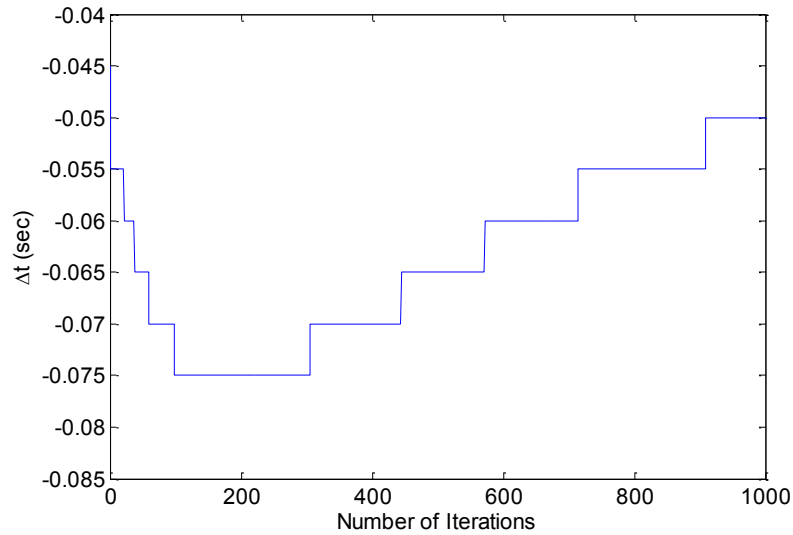


Figure 3.10. A system diagram showing the dimensions and configuration that has been studied and the representation of an inclined structure. The ADV has a cylindrical control volume. The height of the control volume is 7 mm and the diameter is 6 mm.



a.)



b.)

Figure 3.11. Offset associated with the peak seen in the conditionally averaged u results as it is affected by the number of smoothing iterations. a.) Example where multiple iterations are required for the peak to stabilize. b.) Example where no smoothing iterations were necessary for the stabilization of the peak, and an example of a large scale shift in the peak not relevant to when initial motion occurred.

Bed Condition	Location	Height above bed cm	θ Deg	Error θ \pm Deg	Location	Height above bed cm	θ Deg	Error θ \pm Deg
Mobile R-S	SS	0.53	23.0	11.1	T	0.43	+	+
		0.61	6.0	0.9		0.58	8.9	2.4
		0.77	-	-		0.73	40.2	24.6
Fixed R-S	SS	0.79	39.0	18.8	T	0.76	6.1	0.9
		1.1	123.0*	27.3*		1.07	12.1	2.7
		1.4	21.8	5.3		1.37	7.7	1.0
		2.47	16.3	2.2		2.44	7.0	0.5
Fixed S-R	SS	1.22	20.0	5.4	T	1.04	7.9	1.2
		1.68	7.4	0.6		1.49	9.2	1.2
		2.29	6.4	0.4		2.1	8.4	0.7

Table 3.4. Angles of inclined coherent structures associated with the offset of the peak seen in conditionally averaged downstream velocity u relative to when initial motion occurred. (*) denotes angles are oblique which represent angles towards the bed. (-) represents no clear trend in the conditionally averaged downstream velocity u . (+) represents an outlier, where a trend was present in the conditionally averaged downstream velocity u but the peak is not closely related to when initial motion occurred.

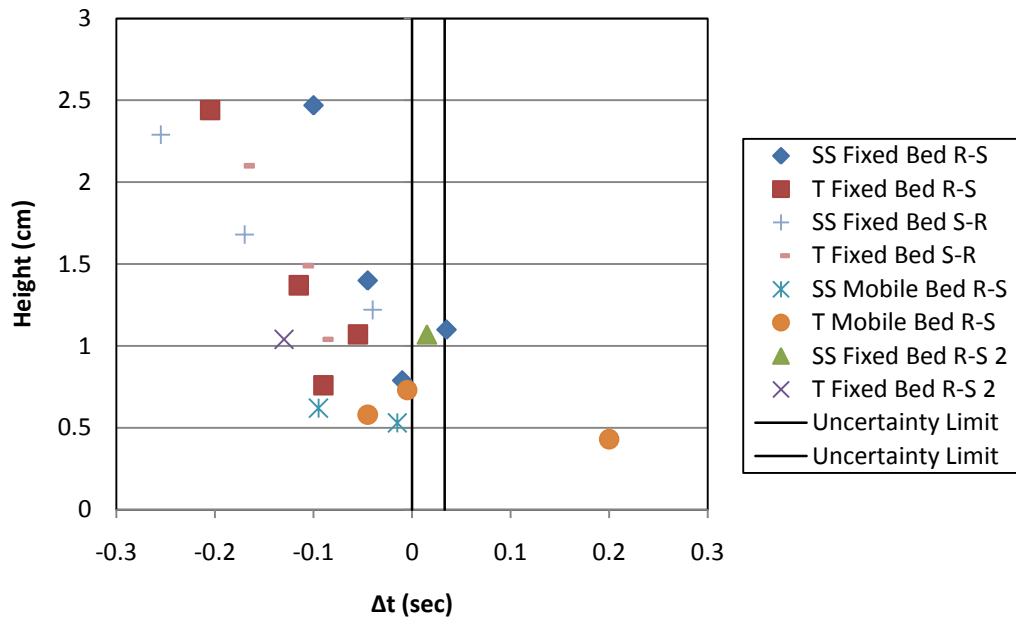
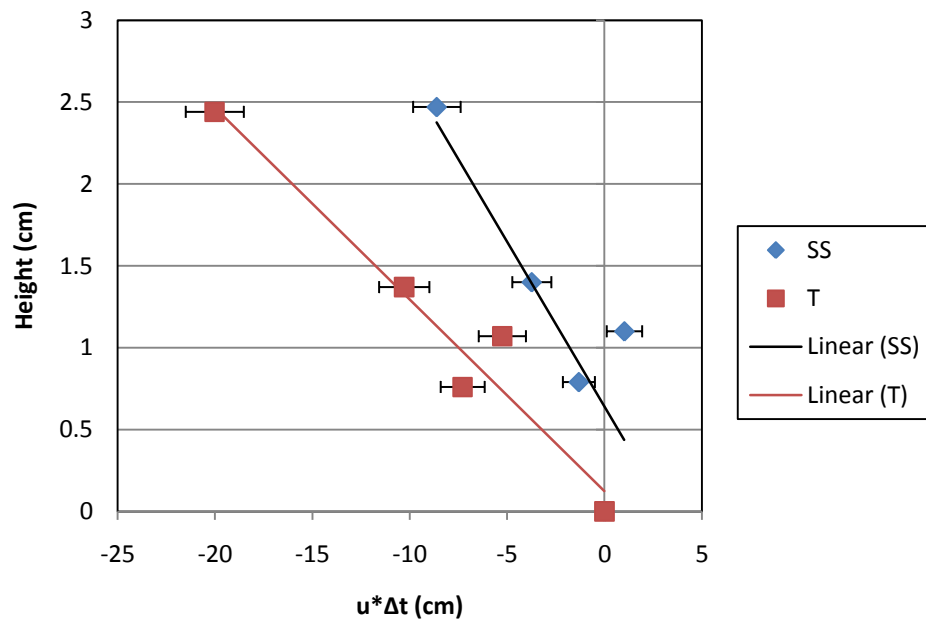
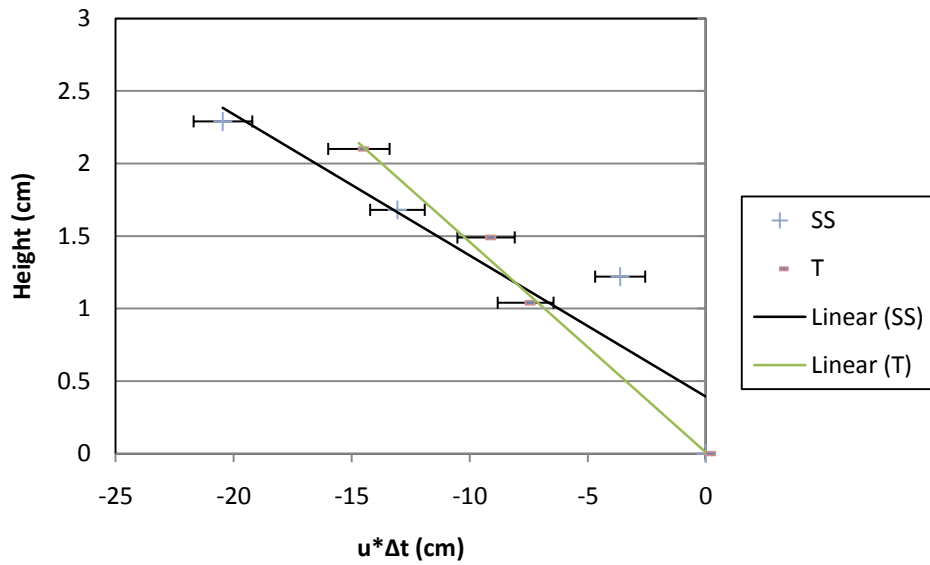


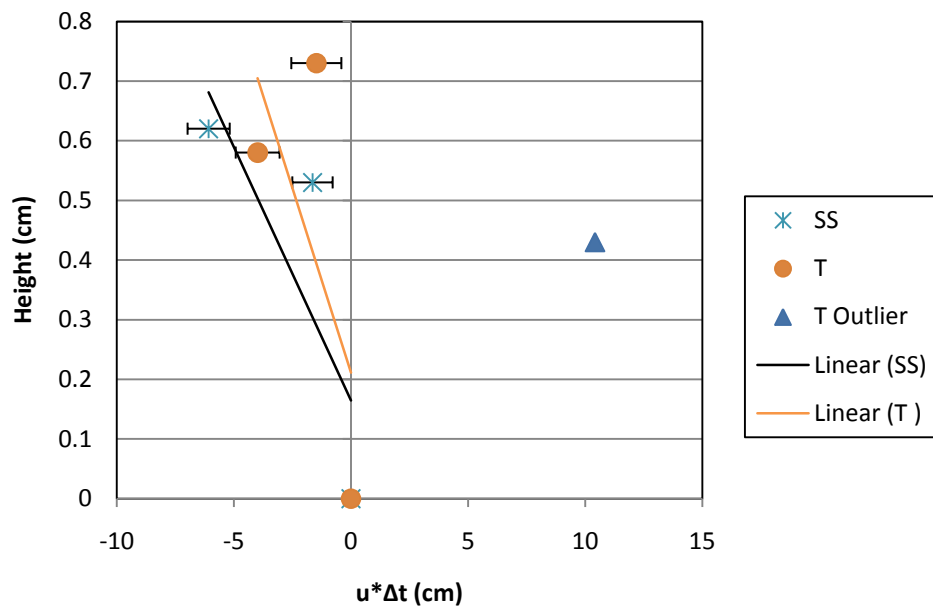
Figure 3.12. All uncorrected offsets associated with the peak in the u velocity of the conditionally averaged results. The limits corresponding to the 0.033 sec window of uncertainty are also plotted.



a.)



b.)



c.)

Figure 3.13. Plots associated with the second method for determining the average angle of inclination representative for the data sets at the SS location and the T location. The equation for the linear trend lines is $y = Ax + B$. a.) Fixed bed R-S transition. SS location: $A = -0.2012$, $B = 0.643$. T location: $A = -0.1171$, $B = 0.1249$. b.) Fixed bed S-R transition. SS location: $A = -0.0972$, $B = 0.3943$. T location: $A = -0.145$, $B = -0.0102$. c.) Mobile bed R-S transition. SS location: $A = -0.085$, $B = 0.1647$. T location: $A = -0.1238$, $B = 0.2111$.

	Method			
	Primary	# of Iterations		
		10	20	Highest Pt
Fixed Bed R-S	11.4	11.9	12.8	13.1
Fixed Bed S-R	5.6	6.0	6.0	8.2
Mobile Bed R-S	4.9	5.7	5.4	4.8

Table 3.5. Comparison of average angles representative of the data sets for the SS locations. The average angles are associated with the offsets of the peak which were determined from different methods. The second method described in the text to determine the angles was used to obtain these results.

	Method			
	Primary	# of Iterations		
		10	20	Highest Pt
Fixed Bed R-S	6.7	3.9	4.3	6.5
Fixed Bed S-R	8.3	8.5	9.0	8.7
Mobile Bed R-S	7.1*	5.6*	6.3*	3.2

Table 3.6. Comparison of average angles representative of the data sets for the T locations. The average angles are associated with the offsets of the peak which were determined from different methods. The second method described in the text to determine the angles was used to obtain these results. (*) Denotes that angles were determined without the outlier point.

3.1.5 Quadrant Analysis

In this section, the results from the quadrant analysis of the data are described. To summarize, the quadrant analysis essentially keeps track of the four contributors to the Reynolds stress $\langle u'w' \rangle$, namely (1) all data points where $u' > 0$ and $w' > 0$, called Q_1 events or termed “outward interactions”; (2) all data points where $u' < 0$ and $w' > 0$, called Q_2 events or termed “ejections”; (3) all data points where $u' < 0$ and $w' < 0$, called Q_3 events or termed “inward interactions”; (4) all data points where $u' > 0$ and $w' < 0$, called Q_4 events or termed “sweeps”. The graphical representation of this is shown for the fixed bed R-S transition in Figure 3.14 (SS position) and Figure 3.15 (T position). In these figures, w' is plotted vs. u' for each data point from the conditionally averaged results

from the entire 2 sec window shown in Figure 3.14a and 3.15a and for a 0.5 sec window around $t = 0$ in Figure 3.14b and 3.15b. Figure 3.16 shows the w' plots of the 2 sec and 0.5 sec window which correlate to the quadrant analysis plots for the SS location and height plotted in Figure 3.14, and the T location plotted in Figure 3.15. Then, the relative frequency of events occurring in each quadrant is presented in table format for the SS location in Table 3.7 and for the T location in Table 3.8.

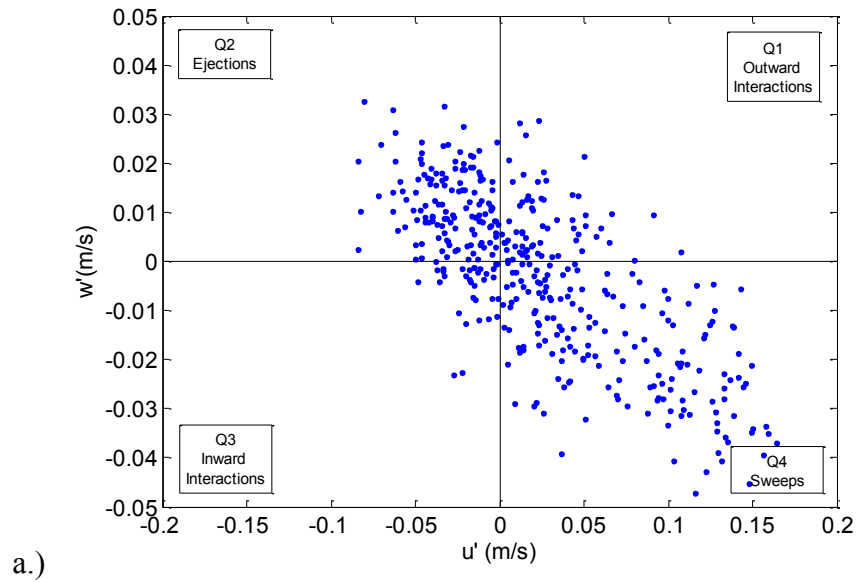
The results of the quadrant analysis for the fixed bed R-S condition are different from the mobile bed R-S condition. For the 2 sec quadrant analysis the dominant quadrant event is Q_4 , which agrees with previous findings linking quadrant events with sediment transport [Nelson *et al.*, 1995; Hofland *et al.*, 2005; Williams *et al.*, 1989; Thorne *et al.*, 1989; Drake *et al.*, 1988; Heathershaw and Thorne, 1985]. Q_1 and Q_2 events contribute nearly equally for both locations, and Q_3 events contribute the least. The percent of Q_1 events was approximately the same whether the calculation was performed over a 0.5 sec window or a 2 sec window, in some instances reducing or increasing by a couple of percent from one window to the next. Figure 3.16a and b show the regions in the w' time series which contribute to Q_1 events in the quadrant analysis for those specific cases plotted in Figures 3.14 and 3.15. These are included to demonstrate that the times when $w' > 0$ and thus the “events” that contribute to the Q_1 events for the 0.5 sec analysis are not near time $t = 0$ when initial motion occurred, but can be seen closer to the outer limits of the 0.5 sec window. The percent of Q_2 and Q_3 events decreased significantly in the percent of events occupied by these quadrants from the 2 sec analysis to the 0.5 sec analysis. In most cases, the percent of events was reduced to 0 for both Q_2

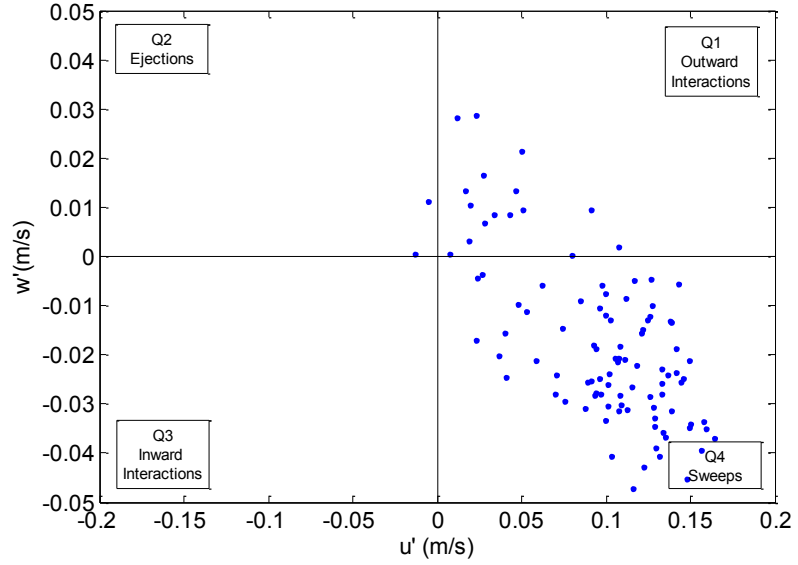
and Q₃ events. For these results, the dominant quadrant is Q₄, and this is even truer for the 0.5 sec window immediately surrounding the entrainment event than for the 2 sec window. On average Q₄ events contribute 72 % and 86 % of the total time of the 0.5 sec window quadrant analysis for the T location and SS location, respectively. This is expected since there are very strong and clear trends in the conditionally averaged u and w results of Figure 3.6.

The results of the quadrant analysis for the fixed bed S-R condition are similar to the results for the fixed bed R-S condition. For the 2 sec window quadrant analysis Q₂ and Q₄ events are the most dominant quadrants for both the SS location and the T location, with Q₄ being most dominant. Q₄ is the dominant quadrant event for the 0.5 sec analysis and occupies 80 % of the total time for both the T location and the SS location. The conditional averaged results also showed clear trends in u and w for the fixed bed S-R condition Figure 3.9, similarly to the fixed bed R-S condition, and thus result in similar conclusions.

The results from the quadrant analysis for the mobile bed R-S condition incur a higher uncertainty of the meaning of the results. This is likely because strong trends were not seen in u or w for the SS location in Figure 3.3. Interestingly though, for the whole 2 sec window the results agree well with previously published quadrant analysis statistics of general flow without correlation with bed-load transport, where Q₂ and Q₄ events are the most dominant quadrant events [*Nelson et al.*, 1995; *Païement-Paradis et al.*, 2010; *Williams et al.*, 1989; *Thorne et al.*, 1989; *Wallace et al.*, 1972]. The 0.5 sec window shifts dominance to Q₁ and Q₄. It is interesting to note that an increase in u (i.e.,

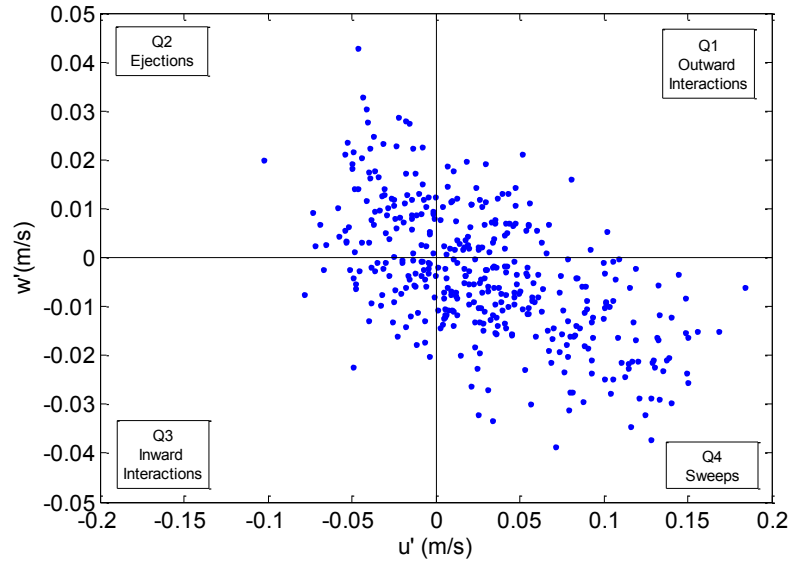
instances of positive u') indicates there should be more contributions to both quadrants Q_1 and Q_4 . An increase in u did occur but the results did not suggest a strong correlation with entrainment. The high frequency of Q_1 and Q_2 events for the mobile gravel bed to smooth bed transition is likely at least partly due to the scour immediately upstream of the transition. As the flow approached the R-S transition near the bed, the water had to flow up in general as it transitioned onto the smooth section. The dominant quadrants of the 2 sec window were Q_1 and Q_2 for the data set at the T location, and the dominant quadrants of the 0.5 sec window were Q_1 and Q_4 , with Q_1 being most dominant.



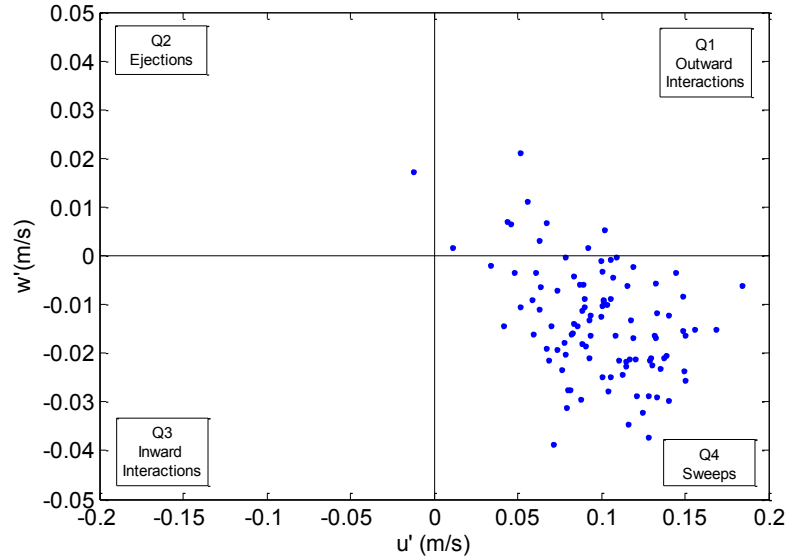


b.)

Figure 3.14. Quadrant analysis plots for a.) 2 second window and b.) 0.5 second window of the SS location for the height 1.4 cm over the fixed bed R-S transition.

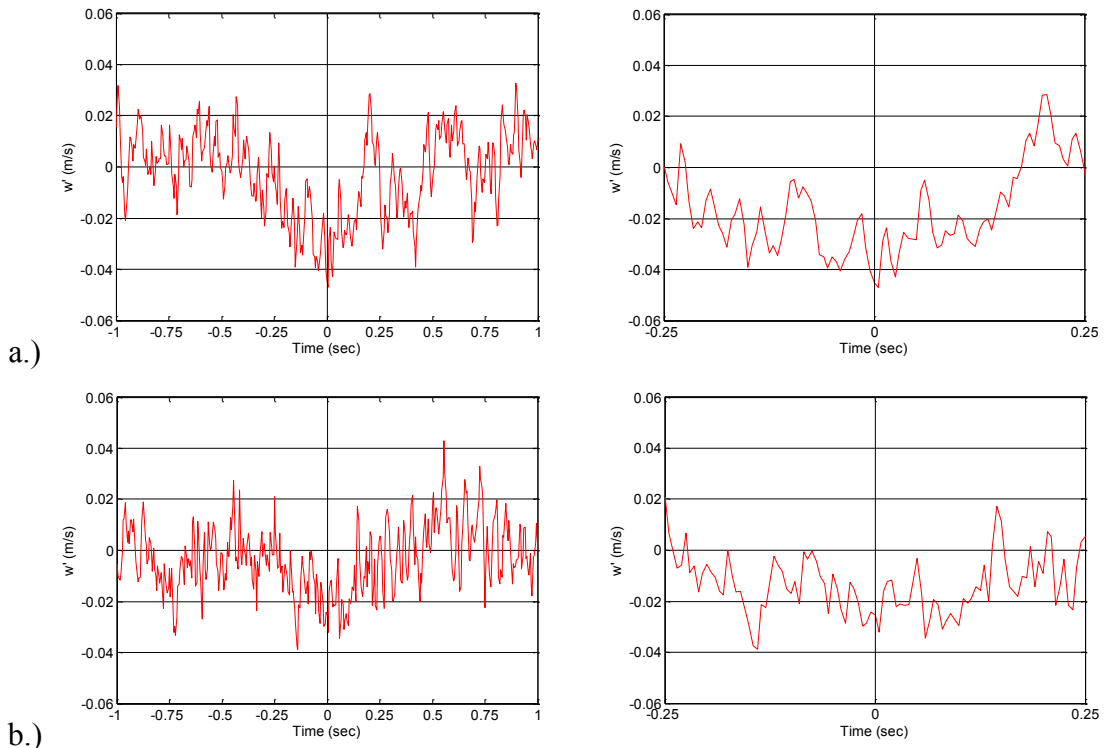


a.)



b.)

Figure 3.15. Quadrant analysis plots for a.) 2 second window and b.) 0.5 second window of the T location for the height 1.37 cm over the fixed bed R-S transition.



b.)

Figure 3.16. The 2 sec and 0.5 sec window of the conditionally averaged w' results for locations a.) SS at 1.4 cm above the fixed bed, and b.) T at 1.37cm above the fixed bed.

Bed Condition	Location	Height Above Bed cm	2 Second Window, 0.5 Second Window			
			Q ₁ Outward Interactions	Q ₂ Ejections	Q ₃ Inward Interactions	Q ₄ Sweeps
Mobile R-S	SS	0.53	12, 24	38, 30	20, 6	30, 41
		0.61	36, 58	33, 15	5, 0	26, 27
		0.77	29, 37	27, 2	5, 0	38, 61
		Ave	26, 40	33, 15	10, 2	31, 43
Fixed R-S	SS	0.79	11, 8	15, 1	14, 1	59, 90
		1.1	24, 19	16, 0	12, 0	48, 81
		1.4	16, 16	33, 2	8, 0	43, 82
		2.47	17, 9	24, 0	10, 0	48, 91
		Ave	17, 13	22, 1	11, 0	50, 86
Fixed S-R	SS	1.22	20, 10	24, 5	13, 2	43, 83
		1.68	15, 20	25, 0	20, 0	40, 80
		2.29	19, 21	22, 0	13, 2	46, 77
		Ave	18, 17	23, 2	15, 1	44, 80

Table 3.7. Quadrant Analysis results for the SS location. The table represents the percentage of time associated with each quadrant event for a 2 sec window and 0.5 sec window surrounding when initial motion occurred.

Bed Condition	Location	Height Above Bed cm	2 Second Window, 0.5 Second Window			
			Q ₁ Outward Interactions	Q ₂ Ejections	Q ₃ Inward Interactions	Q ₄ Sweeps
Mobile R-S	T	0.43	7, 24	37, 14	35, 10	20, 52
		0.58	30, 71	58, 12	5, 1	6, 16
		0.73	44, 75	40, 9	5, 0	11, 16
		Ave	27, 57	45, 11	15, 4	13, 28
Fixed R-S	T	0.76	24, 32	24, 2	11, 1	41, 65
		1.07	26, 49	13, 0	8, 0	53, 51
		1.37	16, 10	21, 1	13, 0	50, 89
		2.44	19, 19	17, 1	13, 0	51, 80
		Ave	21, 27	19, 1	11, 0	49, 72
Fixed S-R	T	1.04	11, 11	26, 2	17, 1	46, 86
		1.49	8, 7	35, 24	27, 4	30, 65
		2.1	21, 10	12, 0	14, 1	53, 89
		Ave	13, 9	24, 9	20, 2	43, 80

Table 3.8. Quadrant Analysis results for the T location. The table represents the percentage of time associated with each quadrant event for a 2 sec window and 0.5 sec window surrounding when initial motion occurred.

3.2 Experiment 2

Experiment 2 was performed to investigate the effects the R-S transition had on a mobile bed upstream of the transition as it develops and reaches a steady state. The experiment was performed with the initial conditions of the fixed bed with the same R-S transition described above. This experiment was performed for both transition locations described in each of the two subsections below.

3.2.1 Fixed Bed Transition Location 1

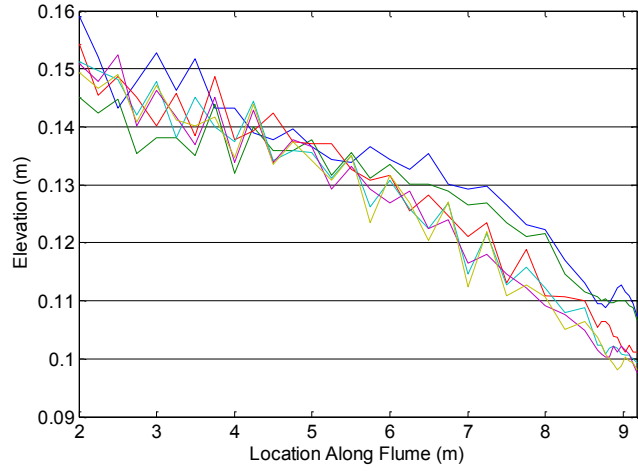
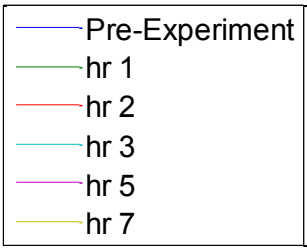
The initial system conditions of this experiment are outlined in Table 2.2. Gravel was fed into the system at $8.56 \times 10^{-6} \text{ m}^3/\text{s}$ for a total of 7 hrs and steady state was reached between 2 hrs of run time and 3 hrs of run time. After hour 2, the system did not

experience significant changes. This can be seen in the WSP's, bed elevations, and depth of Figure 3.17a, b, and c respectively, where all runs are plotted and there are not significant differences seen in the plots for run time after 2 hrs. Though not well-captured using the point gage, some variability was visually apparent after 2 hrs near the sediment feeder. The buildup of the bed progressed down the flume, and during this time there was not very much gravel leaving the system, particularly compared to the feed rate. Finally, after approximately 3 hrs the system conditions started to approach steady state. Since the buildup occurred very quickly, the progression of the front was only captured in the measurements after 1 hour of run time. This can be seen in Figure 3.17b where the front of the buildup is located where the 1 hr bed profile meets the pre-experiment bed profile at about 6 m. This is also clear in Figure 3.18a, c, and d where comparisons were made of each run relative to the initial bed profile, final bed profile, and the percent of the final bed, respectively. In these figures the measurements corresponding to hour 1 are closer to final bed conditions at the beginning of the flume, but transitions to be similar to initial bed conditions further downstream around the 6 m location.

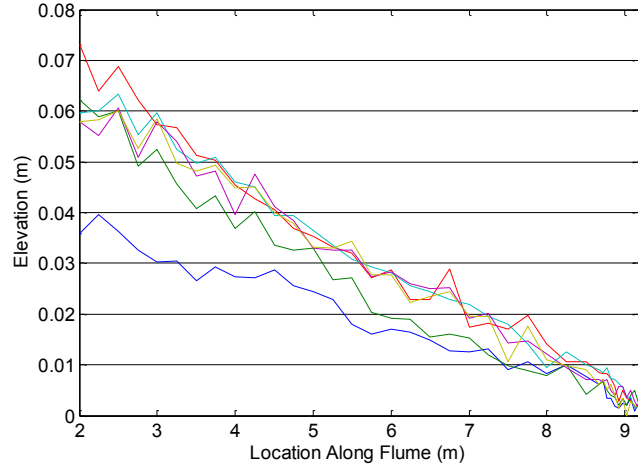
The region that was of interest in this experiment was near the transition, and ultimately the goal was to compare the buildup characteristics near the transition to the general characteristics of the buildup that occurred overall. This was of interest because the impact the R-S transition had on the buildup just upstream of the transition was the primary investigation. Unfortunately, the resolution of the data collected did not provide clear information to see if differences existed. Figure 3.18d shows the instability near the

transition which makes data interpretation difficult. There were not any trends seen in the differences in the bed slopes in the first 0.3 m upstream of the transition in Figure 3.19b, compared to the first 1.17 m upstream of the transition in Figure 3.19a. Table 3.9 lists the slopes and intercepts associated with the linear trend lines in Figure 3.19a and b. Although the results do not provide much quantitative insight, qualitative visual observations taken during the experiment suggest that initially there is not a significant buildup for the 1.5 m immediately upstream of the transition. Build up in this region was limited to streaks of gravel and was only one gravel diameter in height. This is probably because the gravel was more likely to transport through the system when it reached this region compared to depositing, and after steady state was reached this dynamic was still present.

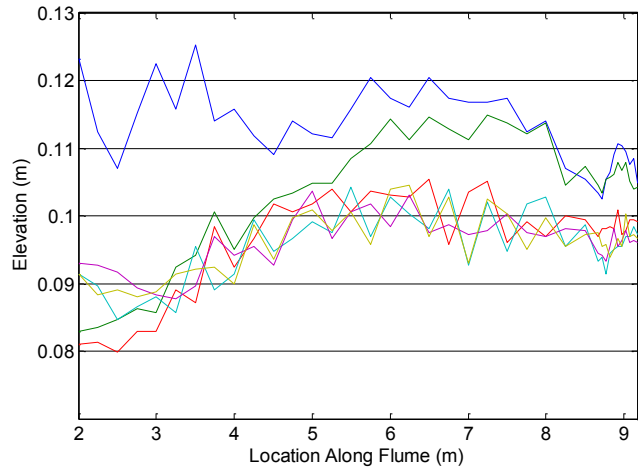
The resolution of the collected profiles created difficulty in interpreting the results. Since large gravel is used in the experiment, there are inherent fluctuations in the bed elevation measurements which may not represent a physical change in bed slope. Instead, this may simply be the result of different arrangements of the asymmetric gravel temporarily on the bed. This has the largest impact when measurements are close together like the bed measurements collected near the transition. Increasing the resolution of the bed profiles would smooth out random variation in the bed and make the results more clear. The resolution could be improved by collecting several points at each location and averaging them together.



a.)

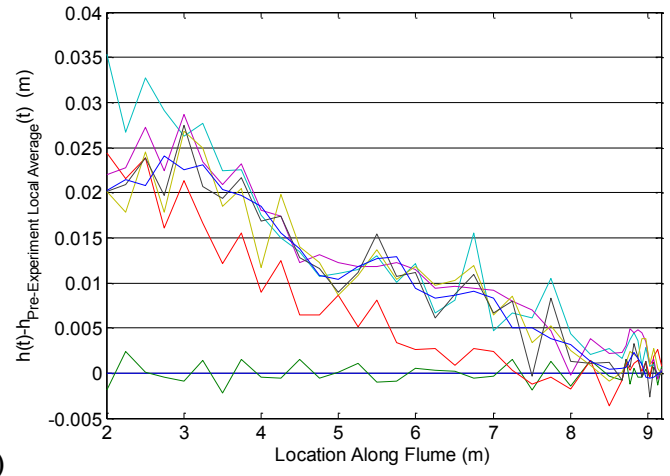
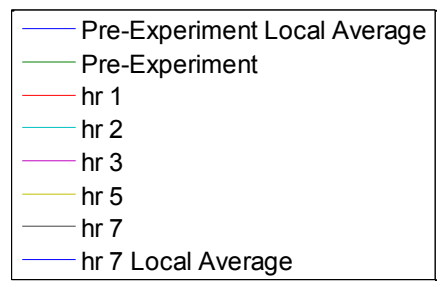


b.)

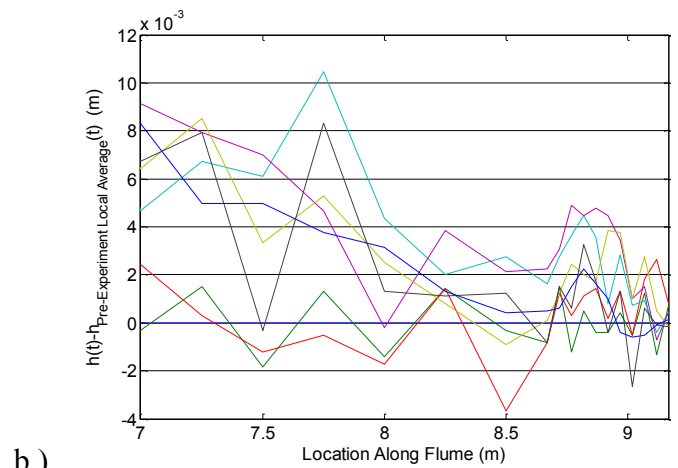


c.)

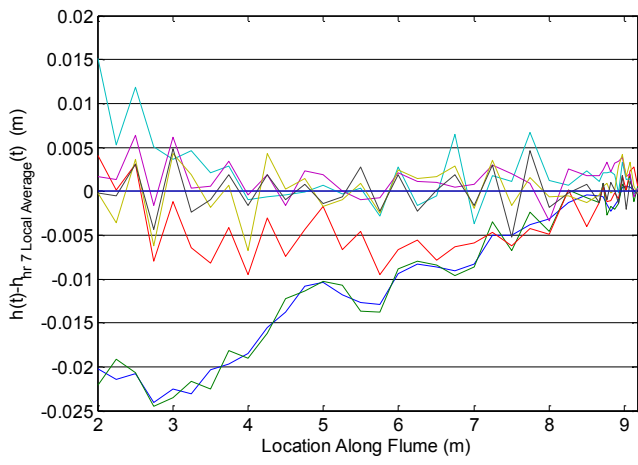
Figure 3.17. a.) WSP's, b.) Bed profile, c.) Depth of flow. Lines were used to guide the eye.



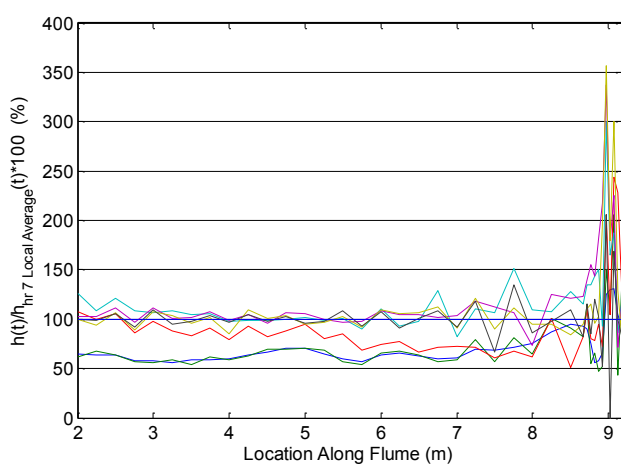
a.)



b.)

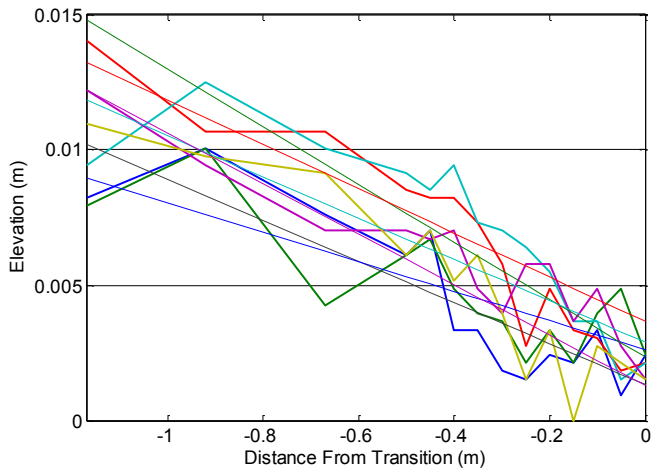
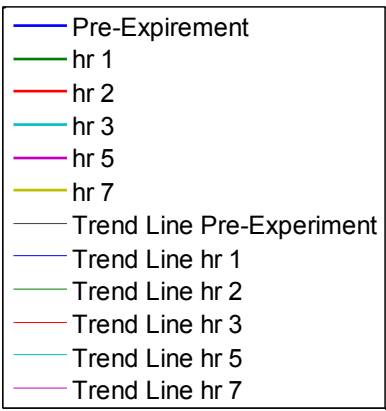


c.)

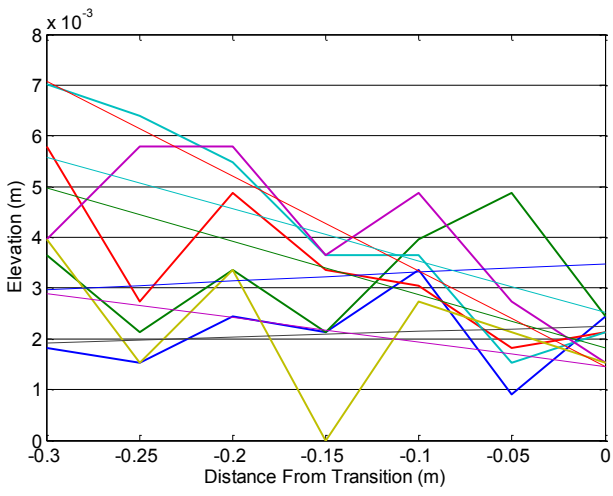


d.)

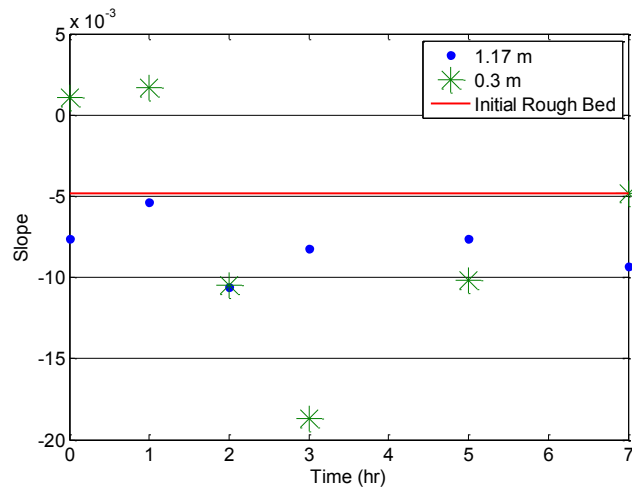
Figure 3.18. a.) Bed elevation change with respect to the pre-experiment local average bed profile. b.) Zoomed in look at the near transition region of the bed elevation change with respect to the pre-experiment local average bed profile. c.) Bed elevation change with respect to the hr 7 local average bed profile. d.) The percentage of the hr 7 local average bed elevation. Lines were used to guide the eye.



a.)



b.)



c.)

Figure 3.19. Zoomed in bed profiles with linear fit trend lines of form $y = ax + b$ where the slope “ a ” and intercept “ b ” are in Table 3.9. a.) 1.17 m. b.) 0.3 m upstream of the R-S transition. c.) the slope changes plotted verses time.

1.17 m			0.3 m		
Time	Slope a	Intercept b	Time	Slope a	Intercept b
0	-0.0076	0.0013	0	0.0011	0.0023
1	-0.0054	0.0026	1	0.0017	0.0035
2	-0.0106	0.0023	2	-0.0105	0.0018
3	-0.0082	0.0037	3	-0.0187	0.0015
5	-0.0076	0.0029	5	-0.0102	0.0025
7	-0.0093	0.0013	7	-0.0048	0.0015

Table 3.9. Slopes and intercepts for the linear trend lines of form $y = ax + b$ in Figure 3.19.

3.2.2 Fixed Bed Transition Location 2

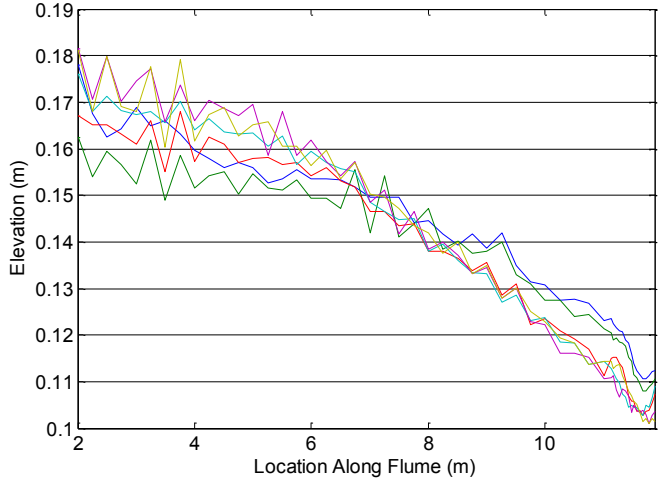
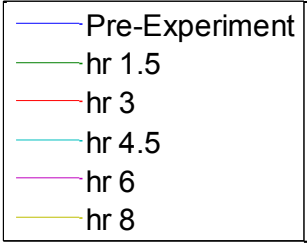
To address some of the limitations of the first experiment of type 2, a few changes were made. First, the sediment feed rate was reduced slightly for this run compared to the feed rate for the first time this experiment was performed in hopes that more of the buildup would be captured. The feed rate was not reduced by much so the overall system would not be much different than the first time the experiment was performed. Second, the resolution of the collected profiles was improved by collecting 3 points at each

location and averaging them together to get a representative measurement. This provided data which was clearer and provided better insight on the differences just upstream of the transition compared to the general buildup that occurred.

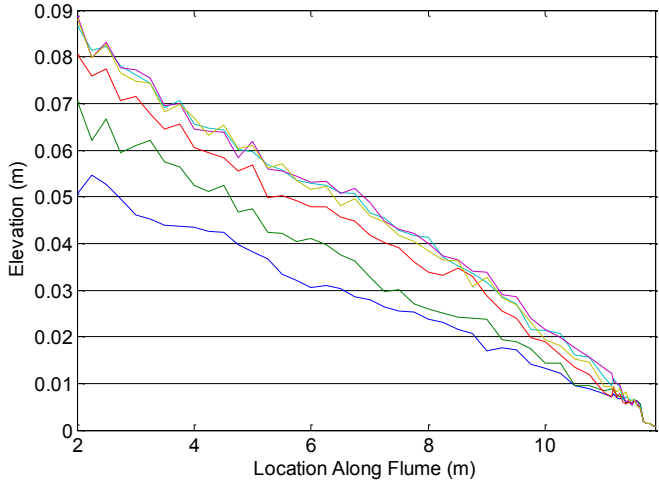
For this experiment, gravel was fed into the system at $7.85E-06 \text{ m}^3/\text{s}$ for a total of 8 hrs and steady state was reached between 3 hrs of run time and 4.5 hrs of run time. After hour 4.5 the system did not experience significant changes. This can be seen in the WSP's Figure 3.20a, bed elevations Figure 3.20b, and depth Figure 3.20c where all runs are plotted and there are not significant differences seen in the plots for run time after 4.5 hrs. From general observation of the development of the bed, variability across the channel was not as prominent for this run. The buildup of the bed progressed down the flume similar to the first time this experiment was performed. As the bed built up, initially there was not very much gravel passing through the system until the progression approached steady state. The progression of the buildup was captured in the measurements after 1.5 hrs of run time and 3 hrs of run time. The progression of the front is not as clear, but the buildup can be seen in Figure 3.20b. The front was not clearly defined and was streaky as the bed built up, and also after the bed had reached steady state near the transition. The buildup is also clear in Figure 3.21a, c, and d where comparisons were made of each run relative to the initial bed profile, final bed profile, and the percent of the final bed, respectively. The measurements after 1.5 hrs of runtime show that the front is roughly located at 8 m, and the streaky front is present in these results because the profiles never fully recover to the pre-experiment profile.

Similar to the first time the experiment was performed, the region of interest was

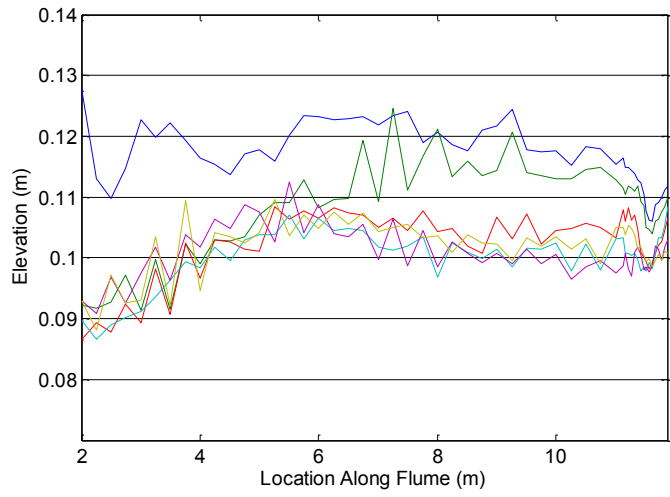
near the transition and ultimately the goal was to compare the buildup characteristics near the transition to the general characteristics of the buildup that occurred overall. When comparing the first 0.3 m before the R-S transition Figure 3.22b, to the first 1.12 m before the R-S transition Figure 3.22a, differences exist in the bed slopes. The slopes and intercepts associated with the linear trend lines in Figure 22a and b are in Tables 3.10. The bed slopes associated with the first 0.3 m for all the measurements are similar to the overall initial bed slope, and if the larger distance is considered the bed slopes are much steeper because of the buildup that occurred. Figure 3.22c shows that the slopes are not significantly different from the initial bed slope in the first 0.3 m upstream of the transition, but is different when you consider 1.12 m upstream of the transition. This provides evidence that the R-S transition impacts transport for a small distance upstream of the transition. General observations taken during the experiment also suggest, similarly to the first time the experiment was performed, that there is not significant buildup just upstream of the transition. Build up in this region was limited to streaks of gravel and was only one gravel diameter in height, as similarly seen before. As before, this is probably because the gravel was more likely to transport through the system when it reached this region compared to depositing, and after steady state was reached this was still noticed to be occurring, Figure 3.22.



a.)

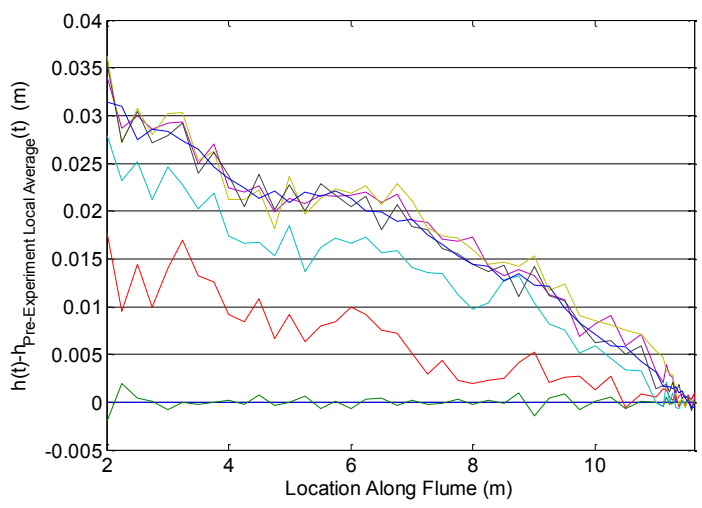
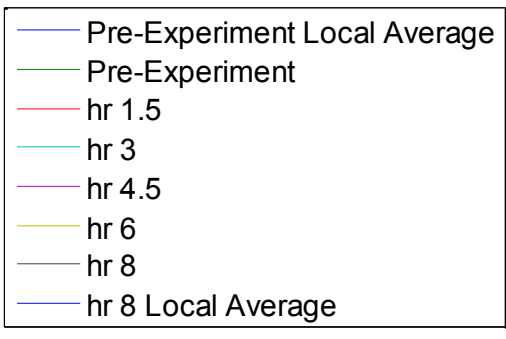


b.)



c.)

Figure 3.20. a.) WSP's, b.) Bed profile, c.) Depth of flow. Lines were used to guide the eye.



a.)

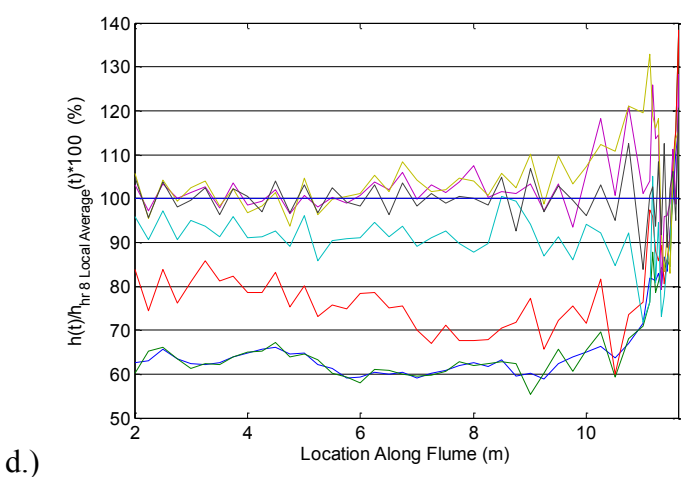
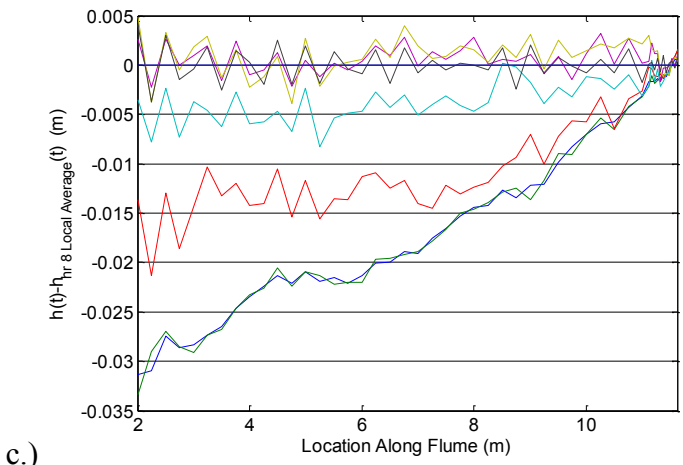
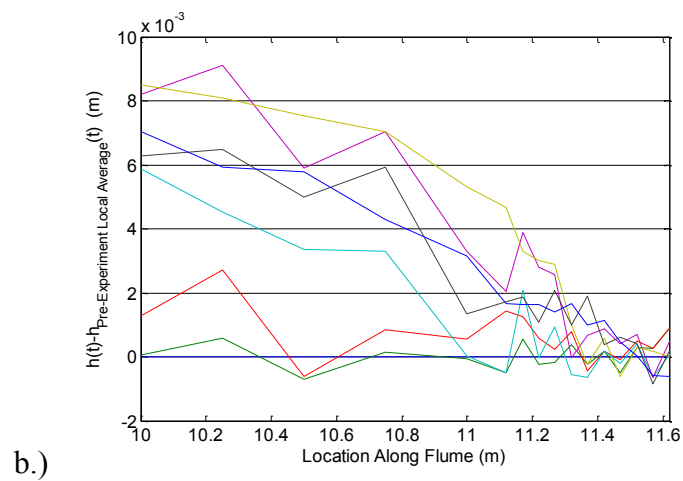
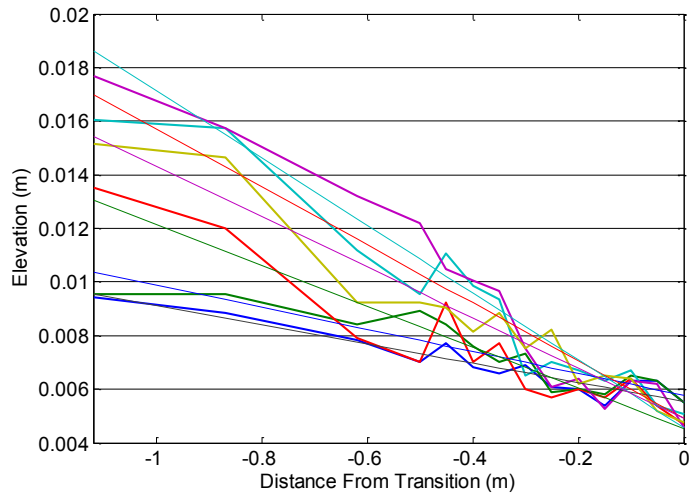
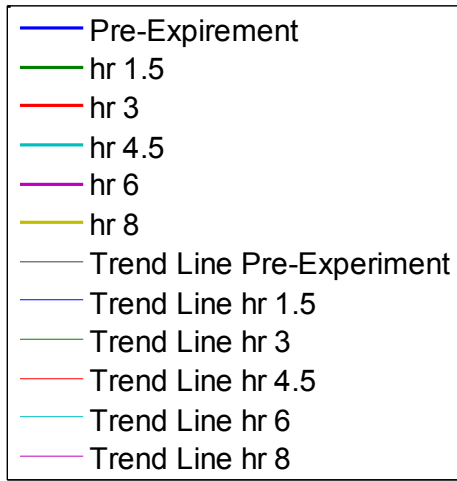
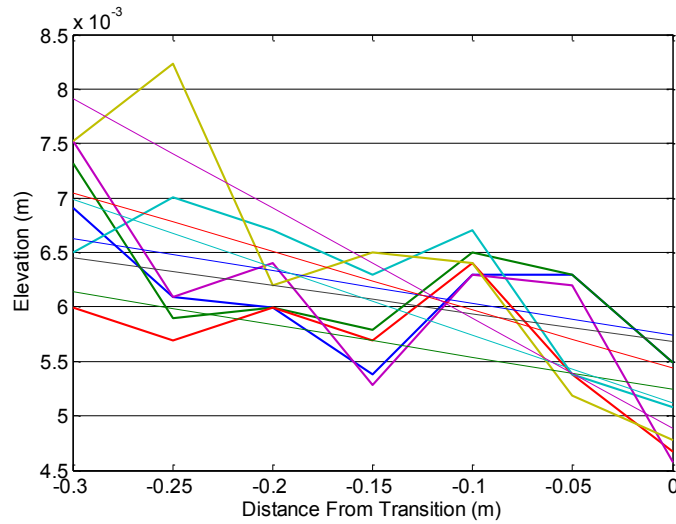


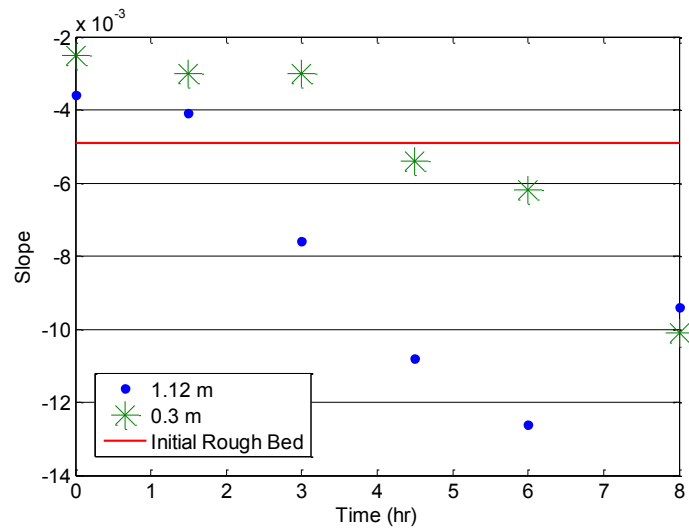
Figure 3.21. a.) Bed elevation change with respect to the pre-experiment local average bed profile. b.) Zoomed in look at the near transition region of the bed elevation change with respect to the pre-experiment local average bed profile. c.) Bed elevation change with respect to the hr 8 local average bed profile. d.) The percentage of the hr 8 local average bed elevation. Lines were used to guide the eye.



a.)



b.)



c.)

Figure 3.22. Zoomed in bed profiles with linear fit trend lines of form $y = ax + b$ where the slope “ a ” and intercept “ b ” are in Table 3.10. a.) 1.12 m. b.) 0.3 m upstream of the R-S transition. c.) the slope changes plotted verses time.

1.12 m			0.3 m		
Time	Slope a	Intercept b	Time	Slope a	Intercept b
0	-0.0036	0.0055	0	-0.0025	0.0057
1.5	-0.0041	0.0058	1.5	-0.003	0.0057
3	-0.0076	0.0045	3	-0.003	0.0052
4.5	-0.0108	0.0049	4.5	-0.0054	0.0054
6	-0.0126	0.0046	6	-0.0062	0.0051
8	-0.0094	0.0049	8	-0.0101	0.0049

Table 3.10. Slopes and intercepts for the linear trend lines of form $y = ax + b$ in Figure 3.22.



Figure 3.22. Photograph of the streaks of gravel upstream of the fixed bed R-S transition as mentioned in the text.

Chapter 4

Discussion

Perhaps the most common characteristic among all of the conditionally averaged velocities presented in Chapter 3 is the correlation between a temporary increase in downstream velocity u with the entrainment of the tracer particle. While certain experiments showed correlations between the particle movement and the other turbulence statistics w , $u'u'$, $u'w'$, and $w'w'$, none of these correlations were as consistent as that of the particle movement with the instantaneous downstream velocities. This Chapter first addresses the question as to how correlations in instantaneous downstream velocity u do not necessarily imply trends in other turbulence statistics, specifically, $u'u'$. Then, in Section 4.2 alternative bed-load transport models are discussed. Section 4.3 is on the implications of the results discussed in a broader context, and Section 4.4 discusses the frequency of the transport events.

4.1 Considerations of Trends in Downstream Velocity Pulses

To address the question as to how correlations in instantaneous downstream velocity u do not necessarily imply trends in other turbulence statistics, specifically, $u'u'$, three different sample data sets, shown in Figure 4.1-4.3 are considered here. In each of these figures, two sample data sets and their conditional average are presented. Specifically, the contents in (a), (b), and (c) in each figure are as follows:

- (a) Contains the instantaneous downstream velocity for a single point above the bed from two sample runs, where in each case, $t = 0$ represents the time at which a hypothetical particle entrainment event occurred and will be referred to as the imagined particle entrainment event; it also contains the “conditionally averaged” velocity from these two sample data sets.
- (b) Contains the instantaneous downstream velocity fluctuation u' for each sample run and the conditionally averaged velocity fluctuation u' , calculated by taking the average of u' from the two sample runs; and
- (c) Contains the instantaneous downstream velocity fluctuation correlation $u'u'$ calculated for each sample run and the conditionally averaged velocity fluctuation correlation $u'u'$ calculated by taking the average of $u'u'$ from the two sample runs.

The sample velocities were chosen to illustrate cases where there could be (I) a trend in u that correlates with a trend in $u'u'$, (II) a trend in u where there is no corresponding trend in $u'u'$, and (III) a trend in $u'u'$ where there is no similar corresponding trend in u . Cases (I) and (II) are most similar to the results from chapter 3 where trends in the conditionally averaged u results were always observed and sometimes correlated with a similar trend in $u'u'$.

For Case I (Figure 4.1) both data runs have similar increases that are in phase with each other around the time of the imagined particle entrainment event Figure 4.1a. As a result, the conditional average shows the same increase. The average run velocities for the slower and faster run results are assumed to be 2 m/s and 3 m/s, respectively. The

increases seen in the sample runs are in excess of the average run velocity. The $u'(t)$ calculated for each run (Figure 4.1(b)) is simply the relevant plots for $u(t)$ shifted downward by the average velocities for each. In this case, the downstream velocity pulses are similar for each run, so the downstream pulse in $u'(t)$ looks similar for both run sets and for the conditionally averaged result. The velocity fluctuations for each run set were calculated as $u'u'(t) = (u(t) - \langle u \rangle)^2$ and the resulting traces are plotted in Figure 4.1(c). Since the entire increases in u for the sample runs are in excess of the average run velocity, there is also an increase seen in $u'u'(t)$ for the two runs. This gives rise to a calculated $u'u'(t)$ with an increase immediately surrounding the imagined particle entrainment event that resembles the conditionally averaged velocity.

In Case (II), shown in Figure 4.2, both sample velocity sets (Figure 4.2(a)) have similar characteristics that are in phase with each other. While the conditionally averaged $u(t)$ is the same as that in Case (I), in Case (II), the average velocities for the slower and faster runs are assumed to be 2.5 m/s and 3.5 m/s, respectively. Therefore, in Case II, over the course of the time surrounding each imagined particle entrainment event, each individual run velocity are never equal to the average run velocity of that run. Therefore, $u'(t)$ is never zero during the 2 sec time interval surrounding the imagined particle entrainment event, and instead has equal parts above and below 0. As a result, $u'u'(t)$ is never 0 either for the individual runs or for the conditional average, and there is no significant trend immediately surrounding a particle entrainment event for either of the results or in the conditionally averaged downstream time series for $u'u'(t)$.

In Case (III), the two sample time series for u exhibit trends surrounding the particle entrainment event, but the trends are exactly opposite to one another relative to the base velocities in each case (2 m/s for sample 1 and 3 m/s for sample 2). In this case, the conditionally averaged $u(t)$, and the conditionally average time series $u'(t)$ do not show a trend. However, the conditionally averaged $u'u'(t)$ does show a trend.

To summarize, these three cases demonstrate sample velocity sets that can give rise to three different cases: (I) a nonzero trend in both u and $u'u'$, (II) a nonzero pulse in u and no trend in $u'u'$, and (III) no trend in u corresponding to a pulse in $u'u'$. Essentially, Case (I) demonstrated that a trend in $u'u'$ can arise when there is a pulse in u for each sample run immediately surrounding the particle entrainment event, and the average downstream velocity for each sample run is in line with the baseline velocity of the event sample. As a result of these conditions being met, trends are seen in u and $u'u'$. Case (II) demonstrated that a pulse in the conditionally averaged $u(t)$ can occur without a pulse in the conditionally averaged $u'u'(t)$ if the average downstream velocity for each sample run is actually above the baseline velocity of the event sample. This suggests that the downstream pulse of $u(t)$ corresponding to each entrainment event may be accompanied by a longer term decrease in velocity suggesting the existence of a wider area of influence of the structure associated with the particle entrainment event than can be captured by our data. Case (III) represents a situation where there is no change in the conditional averaged velocity $u(t)$ but there is an increase in $u'u'(t)$, which would be the case if an increase in turbulence correlated with an entrainment event rather than an increase in downstream velocity. Since this is not seen in the results shown in Chapter 3,

this study indicates that average velocity bursts associated with correlated velocity structures rather than bursts of random velocity fluctuations drives particle entrainment events.

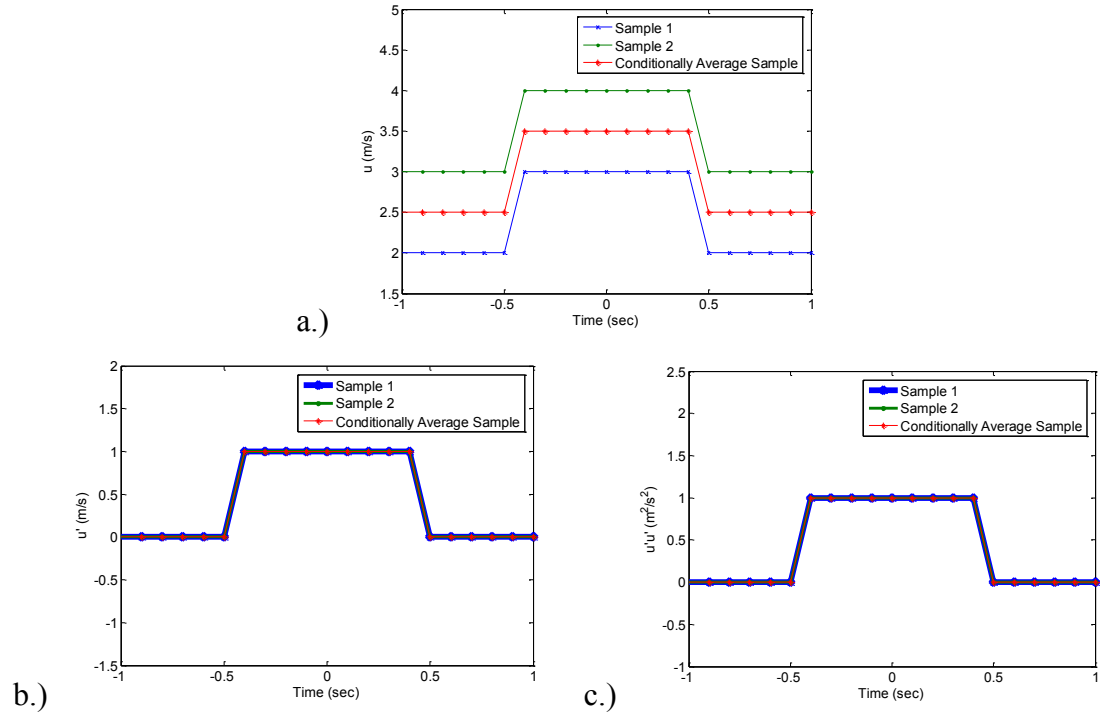
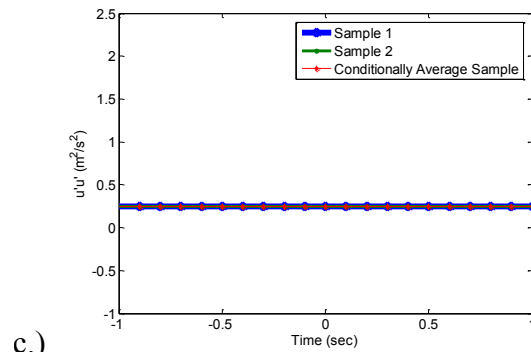
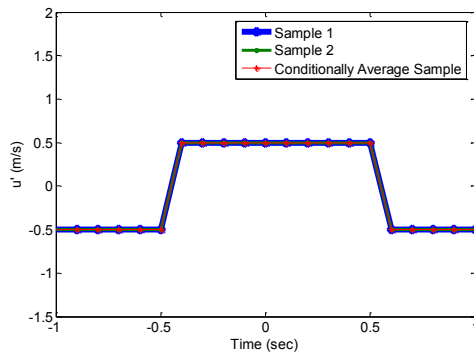
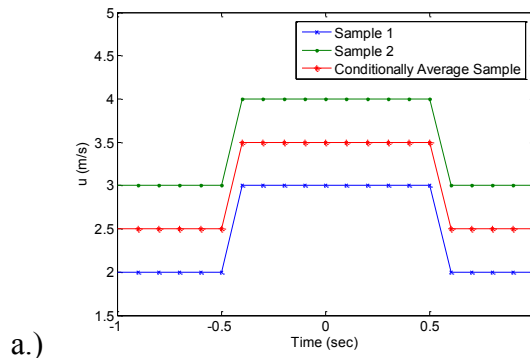


Figure 4.1. Case which demonstrates how event time series can lead to a trend in u and trend in $u'u'$. a.) u velocity run samples and conditionally averaged u . b.) u' velocity fluctuation run samples and conditionally averaged u' . c.) $u'u'$ of the run samples and the conditionally averaged $u'u'$. Lines were used to guide the eye.



b.) c.)
 Figure 4.2. Case which demonstrates how event time series can lead to a trend in u and no trend in $u'u'$. a.) u velocity run samples and conditionally averaged u . b.) u' velocity fluctuation run samples and conditionally averaged u' . c.) $u'u'$ of the run samples and the conditionally averaged $u'u'$. Lines were used to guide the eye.

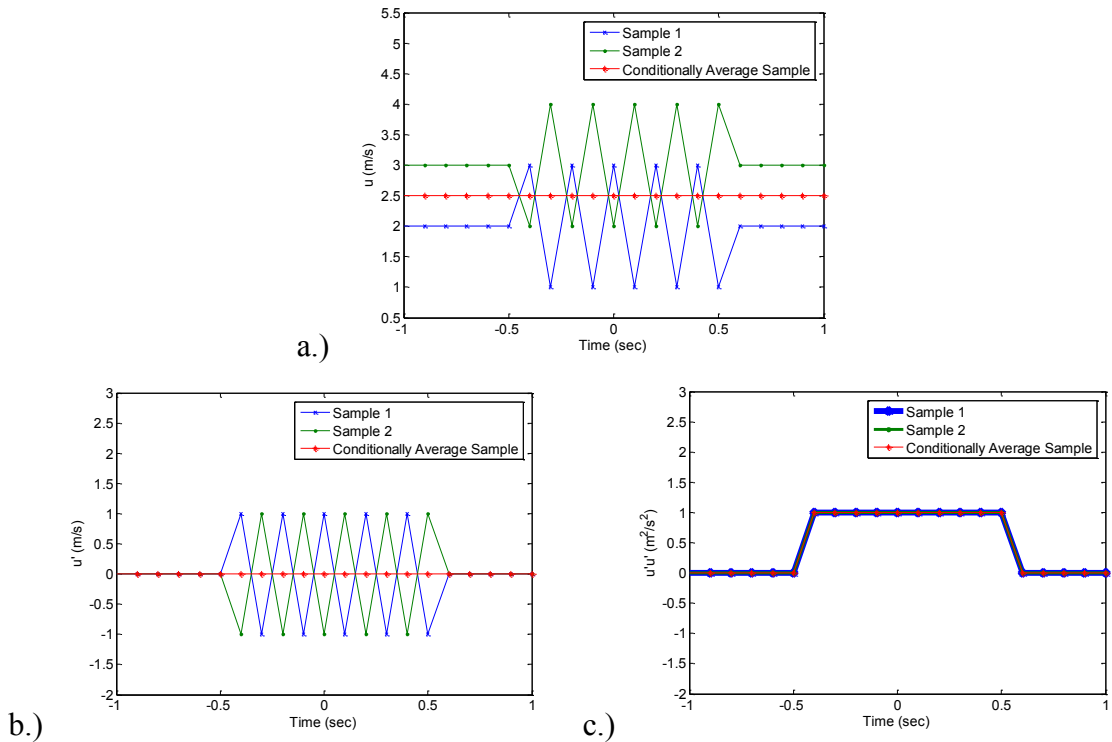


Figure 4.3. Case which demonstrates how event time series can lead to no trend in u and trend in $u'u'$. a.) u velocity run samples and conditionally averaged u . b.) u' velocity fluctuation run samples and conditionally averaged u' . c.) $u'u'$ of the run samples and the conditionally averaged $u'u'$. Lines were used to guide the eye.

4.2 Alternate Bed-load Transport Models

Before considering alternate transport models based on the results described in Section 3.1 and others like these results, it is important to note the relative success of existing transport models. Bed-load sediment transport relationships like the Meyer-Peter and Müller (equation (8)) [Meyer-Peter and Müller, 1948; Wong and Parker, 2006], are developed in flow conditions which are steady and uniform. The predictive power of bed-load sediment transport relationships is apparent in that they provide results that are reliable when applied to systems which are steady and uniform. Conditionally averaged analysis for the SS location over the fixed bed show that in steady state conditions, (e.g., Figure 3.6), there are strong correlations among nearly all turbulence

statistics. In these cases, therefore, it is unlikely for bed-load transport relationships to perform better under alternative measures of different turbulence statistics as different predictors.

On the other hand, the turbulence statistics correlate less with one another under non-uniform and unsteady conditions. Historically, in these non-uniform or unsteady conditions, the turbulence statistics have shown not to scale similarly. Correlation between sediment transport and downstream velocities u has been previously reported for non-uniform flows [Nelson *et al.*, 1995; Williams *et al.*, 1989; and Schmeeckle *et al.*, 2007]. These results appear to pertain for entrainment near roughness transitions as shown in section 3.1. A model which predicts the bed shear stress based on u may provide a framework that could be more stable under multiple flow regimes. A model was proposed by Marusic *et al.* [2001] which estimates the bed shear stress based on the downstream velocity.

$$\tau_m(x, y, z, t) = \langle \tau_w \rangle - \alpha U_\tau [\bar{u}(x + \Delta_s, y, z, t) - \langle \bar{u}(x, y, z, t) \rangle] \quad (13)$$

τ_m is the modeled instantaneous wall shear stress, $\langle \tau_w \rangle$ is the mean wall shear stress, u is the instantaneous streamwise velocity component, $(\bar{\quad})$ denotes spatial filtering operation, and $\langle \quad \rangle$ denotes time average, and α is a characteristic constant equal to 0.10. Perhaps a better model for bed-load transport could be found using this equation for stress in the MPM equation for a time-dependent bed-load transport law that performs better on average under unsteady and/or non-uniform conditions.

4.3 Implications of Results

To understand the physical significance of the results in Chapter 3, it is helpful to note certain limits to the data presented. That is, the correlations between the different turbulent velocity statistics and the particle entrainment events are simply that – correlations – not measures that directly confirm a causal relationship among the different variables. The causal relationship needs to be hypothesized and then hopefully tested by some other means. It is tempting to interpret the correlations between downstream velocity pulse and particle entrainment events as indicators that the downstream velocity pulses are the only physical cause of particle entrainment and the other statistics simply go along for the ride in certain cases. Other interpretations are possible.

One possible alternative interpretation arises from considering that the turbulence velocities at the transitions are larger than the turbulence velocities for the SS locations (Tables 3.1 and 3.2), most noticeable in the values for $u'u'$, and $u'w'$. At the SS location, where critical threshold conditions hold, it is possible that turbulence events need to be much larger than the baseline flow velocity for transport to occur. In contrast, turbulence events likely do not need to be larger than the baseline flow characteristics at the location 5 cm before the R-S transition to cause transport. This could give rise to weak, if any, correlations associated between the initial motion of the gravel particle. It could be possible that if analogous experiments were performed for uniform conditions for higher flows, similar correlations would be seen, only with the downstream velocity pulses, as those near the transition points discussed in Chapter 3.1. This interpretation may extend

to other cases where u rather than $u'w'$ and $u'u'$ have been found to correlate best with particle transport [Williams *et al.*, 1989; Nelson *et al.*, 1995; Schmeeckle *et al.*, 2007].

4.4 Frequency of Transport Events

While collecting the data, the characteristic frequency of transport events seemed to be different between the two locations tested for each bed condition and also bed roughness configuration. For the R-S transition bed configuration, transport events occurred less frequently in the SS location versus the T location for both the mobile bed R-S transition experiments, and the fixed bed R-S transition experiments. For the experiments performed over the fixed bed S-R transition bed configuration, transport events at the SS location occurred as frequently as would be expected at the SS location for the fixed bed R-S transition setup. This makes sense since the two locations are analogous. A completely unexpected situation occurred at the T location for the S-R transition bed configuration. Near the S-R transition, transport events would not occur under the flow conditions which were originally set up. The flow conditions needed to be changed in order to get events to occur, so the flow rate was increased by 15 %. Even with an increase of 15 % to the flow rate, transport events still did not occur very frequently compared to the SS location under the original flow conditions. This could be explained from a study of the response of velocity and turbulence to a S-R transition studied by *Chen and Chiew* [2003]. In their investigation, the results show that a gradual increase in the Reynolds stress and shear velocity occurs after the transition that eventually plateaus at the value for the steady bed conditions. This is different than the conclusion which was reached by *Nezu and Tominaga* [1994], who describe an

overshooting effect which occurs near the transition and then the shear velocity decreases to a plateau. This effect is similar to results obtained in closed conduit flows. An explanation for the difference between open channel flow and closed conduit flows is that in open channel flow the response to a S-R transition is not only in velocity, but also in the depth of flow [Chen and Chiew, 2003]. It is difficult to draw a direct analogy between these results and the entrainment results shown in Chapter 3 which are not clearly linked with a traditional measure of shear stress. However, if one links the downstream velocity bursts with the shear stress as proposed by Marusic *et al.* [2001] (Equation 11), one might imagine a similar issue as to how this measure of shear stress changes after a S-R transition. The relatively low frequency of entrainment events after the S-R transition described in Chapter 3 supports the conceptual framework proposed by Chen and Chiew [2003], namely, that there is no spike in the shear stress as represented by bursts in the downstream velocity immediately following a S-R transition. Instead it seems more likely that there is just a gradual rise, so that the shear stress immediately following a S-R transition is relatively low compared to that at the uniform SS location farther downstream.

Chapter 5

Summary and Conclusions

Experiments have been conducted in a large experimental flume to investigate fluid turbulence and initial motion at an individual gravel particle scale. A conditional averaging analysis, coherent structure analysis, and quadrant analysis were performed to determine how details of turbulence velocities corresponded with particle entrainment events. The following conclusions can be drawn from these results.

1. There is a strong correlation between initial motion and an increase in u for both the SS locations and the T locations of the different bed configurations investigated.
2. The peaks of the increase in the conditionally averaged u results occur before entrainment of the gravel particle takes place. The offset in the peak increases with height from the bed. This suggests that inclined coherent structures are responsible for the entrainment of the individual gravel particle.
3. The conditionally averaged results were the most clear for the fixed bed conditions. Weaker correlations exist between initial motion and decreases in w and $u'w'$, and increases in $u'u'$ for the fixed bed R-S transition SS location. At the T location, weak correlations were seen between initial motion and w , $u'u'$, $u'w'$, and if seen at all. The ability for these correlations to be captured might be sensitive to the flow conditions being studied. Correlations can be seen

when the flow conditions were near the critical threshold for motion, but near the transition where this is not necessarily the case anymore correlations are more difficult to see if at all. If previous studies were not conducted in flows near the critical threshold for motion, this could explain why previous results have not shown strong correlations with turbulent statistics other than u .

4. The angles of inclination of inclined coherent structures associated with the offset of the peak in the conditionally average u results are smaller for the T location than the SS location for the fixed bed R-S transition. The average angle for the T location is 6.7° , and 11.4° at the SS location for the fixed bed R-S transition condition. This suggests, along with the breadth of the trends seen in the u results of the conditionally averaged analysis, that the coherent structure experiences stretching and bending as it moves through the acceleration zone of the transition. The average angle for the T location of the fixed bed S-R transition condition is 8.3° , and 5.6° at the SS location. The spatial deceleration of the flow in the transition region of the S-R transition may cause the coherent structure to tip away from the bed resulting in a larger angle at the T location than compared to the downstream SS location. For the mobile bed R-S transition condition the average angle for the T location is 7.1° , and 4.9° at the SS location.
5. A quadrant analysis for the fixed bed R-S bed configuration shows that Q_4 events are the dominant quadrant event that is associated with initial motion. Q_1 events are also represented in this analysis but are not expected to be

important because the contributing velocity fluctuations are not near time $t = 0$, when initial motion occurred. Q_2 and Q_3 events were non-existent for the 0.5 sec window analysis which is most relevant to when initial motion occurred.

Similar results were obtained for the fixed bed S-R transition bed configuration.

6. A simple model was proposed for a new framework for modeling the instantaneous bed-load transport of particles. A useful test of the model would be using simultaneous transport measurements and fluid velocity measurements in non-uniform conditions such as a meandering river.

References

- Adrian, R. J., C. D. Meinhart, and C. D. Tomkins (2000), Vortex Organization in the Outer Region of the Turbulent Boundary Layer, *J. Fluid Mech.*, 422, 1-54.
- Ashida, K., and M. Michiue (1971), An Investigation of River Bed Degradation Downstream of a Dam, *Proc. 14th Int. Association of Hydraulic Research Congress*, Vol. 3, Wallingford, U.K., 247-255.
- Bottacin-Busolin, A., S. J. Tait, A. Marion, A. Chegini, and M. Tregnaghi (2008), Probabilistic Description of Grain Resistance From Simultaneous Flow Field and Grain Motion Measurements, *Water Resour. Res.*, 44, W09419.
- Brown, G. L., and A. S. Thomas (1977), Large Structure in a Turbulent Boundary Layer, *Phys. Fluids*, 20, S243-S252.
- Brownlie, W. R. (1981), Prediction of Flow Depth and Sediment Discharge in Open Channels, *Report no. KH-R-43A, W.M. Keck Laboratory of Hydraulics and Water Resources*, California Institute of Technology, Pasadena, Calif, 232.
- Buffin-Bélanger, T., A. G. Roy, and A. D. Kirkbride (2000), On Large-scale Flow Structures in a Gravel-Bed River, *Geomorphology*, 32, 417-435.
- Chen, X., and Y. Chiew (2003), Response of Velocity and Turbulence to Sudden Change of Bed Roughness in Open-Channel Flow, *J. Hydraul. Eng.*, 129(1), 35-43.
- Clifford, N. J., J. McClatchey, and J. R. French (1991), Measurements of Turbulence in the Benthic Boundary Layer over a Gravel Bed and Comparison Between Acoustic Measurements and Predictions of the Bedload Transport of Marine Gravels, *Sedimentology*, 38, 161-171.
- Dargahi, B. (1990), Controlling Mechanism of Local Scouring, *J. Hydraul. Eng.*, 192, 193-217.
- Drake, T. G., R. L. Shreve, W. E. Dietrich, P. J. Whiting, and L. B. Leopold (1988), Bedload Transport of Fine Gravel Observed by Motion-picture Photography, *J. Fluid Mech.*, 192, 193-217.
- Einstein, H. A. (1950), The Bedload Function for Sediment Transport in Open Channel Flows, *Tech. Bull. No. 1026. U.S. Dept. of Agriculture. Soil Conservation Service*. Washington, D.C.

- Engelund, F., and J. Fredsoe (1976), A Sediment Transport Model For Straight Alluvial Channels, *Nord. Hydrol.*, 7, 293-306.
- Fenton, J. D., and J. E. Abbott (1977), Initial Movement of Grains on a Stream Bed: The Effect of Relative Protrusion, *Proc. R. Soc. Lond. A.*, 352, 523-537.
- Francalanci, S., and L. Solari (2008), Bed-load Transport equation on Arbitrarily Sloping Beds, *J. Hydraul. Eng.*, 134, 110-115.
- García, M., F. López, and Y. Niño (1995), The Characterization of Near-Bed Coherent Structures In Turbulent Open Channel Flow Using Synchronized High-Speed Video and Hot-Film Measurements, *Experiments in Fluids*, 19, 16-28.
- Haidari, A. H., and C. R. Smith (1994), The Generation and Regeneration of Single Hairpin Vortices, *J. Fluid Mech.*, 277, 135-162.
- Heathershaw, A. D., and P. D. Thorne (1985), Sea-bed Noises Reveal Role of Turbulent Bursting Phenomenon in Sediment Transport by Tidal Currents, *Nature*, 316, 339-342.
- Hill, K. M., L. Dell'Angelo, and M. M. Meerschaert (2010), Heavy-tailed Travel Distance in Gravel Bed Transport: An Exploratory Enquiry, *J. Geophys. Res.*, 115, F00A14.
- Hofland, B., J. A. Battjes, and R. Booij (2005), Measurement of Fluctuating Pressures on Coarse Bed Material, *J. Hydraul. Eng.*, 131(9), 770-781.
- Kline, S. J., W. C. Reynolds, F. A. Schraub, and P. W. Runstadler (1967), The Structure of Turbulent Boundary Layers, *J. Fluid Mech.*, 30, 741-773.
- Lu, S. S., and W. W. Willmarth (1973), Measurements of the Structure of the Reynolds Stress in a Turbulent Boundary Layer, *J. Fluid Mech.*, 60, 481-511.
- Marusic, I., G. J. Kunkel, and F. Porté-Agel (2001), Experimental Study of Wall Boundary Conditions for Large-eddy Simulation, *J. Fluid Mech.*, 446, 309-320.
- McLean, S. R., J. M. Nelson, and S. R. Wolfe (1994), Turbulence Structure Over Two-dimensional Bed Forms: Implications for Sediment Transport, *J. Geophys. Res.*, 99, 12729-12747.
- Meyer-Peter, E., and R. Müller (1948), Formulas for Bed-Load Transport, *Proc. 2nd Meeting*, IAHR, Stockholm, Sweden, 39-64.
- Nelson, J. M., R. L. Shreve, S. R. McLean, and T. G. Drake (1995), Role of Near-Bed Turbulence Structure in Bed Load Transport and Bed Form Mechanics, *Water Resour. Res.*, 31(8), 2071-2086.

- Nezu, I., and A. Tominaga (1994), Response of Velocity and Turbulence to Abrupt Changes from Smooth to Rough Beds in Open-Channel Flow, *Proc. Symposium on Fundamentals and Advancements in Hydraulic Measurements and Experimentation*, Buffalo, N.Y., 195-204.
- Niño, Y., and M. H. García (1996), Experiments on Particle-Turbulence Interactions in the Near-Wall Region of an Open Channel Flow: Implications for Sediment Transport, *J. Fluid Mech.*, 326, 285-319.
- Paiement-Paradis, G., G. Marquis, and A. Roy (2010), Effects of Turbulence on the Transport of Individual Particles as Bedload in a Gravel-Bed River, *Earth Surface Processes and Landforms*, 36, 106-117.
- Parker, G. (1990), Surface-Based Bedload Transport Relation for Gravel Rivers, *J. Hydraul. Res.*, 28(4), 417-436.
- Papanicolaou, A. N., P. Diplas, C. L. Dancy, and M. Balakrishnan (2001), Surface Roughness Effects in Near-Bed Turbulence: Implications to Sediment Entrainment, *J. Eng. Mech.*, 127(3), 211-218.
- Parsheh, M., F. Sotiropoulos, and F. Porté-Agel (2010), Estimation of Power Spectra of Acoustic-Doppler Velocimetry Data Contaminated with Intermittent Spikes, *J. Hydraul. Eng.*, 136(6), 368-378.
- Pope, S. B. (2005), *Turbulent Flows*, Cambridge University Press, New York, N.Y.
- Rajagopalan, S., and R. A. Antonia (1979), Some Properties of the Large Structure in a fully Developed Turbulent Duct Flow, *Phys. Fluids*, 22, 614-622.
- Robinson, S. K. (1991), Coherent Motions in the Turbulent Boundary Layer, *Annu. Rev. Fluid Mech.*, 23, 601-639.
- Roy, A. G., T. Buffin-Bélanger, H. Lamarre, and A. D. Kirkbride (2004), Size, Shape and Dynamics of Large-scale Turbulent Flow Structures in a Gravel-bed River, *J. Fluid Mech.*, 500, 1-27.
- Schmeeckle, M. W., J. M. Nelson, and R. L. Shreve (2007), Forces on Stationary Particles in Near-bed Turbulent Flows, *J. Geophys. Res.*, 112, F02003.
- Sechet, P., and B. Le Guennec (1999), The Role of Near Wall Turbulent Structures on Sediment Transport, *Water Resour. Res.*, 33 (17), 3646-3656.

- Theodorsen, T. (1952), Mechanism of Turbulence, *Proc. Midwest. Conf. Fluid Me.*, 2nd, Columbus, Ohio, 1-18.
- Thorne, P. D., J. J. Williams, and A. D. Heathershaw (1989), In situ Acoustic Measurements of Marine Gravel Threshold and Transport, *Sedimentology*, 36, 61-74.
- Valyrakis, M., P. Diplas, C. L. Dancey, K. Greer, and A. O. Celik (2010), Role of Instantaneous Force Magnitude and Duration on Particle Entrainment, *J. Geophys. Res.*, 115, F02006.
- Van Rijn, L. C. (1984a), Sediment Transport, Part I: Bed Load Transport, *J. Hydraul. Eng.*, 110(10), 1431-1456.
- Van Rijn, L. C. (1984b), Sediment Transport, Part II: Suspended Load Transport, *J. Hydraul. Eng.*, 110(11), 1613-1641.
- Wallace, J. M., H. Eckelmann, and R. S. Brodkey (1972), The Wall Region in Turbulent Shear Flow, *J. Fluid Mech.*, 54, 39-48.
- Wilcock, P. R., and J. C. Crowe (2003), Surface-based Transport Model for Mixed-Size Sediment, *J. Hydraul. Eng.*, 129(2), 120-128.
- Williams, J. J. (1990), Video Observations of Marine Gravel Transport, *Geo-Marine Letters*, 10, 157-164.
- Williams, J. J., P. D. Thorne, and A. D. Heathershaw (1989), Measurements of Turbulence in the Benthic Boundary Layer Over a Gravel Bed, *Sedimentology*, 36, 959-971.
- Willmarth, W. W., and S. S. Lu (1971), Structure of the Reynolds Stress Near the Wall, *J. Fluid Mech.*, 55 (1), 65-92.
- Wong, M., and G. Parker (2006), Reanalysis and Correction of Bed-Load Relation of Meyer-Peter and Müller Using Their Own Database, *J. Hydraul. Eng.*, 132(11), 1159-1168.

Appendix

Appendix 1

Data from Fixed Bed R-S Transition

Location 2

The fixed bed R-S transition location 2 data corresponds to the set of data collected over the fixed bed R-S transition discussed in section 3.1.2. To determine if the R-S transition was responsible for the differences in the results between the two locations, the R-S transition was repositioned to a new location, transition location 2, which was 2.45 m downstream from where the first roughness transition location was. The purpose for repositioning the R-S transition was to confirm that the difference in the results were not caused by flow alterations influenced by flume impurities, but instead caused from the effects of the R-S transition. The SS location selected relative to the new location of the R-S transition was the T location for the initial investigation. The results from the fixed bed R-S transition location 2 confirm that the differences in the results between the SS location and the T location are not a result of flow imperfections introduced by the flume or location specific. This is because the results for the SS location and the T location of Figure A.3, are similar to the results for the SS location and the T location of Figure 3.6.

R-S Transition Fixed Bed			
Transition Location 2			
Flume Dimensions			
A	0.6		m
B	8.52		m
C	11.02		m
D	5		cm
Experiment Properties			
	Rough Section	Smooth Section	
h	0.115	0.111	m
U	0.672	0.701	m/s
Q	0.0387	0.0387	m ³ /s
S	0.0049	0.0051	m/m
Re	77476	77476	
Fr	0.632	0.673	
$D16$	6.2	1.9	mm
$D50$	7.1	2.5	mm
$D65$	7.4	2.8	mm
$D84$	7.8	3.1	mm
$D90$	8.0	3.3	mm

Table A.1. R-S transition location 2 fixed bed flume dimensions and experimental properties. This table corresponds to Table 2.2. Refer to Figure 2.2a for flume dimensions.

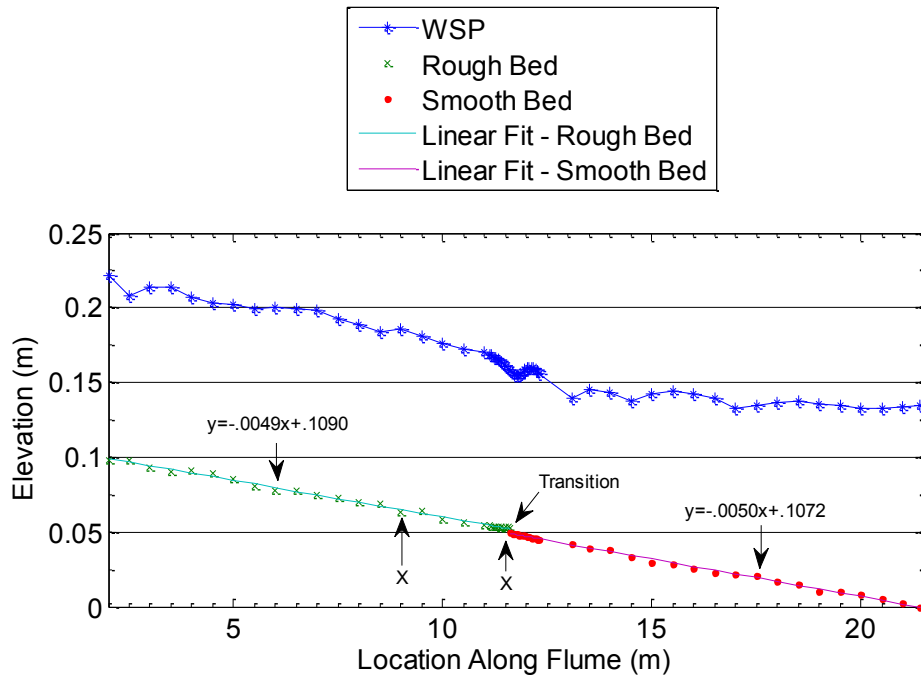


Figure A.1. Bed profile and WSP for the experiments performed to confirm the results over the fixed bed. The data markers are at the points where data were collected. The equations represent the linear trend lines associated with the rough and smooth sections of the bed and provide the slopes of those sections. The two locations where data were collected are marked with an “X”. A line was used for the WSP to guide the eye. This figure corresponds to Figure 3.4.

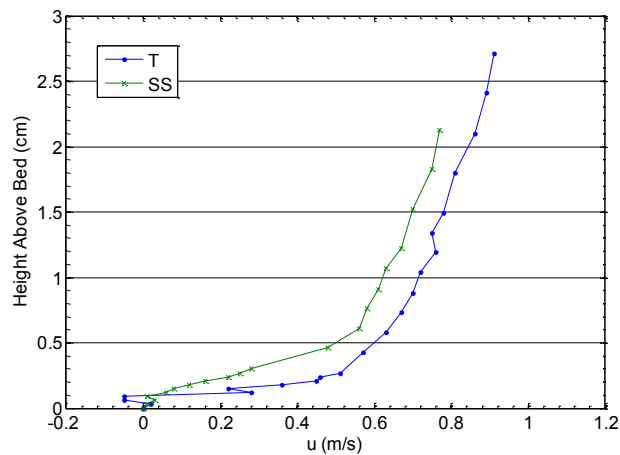
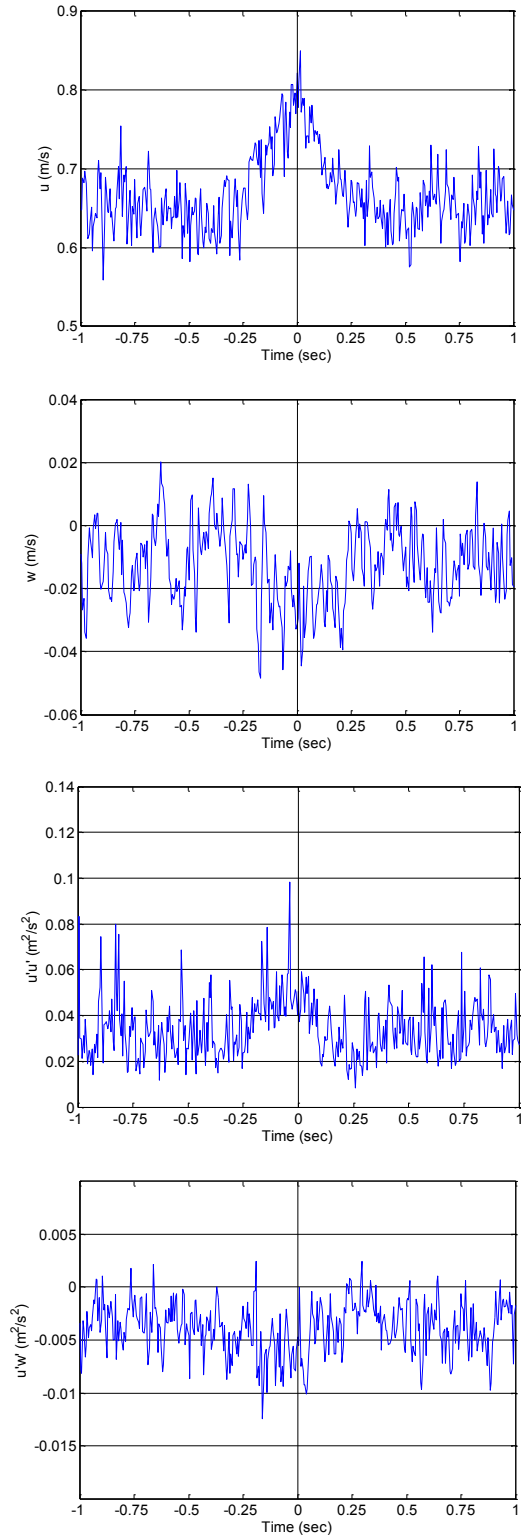


Figure A.2. Velocity profiles for the two locations investigated to confirm the results over the fixed bed. Lines were used to guide the eye. This figure corresponds to Figure 3.5.

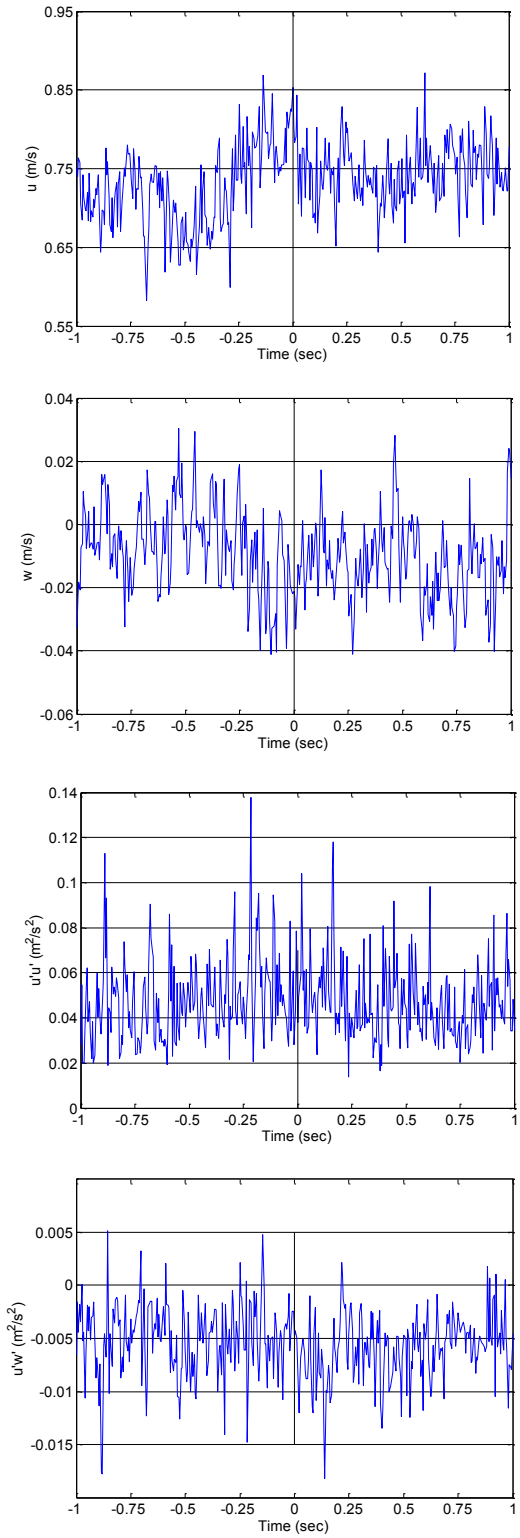
SS

— 1.07 cm



T

— 1.04 cm



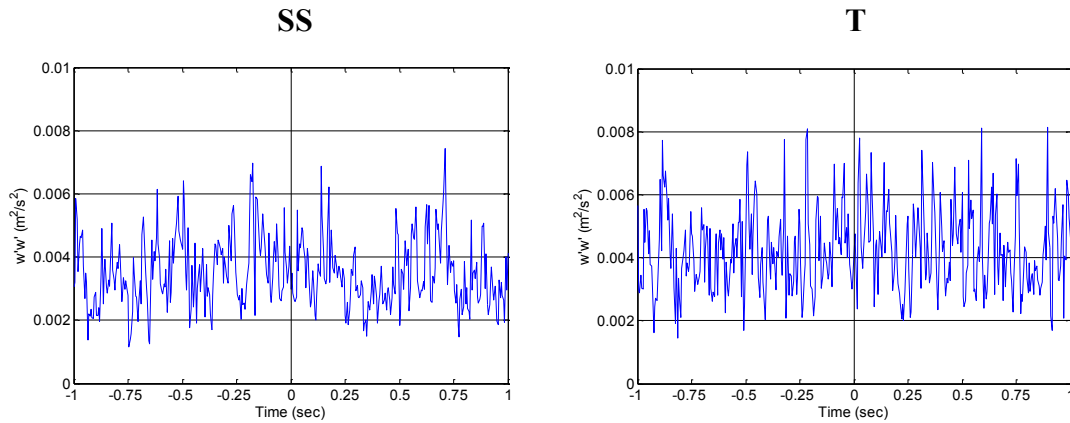


Figure A.3. Conditionally averaged results for the turbulence statistics, u , w , $u'u'$, $u'w'$, $w'w'$, for the two locations investigated to confirm the results over the fixed bed. The left column of figures is the results for the SS location. The right column of figures is the results for the T location. This figure corresponds to Figure 3.6.

Bed Condition	Location	Height above bed cm	u m/s	w m/s	$u'u'$ m^2/s^2	$w'w'$ m^2/s^2	$u'w'$ m^2/s^2	
Fixed	Transition Location 2	SS	1.07	0.64	-0.010	0.029	0.0034	-0.0039
Fixed	Transition Location 2	T	1.04	0.72	-0.008	0.035	0.0041	-0.0052

Table A.2. Average turbulence statistics for the investigation to confirm the results of the fixed bed. This table corresponds to Table 3.2.

Bed Condition	Location	Height above bed cm	θ Deg	Error θ \pm Deg	Location	Height above bed cm	θ Deg	Error θ \pm Deg	
Fixed	Transition Location 2	SS	1.07	87.4*	44.7*	T	1.04	5.7	0.6

Table A.3. Angles of inclined coherent structures associated with the offset of the peak seen in conditionally averaged downstream velocity u relative to when initial motion occurred. This table corresponds to Table 3.4. (*) denotes angles are oblique which represent angles towards the bed.

Bed Condition	Location	Height Above Bed cm	2 Second Window, 0.5 Second Window				
			Q ₁ Outward Interactions	Q ₂ Ejections	Q ₃ Inward Interactions	Q ₄ Sweeps	
Fixed	Transition Location 2	SS	1.07	21, 14	21, 3	12, 0	45, 83
Fixed	Transition Location 2	T	1.04	22, 26	21, 6	14, 11	43, 57

Table A.4. Quadrant analysis results for the investigation to confirm the results of the fixed bed. This table corresponds to Tables 3.7 and 3.8 for the SS location and the T location, respectively.